ERASMUS MUNDUS MSC PROGRAMME

COASTAL AND MARINE ENGINEERING AND MANAGEMENT
COMEM

EROSIVE BAR MIGRATION USING DENSITY AND DIAMETER SCALED SEDIMENT

Delft University of Technology
June 2011

Adam S. Keen
4055179

The Erasmus Mundus MSc Coastal and Marine Engineering and Management is an integrated programme organized by five European partner institutions, coordinated by Delft University of Technology (TU Delft).
The joint study programme of 120 ECTS credits (two years full-time) has been obtained at three of the five CoMEM partner institutions:

- Norges Teknisk- Naturvitenskapelige Universitet (NTNU) Trondheim, Norway
- Technische Universiteit (TU) Delft, The Netherlands
- City University London, Great Britain
- Universitat Politècnica de Catalunya (UPC), Barcelona, Spain
- University of Southampton, Southampton, Great Britain

The first year consists of the first and second semesters of 30 ECTS each, spent at NTNU, Trondheim and Delft University of Technology respectively.
The second year allows for specialization in three subjects and during the third semester courses are taken with a focus on advanced topics in the selected area of specialization:

- Engineering
- Management
- Environment

In the fourth and final semester an MSc project and thesis have to be completed.
The two year CoMEM programme leads to three officially recognized MSc diploma certificates. These will be issued by the three universities which have been attended by the student. The transcripts issued with the MSc Diploma Certificate of each university include grades/marks for each subject. A complete overview of subjects and ECTS credits is included in the Diploma Supplement, as received from the CoMEM coordinating university, Delft University of Technology (TU Delft).

Information regarding the CoMEM programme can be obtained from the programme coordinator and director

Prof. Dr. Ir. Marcel J.F. Stive
Delft University of Technology
Faculty of Civil Engineering and geosciences
P.O. Box 5048
2600 GA Delft
The Netherlands

Erosive Bar Migration Using Density and Diameter Scaled Sediment

by

Adam S. Keen

A thesis presented in partial fulfillment of the
requirements for the degree of

Master of Science

within the group of

Coastal and Marine Engineering and Management (CoMEM)

in the field of

Civil Engineering

at

Delft University of Technology

Submitted for approval on

June 27, 2011

Thesis Committee:

Prof. Dr. Ir. M.J.F. Stive	Delft University of Technology (Chair)
Prof. Dr. Ir. W.S.J. Uijttewaal	Delft University of Technology
Ir. M. Henriquez	Delft University of Technology
Ir. D.J. Walstra	Deltares / Delft University of Technology

Contributions:

Dr. I. Cáceres	Universitat Politècnica de Catalunya

Erosive Bar Migration Using Density and Diameter Scaled Sediment / Adam S. Keen / June 27, 2011

This research was carried out at:

Environmental Fluid Mechanics Laboratory
Faculty of Civil Engineering
Delft University of Technology
Stevinweg 1, 2628 CN Delft
The Netherlands

Preface

This thesis presents the final installment of the Master of Science in Coastal and Marine Engineering and Management (CoMEM) of the Faculty of Civil Engineering at Delft University of Technology, The Netherlands.

I would like to thank my supervisors: prof.dr.ir. M.J.F. Stive, prof.dr.ir. W.S.J. Uijttewaal, and ir. M. Henriquez, for their help and guidance during the realization of this thesis. I would especially like to thank Martijn for his thoughtful insight and patience. And also dr. I. Cáceres for his assistance during the conceptual phase and for providing the SANDS data set.

Furthermore, I would like to thank all the staff at the Fluid Mechanics Laboratory (Delft University of Technology) for their help during the physical modeling phase. The support of ir. S. de Vree and J. van Duin were necessary to the timely delivery of this thesis. Without them, it would not have been possible.

I would finally like to thank my parents for the support they have given me over the last two years and throughout my education.

Adam S. Keen
Delft 2011

Abstract

Mobile bed scaling (for scales smaller than 1:1) does not allow for ideal similarity between all nondimensional parameters. This leads to an exaggerated presence of one process over another or the development of scale effects. The complexity of the surf zone makes it especially difficult to separate and quantify the effect of sediment scaling on each individual process. As a result, the impact of sediment scaling on the holistic morphodynamic process is poorly understood.

Profiles were obtained at TU Delft (scale 1:10) following the testing regime used during the SANDS project. This set made use of density and diameter scaled sediment ($\rho_s = 1200\ kg/m^3$ and $d_{50} = 0.52\ mm$); scaled according to the bed load model of Henriquez, Reniers et al. (2008). The set used for analysis here includes the Hannover (prototype scale 1:1) and Deltares (Froude scale 1:6) profiles obtained during SANDS.

The present work looks to extend what is currently known about the impact of sediment scaling on nearshore transport processes. Three main objectives are identified: 1) Showing profile development and inferred transport rates, compare nondimensional parameters across the nearshore and surf zone; 2) Identify how spatial variance of dominate hydrodynamic and sediment transport regimes across the surf zone are influenced by the subsequent scaling; 3) Explain morphological differences due to scaling by observing the small scale transport process.

Analysis of the profiles showed a marked degree of geometrical similarity between all three facilities. More specifically, the development of a bar-trough system and subsequent offshore migration. The transport rates were, however, divergent. Compared to Hannover, the transport rates at Deltares were low where conversely TU Delft was high.

Using ideal scaling theories as a basis, the cross shore distribution of the nondimensional parameters at TU Delft suggested that both sediment mobility and near bed suspension were similar with prototype. However, due to a large fall velocity, the Dean number was underestimated. From the use of Froude scaling at Deltares, the nondimensional parameters suggested that neither near bed nor suspended load transport regimes were reproduced correctly. This can mostly be attributed to the rippled bed state and reduced Shields value.

A simple depth and time averaged model was also used to decompose the sediment concentrations. These concentrations were used to check consistency of the nondimensional parameter agreement with the manifestation of the physical process. Inconsistent with the nondimensional results, TU Delft showed that near bed sediment mobility and suspension was high. It is believed this led to the exaggerated sediment fluxes. Concentrations at Deltares suggest the rippled bed introduced a thinned boundary layer which caused decreased sediment mobility and the decreased sediment fluxes.

Contents

1 INTRODUCTION

1.1 A Need for Scaling in Nearshore Mobile Bed Experiments

The nearshore is a highly active hydrodynamic and morphodynamic environment. It is under constant influence from a number of different processes. In order to describe the processes which take place in the nearshore, a number of nondimensional parameters have been derived to describe the relative influence of each forcing component. Parameters like Froude or Shields express numerically the relative influence of one process over another.

The nature of the nearshore provides a unique challenge to physical modeling. Through mobile bed experimentation, researchers strive to reproduce in situ conditions in the laboratory. However, for many experiments, the facility size and cost required for full scale experiments is beyond the capability. Therefore, some physical models have to be simplified and scaled down generating what are known as model and scale effects.

There is the possibility even at prototype scale, where all scale relations should theoretical be preserved, comparison with in situ profiles present inconsistent results. These are what are known as model effects. They are a consequence of the artificialness of model testing. Environmental factors such as wind, tide and longshore currents are usually neglected and consequently their contributions to transport. Even at prototype scale, model setups in 2D and 3D over simplify nature limiting the number of factors which influence the morphology. This oversimplification leads to these inconsistencies.

Once a model needs to be reduced in size, process scaling can lead to what are known as scale effects. Scale effects are an exaggerated importance of some physical process in a model which is not as important in prototype. Like model effects, scale effects can also give inconsistent and erroneous results. These require modeler interpretation to deciding what is valid and what is not.

With a large number of coexisting processes and scale effects, it can be difficult to quantify the relative effect of sediment scaling on each individual process. As a result, the impact of sediment scaling on individual processes and resultant morphodynamics is poorly understood. Depending on the process being reproduced, different scaling theories have been proposed to deal with especially scaling problems. Specialized scaling theories attempt to correctly capture dominant processes while minimizing scale effects found in secondary processes. It is through techniques such as these that valid results can be found.

1.2 Study Objectives

The following work looks at a theory using density and diameter scaled sediment to reproduce, at scale 1:10, bed load transport in the offshore migration of a shore parallel sand bar. There are four objectives:

- Obtain a 1:15 erosive profile set using similar testing methods to the Hannover and Deltares facilities during the SANDS project. This erosive set is to employ density and diameter scaled sediment; scaled according to the bed load method of Henriquez, Reniers et al. (2008).

- Showing profile development and inferred transport rates, compare nondimensional parameters across the nearshore and surf zone.

- Identify how spatial variance of dominate hydrodynamic and sediment transport regimes across the surf zone are influenced by the subsequent scaling.

- Explain morphological differences due to scaling by relating the small scale process.

With these objectives, and using the unique data sets available to the project, the intent is to explain the physics relating the influence of sediment scaling on coexisting process and subsequent morphological development.

1.3 Outline of Thesis

In Chapter 2 the complex hydrodynamic and morphodynamic nature of the nearshore is discussed. After, a number of nondimensional parameters are presented which are used to scale nearshore processes. This is followed by a discussion on scaling theories. Finally is a short summary of the experiments conducted during the SANDS project in the facilities at Hannover and Deltares.

Chapter 3 focuses on the experimental test setup. First is a description of the lab setup and materials. Then the hydraulic boundary conditions are presented. Thereafter is a summary of the testing schedule.

The results and analysis are presented in Chapter 4. The hydraulic conditions are presented first. This is followed by an analysis of the cross shore variance of the ideal scaling sets. Scaling results are presented for both bed and suspended load similarity sets. Finally the cross shore variance of the undertow and time averaged concentration quantities are presented. Both depth averaged and reference level concentrations are resolved.

Conclusions and recommendations for further research are presented in Chapter 5.

Chapter 6 contains a list of references.

2 THE NEARSHORE AND MOBILE BED SCALING

2.1 The Complex Nature of the Nearshore

Sediment transport processes can be broken into two dominant regimes: bed load and suspended load transport. According to Bosboom and Stive (2010), bed load transport is the transport of sediment particles in a thin layer close to the bed. These particles are more or less in constant contact with the bottom. In contrast to bed load transport, suspended load transport is defined by Bosboom and Stive (2010) as the transport of sediment particles in the water column without any contact with the bed. The particles are kept in suspension mainly by turbulent diffusive forces and are characterized by the fact that they do not respond instantly to forcing.

The complex nearshore brings with it a strong cross shore variance in the physical cross shore transport processes. Nondimensional parameters are able to relate numerically the presence of these processes. However, a physical understanding of these transport processes is first needed to better understand this relationship. Therefore, a brief summary of the dominant suspension and transport processes is presented hereafter.

With a strong spatial variance in transport processes, the nearshore can be compartmentalized into five characteristic regions (Figure 2.1): the rippled bed region, the plain bed, the outer surf zone, the inner surf zone and swash zone.

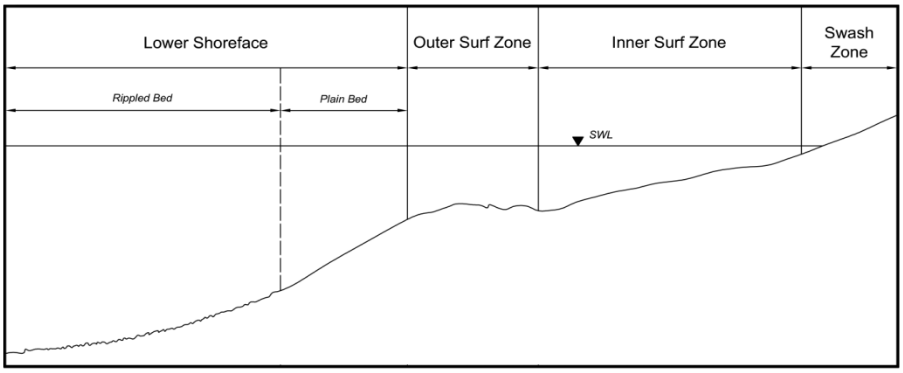

Figure 2.1 *Transport regimes across the nearshore can be divided into transport zones. Each zone defines transport modes ranging from bed load dominated to suspended load dominated. The degree of transport contributed by each regime can be defined numerically using nondimensional parameters.*

The rippled bed region is the outer most boundary of the nearshore. Within this region, the influence of waves has a reduced but significant presence. With large relative water depths, the oscillatory wave influence is lessened, reducing the shear stress and causing the bed to ripple. With waves and ripples, adverse pressure gradients develop causing flow separation. This flow separation generates the development of a ripple vortex. This small vortex moves across the ripple with the oscillatory motion approximately 90 degrees out of phase.

Ripple vortices have a strong influence on near bed processes and sediment suspension. Ribberink, van der Werf et al. (2008) state that ripples, flow separation and coherent vortex motions dominate the entrainment, transport and resettling of sand grains. In particular, turbulence associated with vortex shedding around the ripples leads to an accentuated role of suspended sediment in the transport processes (compared to similar smooth bed processes). As the vortex moves across the ripple, it mobilizes and entrains sediment. This sediment moves with the vortex and during vortex shedding, is released into the water column. This causes the sediment mobilization and suspension process to become organized, correlating but out of phase with the oscillatory motion.

The nearshore also contains a smooth bed region on the outside of the breaker bar known as the sheet flow region. As waves propagate onshore, decreased water depth and increased wave shoaling increase orbital velocities near the bed. This process increases the near bed shear stress and smoothes the bed. Instead of rippling, the bed now becomes plain. With a plain bed, sediment pickup and suspension is determined by the boundary layer processes. In this region, the boundary layer processes are strong enough to not only induce bed load transport but also generate a certain degree of suspension. However, without the presence of added turbulence to the water column, transport remains close to the bed defined here as sheet flow.

As the waves transition from the lower shoreface to outer surf zone, the degree of shoaling causes the waves to begin to break. Church and Thornton (1993) have shown that wave breaking introduces a significant degree of turbulence that enhances mixing. Ting and Kirby (1994) have also shown that the degree of mixing is often dependent on the type of breaking. While various types of breaking do occur, the outer surf zone is mostly defined by plunging breakers. These waves distribute a large amount of turbulence throughout the water column. This turbulence is introduced by the wave jet plunging into the forward wave trough. The wave jet is so significant it has implications on both the sediment mobility and suspension. Sediment mobilization by the wave jet minimizes the near bed processes, causing the region to be suspension dominated.

The inner surf zone is one of the most complex regions across the surf zone and therefore one of the most difficult to scale. Because of the bathometric influence, the breaking process in the inner surf zone is dominated by spilling breakers. Unlike plunging breakers, Ting and Kirby (1994) have shown that spilling breakers tend to focus the breaking induced turbulent mixing toward the surface. The lack of a wave jet simply does not distribute turbulence thorough the water column. Waves that break or have broken progress shoreward with a roller which acts as a temporary energy storage and dissipation mechanism. Many authors [Ting and Kirby (1994) & Boers (2005)] have shown this roller is also continuously contributing turbulence to the water column, which especially enhances sediment suspension. However, at present, there is some disagreement about the contribution of a spilling breaker and surface roller to turbulence induced sediment mobility.

Due to the irregularity of the sea state, wave breaking is not solely responsible for sediment suspension in this region. In addition, there are a certain number of waves which shoal as they progress over the breaker bar but remain stable and do not break. As these waves propagate into the trough, they de-shoal and subsequently re-shoal with an approach to the shoreline. The resulting waveform is a rearrangement of the incident and high frequency components. Eventually these waves break in a spilling type manner. The contributions of breaking, de-shoaling and re-shoaling to the result sediment transport process is poorly understood and therefore makes transport in this region complex. However, compared to a plunging breaker, the presence of spilling and roller induced turbulence has fewer implications on suspended and near bed processes. Therefore, it is believed that both bed load and suspended processes generate joint contributions to the resultant sediment transport process in this region.

At the inner most edge of the profile is the swash zone. Elfink et al. (2002) define this area as the region where the beach face is intermittently exposed to the atmosphere, ranging on time scales of minutes to seconds. The swash zone therefore represents the interface between land and sea and does have influence on the surf zone processes. However, as the aim of the present work is submerged transport, processes here will not be focused upon.

It is quite evident that across the nearshore, the processes that contribute to sediment suspension and transport are quite localized and heterogeneous. Because all these processes are occurring at the same time and each contributes to the holistic development makes scaling quite difficult. However, it is the dominance of one regime over the other which determines the resultant morphology. This allows scaling emphasis to be placed on particular processes. Therefore, to determining the net resultant transport of these processes, transport is usually quantified solely by the hydraulic terms. Because these terms represent the main sediment advection constituents, their respective contributions are able to embody the net sediment transport. Deigaard, Fredsøe et al. (1999) defined net sediment transport by three advective constitutes (Figure 2.2): boundary layer streaming, sediment drift and return flow transport.

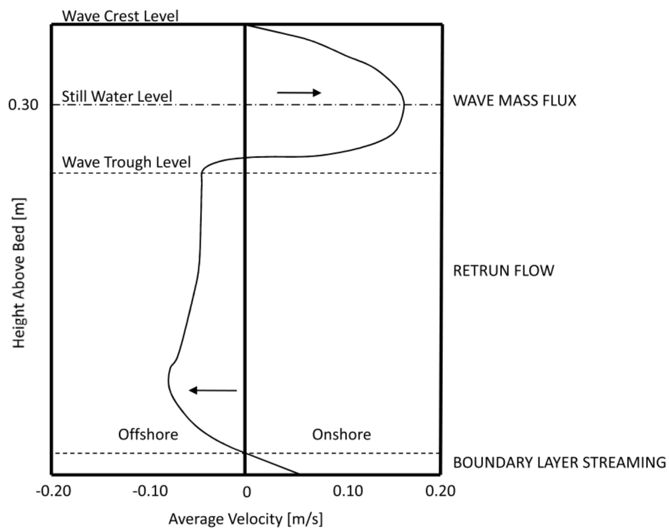

Figure 2.2 *A typical vertical velocity profile responsible for on- and offshore sediment transport [after Bosboom and Stive (2010)].Onshore transport is defined in the upper part of the water column by the wave mass flux and near the bed by boundary layer streaming. The undertow represents the dominant offshore transport component.*

Sediment drift is a well documented transport mechanism. The oscillatory motion of waves induces a net fluid drift in the direction of wave propagation known as Stokes drift. As the main advective component to sediment transport is by the fluid, this fluid drift also influences the transport. Deigaard, Fredsøe et al. (1999) explain that because of the non-uniformity of the flow and the presence of vertical velocities, the suspended sediment concentration is stretched under the wave crest and suppressed under the wave troughs. Because this process is unequal, an onshore directed drift of sediment is generated.

Demonstrated by Longuet-Higgins (1953), the non-uniformity of wave motions also causes the expansion of the boundary layer under wave crests and suppression under the troughs. This induces a transfer of momentum within the boundary layer and an onshore directed velocity in the direction of wave propagation. This is known as boundary layer streaming. Sediment which remains close to the bed is advected onshore by these velocities.

The return flow constitutes the dominant offshore contribution to surf zone sediment transport. According to the mass balance, water cannot accumulate at the shoreline. Therefore an offshore directed return flow must compensate for the onshore wave induced mass flux. Highly energetic conditions however increase the amount of wave induced setup within the surf zone. Using a momentum balance, a pressure term accounts for the effect of the water level gradient. Reniers, Thornton et al. (2004) have suggested that this term causes the return flow to dominate the momentum balance with the bottom boundary layer and wave drift generating a dominant offshore flow. Many authors have determined [Stive and Battjes (1984) & Vellinga (1986)] that resultant offshore transport is strongly correlated with the return flow. Stive and Battjes (1984) suggest that a first order estimate of offshore sediment transport can be determined by the depth average return flow velocities and sediment concentrations alone.

The leading theory which explains the location of the breaker bar is strongly correlated with the magnitude of the advective components. Thornton, Humiston et al. (1996) suggested that the breaker bar is located at the convergence location of the short wave skewness and return flow. Before the return flow migrates over the bar, it reduces in strength due to an increase in depth. At the location where the onshore and offshore terms converge due to this reduction, the material is deposited. It is this mechanism which forms and dictates the bar location.

2.2 Surf Zone Parameters and Scaling

Nondimensional parameters relate numerically the relative presence of hydrodynamic and sediment transport regimes. They therefore provide a means to reduce mobile bed physical models in scale while attempting to preserve similar relative processes. Even though the hydrodynamics and transport process are interrelated through the morphodynamics, the two components are usually scaled independently.

2.2.1 Hydraulic scaling

Hydrodynamic scaling theories focus on scaling either individual wave components or an entire time series in order to correctly reproduce dominant hydrodynamic regimes. While the following relations are rather well known, it is important that they are scaled correctly. The hydrodynamics represent the major forcing component of the research.

Reynolds number

The Reynolds number is a nondimensional quantity which expresses the relation of the inertial and viscous forces. It is given as the ratio of the inertial to the viscous forces in the form:

$$Re = \frac{\rho l^2 {U_o}^2}{\mu V l} = \frac{\rho l U_o}{\mu} = \frac{l U_o}{\nu} \tag{2.1}$$

where:

ρ	Density of fluid	kg/m^3
l	Characteristic length	m
U_o	Mean flow velocity	m/s
μ	Dynamic viscosity of fluid	kg/m-s
ν	Kinematic viscosity of fluid	m^2/s

In physical processes, the Reynolds number characterizes whether a flow is under a laminar or turbulent regime. Turbulent fluid flow undergoes irregular fluctuations, or mixing, in contrast to laminar flow, where the fluid moves in smooth paths. Values less than a critical value are classified as laminar flow whereas, conversely, flows greater than the critical value are turbulent. Many nearshore coastal processes fall within the turbulent regime.

It is important that the regime classification is represented properly in the laboratory model. In order to obtain model and prototype scale similarity, the Reynolds number in model scale and prototype scale are set equal to each other:

$$\left(\frac{\rho l U_o}{\mu}\right)_p = \left(\frac{\rho l U_o}{\mu}\right)_m \tag{2.2}$$

Rearranging these equations leads to:

$$\left(\frac{\rho_p}{\rho_m}\right)\left(\frac{l_p}{l_m}\right)\left(\frac{{U_o}_p}{{U_o}_m}\right) = \left(\frac{\mu_p}{\mu_m}\right) \tag{2.3}$$

To simplify this relation, model and prototype parameter values are usually expressed in the form of scale ratios:

$$n = \frac{p_p}{p_m} \tag{2.4}$$

where:

p	Arbitrary parameter in model (m) and prototype (p)	-

Inserting this simplification into Equation 2.3 leads to:

$$n_{Re} = \frac{n_\rho n_l n_{U_o}}{n_\mu} \tag{2.5}$$

where:

n	Scale ratio of prototype value to model value	-

As it is often difficult to fill a flume or wave tank with a fluid other than water (due to the volume required), the fluid density (n_ρ) and viscosity (n_μ) terms are often assumed to be equal to one, leading to:

$$n_{Re} = n_l n_{U_o} \tag{2.6}$$

For similarity, it is often sufficient to ensure that the scaled experiment is within the turbulent regime without scaling exactly to precision.

Froude number

The Froude number is a nondimensional quantity which expresses the relation of the inertial and gravity forces. It is given as the ratio of the inertial to the gravity force in the form:

$$Fr = \sqrt{\frac{\rho l^2 U^2}{\rho l^3 g}} = \frac{U}{\sqrt{gl}} \tag{2.7}$$

where:

U	Characteristic velocity	m/s
g	Gravitational acceleration	m/s^2

In order to obtain model and prototype similarity, the Froude number in model scale and prototype scale are set equal:

$$\left(\frac{U}{\sqrt{gl}}\right)_p = \left(\frac{U}{\sqrt{gl}}\right)_m \tag{2.8}$$

Rearranging this equation leads to:

$$\frac{U_p}{U_m} = \sqrt{\left(\frac{g_p}{g_m}\right)\left(\frac{l_p}{l_m}\right)} \tag{2.9}$$

Assuming the gravity scale is equal to one, the above equation (Eq. 2.9) can further be expressed in terms of scale ratios, $n = p_p/p_m$.

$$n_{Fr} = \frac{n_U}{{n_l}^{0.5}} \tag{2.10}$$

Using the scale relation of Equation 2.10 with the characteristic velocity and length, a number of wave parameters can be scaled. The following relations have been proposed by Noda (1972), Kamphuis (1972) and Vellinga (1986):

$$n_u = n_T = (n_L)^{0.5} = (n_H)^{0.5} = (n_h)^{0.5} \qquad 2.11$$

where:

u	Orbital velocity	m/s
T	Wave period	s
L	Wavelength	m
H	Wave height	m
h	Water depth	m

These relations were obtained using the linear wave theory dispersion relation. In this form, Froude scaling allows for the correct representation of wave dynamics and is the generally accepted method for scaling hydraulic model components.

Surf similarity parameter

Battjes (1974) showed within the surf zone, the type of wave breaking is guided by the surf similarity parameter. This parameter first derived by Iribarren and Nogales (1949) is defined as:

$$\xi = \frac{\tan\beta}{\sqrt{H_o/L_o}} \qquad 2.12$$

where:

β	Beach slope outside surf zone	-
H_o	Wave height in deep water	m
L_o	Wave length in deep water	m

The type of wave breaking as defined by the surf similarity parameter falls into four categories:

$\xi > 5$ Surging Breaker	$3.3 < \xi < 5$ Collapsing Breaker
$0.5 < \xi < 3.3$ Plunging Breaker	$\xi < 0.5$ Spilling Breaker

To ease similarity analysis, $\tan\beta$ is simplified with $\tan\beta = \mathrm{h}/l$. Utilizing this slope relationship, the surf zone parameter can be taken in terms of parameter scaling ratios:

$$n_\xi = \frac{(n_h/n_l)}{(n_H/n_L)^{0.5}} \qquad 2.13$$

Surf similarity will be preserved as long as the hydrodynamic forcing is scaled according to Froude scaling and the model remains undistorted ($n_h/n_l = 1$).

2.2.2 Scale relations for mobile sediment

Morphological development within the surf zone is dependent upon a number of coupled processes described in Section 2.1. In the following section, the scaling of coastal processes will be discussed. Sediment scaling usually focuses on scaling the sediment diameter and/or sediment density in order to preserve a regime in the laboratory setting.

Bed Load Scaling

Shields parameter

The initiation of motion is an important concept within sediment transport mechanics especially concerning bed load processes. Bed load transport will occur when the wave induced bed shear stress exceeds a critical value. This relationship is given by the Shields parameter which takes the form:

$$\theta = \frac{\tau_b}{(\rho_s - \rho) g d_{50}} \tag{2.14}$$

where:

τ_b	Bed shear stress	N/m^2
ρ_s	Density of sediment	kg/m^3
d_{50}	Mean sediment diameter	m

The Shields parameter represents the forcing on the sediment grains as a ratio of the flow drag force to the sediment gravity force.

As a scale relation expressing bed load, the Shields parameter is often given in terms of the densmetric Froude number. This quantity is expressed as:

$$\theta_F = \frac{\rho\, {u_*}^2}{\gamma\, d_{50}} \tag{2.15}$$

where:

u_*	Bed shear velocity	m/s
γ	Buoyant weight of sediment ($= (\rho_s - \rho) g$)	N/m^3

The use of the buoyant weight makes the form of the Shields equation much more suitable for scale relations which now can be expressed non-dimensionally as:

$$n_\theta = \frac{{n_{u_*}}^2}{n_\gamma\, n_{d50}} \tag{2.16}$$

Given that Equation 2.16 is a similar form of the Shields parameter, for the remainder of this work, it will be referred to as the Shields scale parameter.

Particle Reynolds number

Similarly to the scaling of the flow using the Reynolds number, the flow regime at the bed can be classified as laminar, turbulent or transitional. For sand on a flat bed, the initiation of motion depends upon the flow regime. In order to quantity this relation, the particle Reynolds number is used.

$$Re_p = \frac{u_* d_{50}}{\nu} \qquad 2.17$$

In contrast to the Reynolds number, the particle Reynolds number characterizes more directly the interaction of the sediment and flow properties close to the bed. Both having input into the motion of a sand particle at the bed, the Shields and particle Reynolds number are interrelated. The two quantities represent the uplift force and resisting force on the sediment particle, respectively. They are defined here as the sediment pickup function determining how much sediment is contributed to the water column.

As a scale relation, the quantity can be quite easily derived:

$$n_{Re_p} = n_{u_*} n_{d50} \qquad 2.18$$

With the viscosity removed, it is easier to see the resistive forcing of the particle Reynolds number by observing the dependence of the bed shear velocity and particle diameter. This is in contrast to the Shields parameter where the bed shear velocity and diameter have an inverse relationship.

Sleath number

To describe the oscillatory movement of sediment in a water column Flores and Sleath (1998) introduce the following parameter known as the Sleath number:

$$S = \frac{2\pi \, \rho \, u}{(\rho_s - \rho) \, g \, T} \qquad 2.19$$

This parameter represents the ratio of inertial to gravity forces acting on individual grains of sediment. For low values of the Sleath number, the mobile layer of sediment behaves as if the flow is quasi-steady. At high values ($S > 0.3$) the flow is dominated by the pressure gradient and inertial forces. This suggests that sediment will start to move earlier than predicted by the Shields curve.

Similarly to the Shields relation, as a scale relation, the Sleath number is usually represented using the buoyant weight of the sediment:

$$n_S = \frac{n_u}{n_\gamma \, n_T} \qquad 2.20$$

Using Froude relationships (Section 2.2.1), the oscillatory (n_u) and periodic (n_T) terms cancel leaving:

$$n_S = \frac{1}{n_\gamma} \qquad 2.21$$

This gives a unique formulation which shows the Sleath parameter is only dependent upon the sediment density.

Suspension Load Scaling

Relative fall velocity

The relative fall velocity was introduced by Van Rijn (1984). Similar to the Rouse number except with the von Kármán constant removed, the relative fall velocity takes the form:

$$V = \frac{w_s}{u_*} \qquad 2.22$$

where:

w_s Sediment fall velocity m/s

The suspended sediment process is described by Van Rijn (1984) as the relative influence of the upward directed turbulent velocities to the downward directed fall velocity. Hughes (1993) states that the inclusion of the relative fall velocity accounts for suspended transport occurring simultaneously with bed load transport.

As a scaling parameter, the relative fall velocity was expressed by Kamphuis (1991):

$$n_V = \frac{n_{w_s}}{n_{u*}} \qquad 2.23$$

However, the above equation is left in terms of the sediment fall velocity. This is a small problem since the fall velocity is usually, not only empirically found, but also is a function of particle size and density. Dependent on the flow regime around the grain, the formulations must be valid for both prototype and model scale. One popular formulation for the settling velocity of natural grains is that of Hallermeier (1981):

$$w_s = \frac{\gamma^{0.7} {d_{50}}^{1.1}}{6\rho^{0.7} \upsilon^{0.4}} \qquad 2.24$$

This formulation is convenient as the relation allows for easy transfer into a scale relation.

$$n_{ws} = \frac{{n_\gamma}^{0.7}\,{n_{d50}}^{1.1}}{{n_\rho}^{0.7}\,{n_\upsilon}^{0.4}} \qquad 2.25$$

Assuming similarity between fluid viscosities and densities, the fall velocity scale relation is inserted into the relative fall velocity (Eq. 2.23):

$$n_V = n_{u*}\,{n_\gamma}^{0.7}{n_{d50}}^{1.1} \qquad 2.26$$

Dimensionless fall velocity (Dean number)

During beach and erosion events, due to breaking waves over a sandy bed, the amount of material suspended in the water column is largely controlled by the suspension processes. In order to characterize this process in the form of a parameter Dean (1973) introduced the dimensionless fall velocity:

$$\Psi = \frac{H}{w_s\,T} \qquad 2.27$$

The parameter represents the time taken by one sediment particle to move a vertical distance equal to the wave height.

Wright and Short (1984) link a dependence of beach states to the dimensionless fall velocity and surf similarity parameter. Reflective beaches which are characterized by a relatively steep and narrow face and a narrow surf zone usually have values of $\Psi < 1$ and $\xi > 2$. Dissipative beaches are characterized by a wide and flat sandy coastal zone with multiple bars. These types of beaches have a $\Psi > 6$ and $\xi \approx 0.2 - 1.3$. Most importantly, this concept shows the coupled link between the hydrodynamics and profile development.

Dean (1973)'s original formula introduced the deep water wave steepness into Equation 2.27 by dividing by the deep water wavelength.

$$\mathrm{L_o} = \frac{gT^2}{2\pi} \qquad 2.28$$

He then compared the resulting expression with data from wave tank tests that had resulted in either erosive or accretive profiles. This yields the following dimensional form of the Dean number:

$$\frac{\mathrm{H_o}}{\mathrm{L_o}} = 1.7\,\frac{\pi\,w_s}{gT} \qquad 2.29$$

Using Equation 2.29, Ting and Kirby (1994) correlate the influence of turbulence to fluid velocity and suspended sediment concentrations as related to beach states. They assume that turbulent velocity fluctuations (focusing primarily on breaking) are responsible for keeping sediment in suspension.

Ting and Kirby (1994) consequently provide a second understanding of the Dean number as a ratio of turbulence generated by wave breaking and the settling velocity. This conclusion shows that the dimensionless fall velocity is inherently different from the relative fall velocity in that it describes suspension due to wave breaking and not boundary layer shear.

The scale relation can be easily obtained from Equation 2.27.

$$n_{\Psi} = \frac{n_H}{n_{ws}\, n_T} \qquad 2.30$$

Using the Hallermeier (1981) fall velocity relationship and assuming the same fluid viscosity and density in both model and prototype gives:

$$n_{\Psi} = \frac{n_H}{{n_{\gamma}}^{0.7}\, {n_{d50}}^{1.1}\, n_T} \qquad 2.31$$

And using Froude scaling to reduce the fluid properties gives:

$$n_{\Psi} = \frac{{n_h}^{0.5}}{{n_{\gamma}}^{0.7}\, {n_{d50}}^{1.1}} \qquad 2.32$$

Bed Forms

Most of the time, in situ mobile beds are not flat but rather contain topographic features often referred to as bed forms or ripples. As a nondimensional parameter, representation of bed forms has been proposed by Kamphuis (1985) using the bed form length:

$$l_s = \frac{\lambda}{d_{50}} \qquad 2.33$$

where:

λ	Bed form length	m

Kamphuis (1991) suggests for scaling that the bed form length scale should be the average of the wave amplitude for short-wave models. As a scale relation, the quantity takes the form:

$$n_{l_s} = \frac{n_{\lambda}}{n_{d50}} \qquad 2.34$$

The formation of bed forms in mobile bed models has been studied by Mogridge (1974). Experiments were carried out in the laboratory using a flume and oscillatory wave tunnel. Using both sand and lightweight material, Mogridge (1974) suggests that the correct representation of bed forms is necessary in the model to assure correct near bed transport.

Dingler (1974) has shown that the presence of ripples can also be defined numerically by analyzing the Shields number (Eq. 2.14). The presence of ripples is defined by a low Shields parameter (ϴ < 1). Once the Shields number moves above one, the shear stress increases and the bed becomes plain.

Ribberink, van der Werf et al. (2008) have proposed a nondimensional phase lag parameter to quantify the contribution of the ripple vortex to sediment suspension. However, they state that this parameter can be approximately equated to the relative fall velocity (Eq. 2.23). For small relative fall velocity values ($u_*/w_s < 0.8$), phase lag effects are relatively small and bed load is the dominate transport mode. Ripples may still be present but the magnitude of suspended sediment due to the vortex process is small compared to the bed load. As a converse, for large values ($u_*/w_s \geq 0.8$), the vortex process has strong effects damping out the bed load process and amplifying suspension.

2.2.3 Time scales of morphological development

Time scales of morphological development are used to compare the development rate of scaled down models to those in prototype scale. Hughes (1993) states that morphological time scales in mobile-bed physical models are very subjective. Kamphuis (1975) suggest these time scales are best determined by comparing model response time to known prototype response. However, a number of methods have been proposed to estimate this time scale, a few of which will be discussed in the section following.

Direct Time Scale Models

Ito and Tsuchiya (1986) propose the following morphological time scale:

$$n_{Tm} = {n_h}^{0.5} \qquad 2.35$$

Using storm erosion profiles (14-18 March, 1981) of the Ogata coast of Japan, the results of small scale experiments were compared. Using these results, Ito and Tsuchiya (1986) define similitude between bed profiles to exist when the difference is less than twice the experimental error when based on repeated tests.

Hughes and Fowler (1990) preformed similar experiments at large and small scale using regular and irregular waves. The time scale relation of Equation 2.35 was used with a depth scale equal to 7.5. In general, agreement was found to be very good with about a 10% under estimation in the upper part of the profile.

Grasso, Michallet et al. (2009) propose a similar time scale for lightweight sediment based on the square of the characteristic length scale:

$$n_{Tm} = {n_l}^{0.5} \qquad 2.36$$

However, as long as the model remains undistorted this relation is equivalent to Equation 2.35 through Froude scaling. Grasso, Michallet et al. (2009) therefore propose that even with the introduction of diameter and density scaling, morphological development is only a function of Froude scaling.

Suspended Transport Model

Vellinga (1986) introduced a scale relation for dune erosion based on suspended sediment concentration. This model was one of the first to propose that morphological time scales are not only a function of the fluid dynamics but also the sediment properties. This is inherently different from the direct scaling models discussed previously.

Within the surf zone, the suspended sediment transport rate can be given by:

$$q_s = h\, U_r\, C \tag{2.37}$$

where:

U_r	Undertow velocity	m/s
C	Suspended sediment concentration	m^3/m^3

In order to derive the scale relation, Vellinga (1986) assumes that the suspended sediment concentration is approximately constant over the water column at the dune foot. Van Rijn, Tonnon et al. (2010) assume the suspended sediment concentration to be proportional to:

$$C \approx \frac{(\hat{u})^a\, (SL)^b}{(T)^c\, (d_{50})^d\, (s-1)^e} \tag{2.38}$$

where:

$\hat{u}$	Peak orbital velocity	m/s
SL	Bed slope	-
s	Relative density $(= \rho_s/\rho)$	-

The exponential constants (a, b, c d, and e) of Equation 2.38 are empirically found values requiring the development to be derived. From basic research in laboratory flumes Van Rijn (1993) found these constants are approximately:

$$a \approx 3$$
$$c \approx 1 - 2$$
$$d \approx 1 - 2$$
$$e \approx 1$$

The effect of bed slope on the depth-averaged concentration is not well known. It is assumed that the concentration will increase with increasing bed slope within this approximate relationship:

$b \approx 0.5 - 2$

Using Equation 2.38 and a relation for the bed slope, $n_{SL} = n_h/n_l$ yields the scale relationship for the suspended sediment concentration:

$$n_c = (n_h)^{0.5a-0.5c}\,(n_{d50})^{-d}\,(n_{s-1})^{-e}\,(n_h/n_l)^{-b} \qquad 2.39$$

And inserting it into Equation 2.37, the equation for the suspended sediment transport rate similarity in the water column can be derived:

$$n_{qs} = (n_h)^{1.5+0.5a-0.5c}\,(n_{d50})^{-d}\,(n_{s-1})^{-e}\,(n_h/n_l)^{-b} \qquad 2.40$$

Further, using Equation 2.40, the erosion time scale can also be derived. At the dune face, the erosion rate is derived using a per unit width assumption:

$$q_s = \frac{A_e}{T_m} \qquad 2.41$$

where:

A_e	Dune erosion area	m^2
T_m	Time scale to erode the duce face	s

Using the dune face erosion rate, this leads to the following scale relation:

$$n_{qs} = \frac{(n_h/n_l)(n_h)^2}{n_{Tm}} \qquad 2.42$$

And setting the suspended sediment transport rate similarity equations equal to each other leads to the time scale of erosion:

$$n_{Tm} = (n_h/n_l)^{b+1}\,(n_{d50})^{d}\,\,(n_{s-1})^{e}(n_h)^{0.5a-0.5c-0.5} \qquad 2.43$$

2.3 Sediment Scaling Theories

2.3.1 Ideal scaling theories

To scale down sediment transport processes from prototype to model scale, the classical method of dimensional analysis has been used. First, a set of parameters is selected based on the process being described. These parameters are then used to derive a set of nondimensional relations. A number of nondimensional parameter sets have been proposed.

Kamphuis (1991) proposed the following parameters be used to describe both fluid and sediment characteristics:

$$f(\rho, \upsilon, \lambda, \tau_b, d_{50}, \rho_s, g) \tag{2.44}$$

where:

τ_b	Bed shear stress	N/m^2

These terms were selected as those which would be most appropriate for sediment transport from bottom shear stress or that of bed load transport. Using these characteristic values along with dimensional analysis, Kamphuis (1985) proposed the following set of nondimensional parameters:

$$\Pi = g\left(\frac{u_* d_{50}}{\nu}, \quad \frac{\rho\, u_*}{\gamma\, d_{50}}, \quad \frac{\rho}{\rho_s}, \quad \frac{\lambda}{d_{50}}\right) \tag{2.45}$$

where:

u_*	Bed shear velocity $\left(=\sqrt{\tau_b/\rho}\right)$	m/s
γ	Buoyant weight of sediment $(=(\rho_s-\rho)g)$	N/m^3

Kamphuis (1991) added a fifth term to the group described previously as the dimensionless fall velocity (Eq. 2.22):

$$\Pi' = g'\left(\frac{u_* d_{50}}{\nu}, \quad \frac{\rho\, u_*}{\gamma\, d_{50}}, \quad \frac{\rho}{\rho_s}, \quad \frac{\lambda}{d_{50}}, \quad \frac{w_s}{u_*}\right) \tag{2.46}$$

As these terms are mostly intended to describe bed load transport, the relative fall velocity was added to account for near bed suspended transport occurring simultaneously with bed load transport. In addition, it should be observed that each of these derived quantities describes some physical process within the surf zone (Section 2.1). For this reason, Hughes (1993) states that for complete similitude of sediment transport, all terms of Equation 2.46 must be maintained. Otherwise, scaling will not reproduce the correct contribution of each physical process leading to scale effects.

Dalrymple (1989) proposed a similar set of parameters to described sediment characteristics:

$$f(\rho, \upsilon, \tau_b, d_{50}, \rho_s, w_s, H, T, g) \tag{2.47}$$

In this parameter set, the bed form characteristic length (λ) has been removed and replaced with the sediment fall velocity (w_s), wave height (H), and wave period (T). The resulting nondimensional parameter set is given as:

$$\Pi = g\left(\frac{u_* d_{50}}{\nu}, \quad \frac{\rho\, u_*}{\gamma\, d_{50}}, \quad \frac{\rho}{\rho_s}, \quad \frac{H}{w_s\, T}\right) \qquad 2.48$$

This set is very similar to Equation 2.46 except that the relative fall velocity has been replaced with the dimensionless fall velocity. Dalrymple (1989) proposes that this parameter better represents the transport of both near bed and suspended sediment. Similarly, correct similitude of the sediment transport process requires that all four parameters must be the same in both model and prototype.

2.3.2 Problems in scaling

Similitude of hydraulic processes in both model and prototype represent the basis for sediment transport modeling. As has been discussed previously, similarity of free surface waves can be achieved whenever Froude scaling is applied. However, hydraulic similarity does not imply transport similarity and must be dealt with separately.

Following the reasoning of Hughes (2003) in the previous section, Hughes and Fowler (1990) state that for coastal models it is often important to attain similarity of the cross shore equilibrium bed profiles. This is the case particularly in the surf zone, however, limitations of modeling do not allow for similarity between all parameters. For instance, grain size can be scaled at approximately the square of the characteristic length scale of the model. With this, there is a possibility that the grains become so small that the cohesive characteristics of the sediment contribute to the transport therefore generating scale effects.

As a result of these scaling problems, Sutherland and Soulsby (2010) propose that the most dominate mode of transport (either bed load or suspended load) be reproduced within the model.

2.3.3 Scaling in practice

In order accommodate the sediment scaling problems, a number of scaling methods have been proposed in order to preserve the dominant transport process. Defining two regimes (bed load transport and suspended load transport), Henriquez, Reniers et al. (2008) propose a scaling method in which both the sediment diameter and sediment density are scaled.

Bed Load Model

The bed load model of Henriquez, Reniers et al. (2008) use the Shields parameter (Eq. 2.16), the Reynolds particle number (Eq. 2.18), and the relative fall velocity (Eq. 2.26). Selection of these three parameters allows for preservation of the turbulence regime in the wave boundary layer, mobility of sediment by bed friction and settling of suspended sediment generated by these processes. These combinations represent the most important processes of the bed load transport regime.

Scaling of transport is done by scaling both the sediment diameter and density. In the previous section, all terms of the parameters have been described. However, the determination of the bed shear velocity requires consideration by the modeler. Henriquez, Reniers et al. (2008) propose the computation of the bed shear velocity be done using the relation of Jonsson (1966):

$$u_*{}^2 = 0.5\, f_w u^2 \qquad 2.49$$

where:

f_w	Wave friction factor	-

Johnson proposed this formulation based on experiments with oscillatory wave motion. These motions are most responsible for bed load transport over a flat bed. The arrangement of this relation also allows for easy transfer into a scale relation:

$$n_{u_*}{}^2 = n_{f_w}\, n_u{}^2 \qquad 2.50$$

With the velocity term transformed using Froude scaling, the friction factor scale must also be derived. Henriquez, Reniers et al. (2008) propose an approximation of the Swart (1974) formlation:

$$f_w = 0.078 \left(\frac{k_s}{A}\right)^{0.3} \qquad 2.51$$

where:

A	Horizontal excursion of the orbital motion	m
k_s	Effective bed roughness height ($= 3\, d_{50}$)	m

This simplified formulation allows for easy transfer to a scale relation. With the horizontal excursion scaled according to the water depth, the scale relation follows:

$$n_{f_w} = \left(\frac{n_{d50}}{n_h}\right)^{0.3} \qquad 2.52$$

The expression is then substituted into the scale relation of Johnson to obtain a scale relation for the bed shear velocity:

$$n_{u_*} = \frac{n_{d50}{}^{0.3}\, n_u{}^2}{n_h{}^{0.3}} \qquad 2.53$$

Using Froude scaling ($n_u{}^2 = n_h$), the bed shear velocity is expressed in terms of water depth and sediment diameter:

$$n_{u_*} = n_{d50}{}^{0.3}\, n_h{}^{0.7} \qquad 2.54$$

With this, the scale Shields parameter, particle Reynolds number and relative fall velocity are expressed in terms of sediment diameter, sediment density and water depth.

$$n_\Theta = \frac{{n_h}^{0.7}}{n_\gamma \, {n_{d50}}^{0.7}} = 1 \tag{2.55}$$

$$n_{\mathrm{Rep}} = {n_h}^{0.7} \, {n_{d50}}^{2.3} = 1 \tag{2.56}$$

$$n_{\mathrm{V}} = \frac{{n_\gamma}^{1.4} \, {n_{d50}}^{1.9}}{{n_h}^{0.7}} = 1 \tag{2.57}$$

From these equations, selection of the sediment density and diameter can be done based upon any arbitrary depth scale. When plotted as a function of density and diameter, the intersection of three lines gives the properties by which the scale relations are preserved.

Suspended Load Model

The energy required for suspended load transport is mostly generated by breaking waves. Henriquez, Reniers et al. (2008) propose a method based on breaking energy dissipation using the dimensionless fall velocity and Shields parameter. Treatment of the suspended sediment in this way allows for preservation of mobility by bed friction and settling of suspended sediment processes.

To evaluate the dimensionless fall velocity, Henriquez, Reniers et al. (2008) make use of the Ting and Kirby (1994) understanding of the Dean number: the ratio of turbulence generated by wave breaking and the settling velocity. They validate this assumption by comparing the breaking process to that of a hydraulic jump following the method by Battjes (1975) and Fredsøe and Deigaard (1992).

Using Equation 2.32 along with Froude scaling, the relationship can be expressed:

$$n_\Psi = \frac{{n_h}^{0.5}}{{n_\gamma}^{0.7} \, {n_{d50}}^{1.1}} = 1 \tag{2.58}$$

For continuity, the Shields parameter (Eq. 2.55) is repeated below.

$$n_\Theta = \frac{{n_h}^{0.7}}{n_\gamma \; {n_{d50}}^{0.7}} = 1$$

Along with the dimensionless fall velocity, these two quantities represent the similarity set. From these equations, the selection of the sediment density and diameter can be done based upon any arbitrary depth scale. When plotted as a function of density and diameter, the intersection of two lines gives the properties by which the scale relations are preserved.

Preservation of the Sleath and Bed Form Parameters

Henriquez, Reniers et al. (2008) provide a brief discussion of some expected scale effects based on the density and diameter scaling method. Using the bed load model, both the Sleath and bed form relations will not be preserved. The mismatch of the Sleath parameter is given as:

$$n_S = \frac{1}{{n_h}^{0.9}} \qquad 2.59$$

This suggests that the mobility of the sediment can begin sooner than expected. This process was observed by Flores and Sleath (1998) who note that lightweight granules move quickly into motion (responding almost instantly to the flow) but settle much slower. They also note that under certain regular oscillatory conditions, a transport regime known as plug flow could occur. The unique regime causes the sediment to move as a discrete block. Plug flow is not normally observed with natural sediment.

The mismatch of the bed form parameter is given as:

$$n_{\lambda/d} = {n_h}^{1.3} \qquad 2.60$$

This mismatch of the bed form parameter suggests that the ripple geometry will not be scaled correctly causing the mobile bed porosity to be quite large. Kamphuis (1991) suggests this will result in greater wave energy absorption due to these porosity effects.

A mismatch of the Sleath parameter is also seen in the suspended load model:

$$n_S = \frac{1}{{n_h}^{0.7}} \qquad 2.61$$

And for the bed form parameter:

$$n_{\lambda/d} = n_h \qquad 2.62$$

The parameter mismatches will result in similar scale effects to the bed load model. However, the magnitude should be less.

2.4 The SANDS Project

The SANDS (Scaling and Analysis and New instrumentation for Dynamic bed testS) project was a Joint Research Activity of the Integrated Infrastructure Initiative HYDRALAB III within the EC Framework 6. The project had three main goals:

- Improve the scaling and analysis procedures and achieve more “repeatable” and compatible mobile bed tests (with known error bounds).

- Innovative data capture and analysis using advanced optical and acoustic equipment on non-intrusive probes.

- Develop new protocols for the design and interpretation of the movable bed test results.

The SANDS project dealt with the beach erosion and accretion tests preformed as three different European research facilities with each facility focusing on a different characteristic scale:

- 1:1 (defined as prototype) in the Large Wave Channel (GWK) of the Coastal Research Centre FZK, *Hannover* (UHANN)

- 1:1.9 in the Large Wave Flume (CIEM) of the Maritime Engineering Centre of *UPC*, Barcelona

- 1:6 in the Scheldt Flume of *Deltares* (former Delft Hydraulics), Delft

In each facility, the same geometric and hydraulic boundary conditions were kept, but with different undistorted scales defined above. Both the hydraulic boundary conditions and sediment grain size were scaled using Froude scaling [Grüne, Cáceres et al. (2009)].

While data was taken at all three facilities, only the erosive 1:15 profiles obtained from Hannover and Deltares will be used within. Hannover is defined as prototype with Deltares being a scaled comparison.

2.4.1 Initial profile and data collection

Hannover

Tests at Hannover were conducted in the Large Wave Channel (GWK) of the Coastal Research Centre FZK (Figure 2.3). The constructed profile was defined as the prototype setup for the SANDS project.

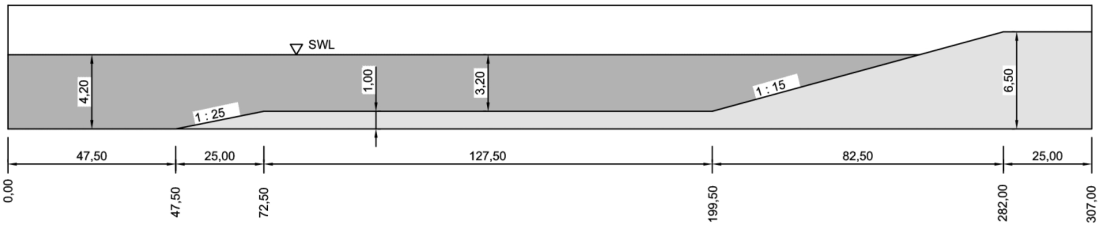

Figure 2.3 *Foreshore and beach installed at GWK flume (1:1)*

The flume has a total length of 307 m, a width of 5 m, and a depth of 7 m. The maximum depth at the wave generator is 5 m. Both regular and irregular waves can be simulated by the oil-hydraulically driven plunger type wave generator.

The foreshore and beach profiles were recorded with a computer controlled wheel driven bed profiler. The profile arm is linked to a measuring carriage which is moved along the flume. The measuring sensory arm pulley consists of three side by side fastened nylon rolls with 300 mm diameter and 50 mm width. From the measurements of the x-position and angularity of the sensor arm the bed profile can be calculated by the computer. The accuracy of the system is in the range of +/- 10 mm. This corresponds to +/- 0.2% full scale caused by the bed profiler wheel compressing of the sand by the.

Deltares

Tests at Deltares were conducted in the Scheldt flume. The flume consists of a metal bottom and glass walls. The flume is 56 m long, 1 m wide and 1.2 m deep. The wave generator is a piston type wave generator.

The constructed profile (Figure 2.4) was a scaled profile of Hannover at a scale of 1:6.

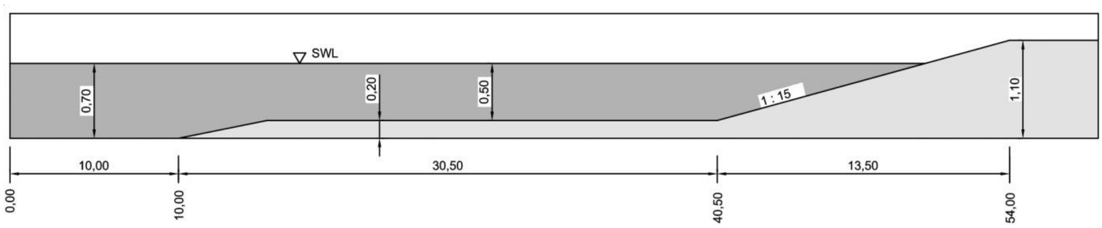

Figure 2.4 *Foreshore and beach installed at of Scheldt flume (1:6)*

Upon closer inspection, it can be seen that the water depth scales across the profile do not maintain a constant 1:6 scale in line with Froude scaling.

Table 2.1 *Vertical scale ratios in Scheldt flume (characteristic scale 1:6). While the water depth at the paddle does coincide to Froude scaling, the other scale ratios are distorted. The implications of the distortion on the results was not discussed in published SANDS reports.*

	Hannover	Deltares	Scale Ratio [-]
Water depth at wave paddle [m]	4.2	0.70	6
Water depth at toe [m]	3.20	0.50	6.4
Thickness of sand bed [m]	1	0.20	5
Mean grain size, d_{50} [mm]	0.27	0.13	2.08

Due to testing limitations in the GWK flume, a minimum 1 m sand bed was needed. This was not accounted for prior to the test setup. While the scale of the water depth at the wave paddle is correct, there is some vertical distortion in the water depth at the toe (see Figure 2.4 and Table 2.1). The implications of this were not discussed in published SANDS reports.

There are also some inconsistencies with respect to the the sediment diameter. Hoyng (2008) state that sediment was scaled according to Froude scaling laws. However, an incorrect prototype sediment diameter was used which resulted in a slightly larger sediment grain.

Profile measurements were taken using an Amphibious Profile Indicator (PV) system. The device consists of three high sensitive sounding probes mounted on a carriage. The profiler has a maximum resolution of 0.8 mm. It was programmed to generate profiles along three trajectories through the flume at y = 0.25 m, 0.50 m and 0.75 m with an equidistant step size of 0.01 m for equidistant step sizes of 0.2 for all other soundings.

2.4.2 Hydraulic forcing

The spectrum used in both the GWK and Scheldt flumes was defined by a JONSWAP spectrum with a gamma of 3.3. The wave characteristics can be found below (Table 2.2).

Table 2.2 *Scales and parameters used at Hannover and Deltares*

	Hannover	Deltares	Scale Ratio [-]
Wave height, Hs [m]	1	0.17	5.88
Wave period, Tp [s]	5.70	2.32	2.46
Number of waves, N [-]	500	500	---

In both facilities, tests were performed using identical time series. Each time series consists of 500 waves. The series used in the Scheldt flume was scaled down using Froude scaling.

While second order generation and active adsorption are possible in both facilities, these capabilities were turned off limiting the generated time series to a 1st order approximation. This was done to limit differences and associated uncertainties in wave generation and influences from the kind of paddle at each facility.

2.4.3 Testing Regime

Hannover

Wave series were run and allowed to propagate starting from N = 1 to N = 500 with the series started and stopped in the same position. In between each time series, testing was stopped giving the sediment time to settle. This provides a consistent and uniform time series across the whole campaign. During Series 021, the time series was stopped approximately 50 waves short. This resulted in a slight discontinuity in the total testing regime

Bottom profiles were taken in a semi-regular sequence.

Table 2.3 *Hannover testing and data acquisition program*

Series Number	Number of Waves	Cumulative Number of Waves	Duration [min]	Cumulative Duration [hr]
---	Profile 000			
1	500	500	42	0.70
---	Profile 001			
2	500	1000	42	1.40
3	500	1500	42	2.10
---	Profile 002			
4	500	2000	42	2.80
5	500	2500	42	3.50
---	Profile 003			
6	500	3000	42	4.20
7	500	3500	42	4.90
---	Profile 004			
8	500	4000	42	5.60
9	500	4500	42	6.30
---	Profile 005			
10	500	5000	42	7.00
11	500	5500	42	7.70
12	500	6000	42	8.40
---	Profile 006			
13	500	6500	42	9.10
14	500	7000	42	9.80
15	500	7500	42	10.50
---	Profile 007			
16	500	8000	42	11.20
17	500	8500	42	11.90
18	500	9000	42	12.60
---	Profile 008			
19	500	9500	42	13.30
20	500	10000	42	14.00
21	450	10450	38	14.63
---	Profile 009			
22	500	10950	42	15.33
23	500	11450	42	16.03
24	500	11950	42	16.73
25	500	12450	42	17.43
---	Profile 010			
26	500	12950	42	18.13
27	500	13450	42	18.83
28	500	13950	42	19.53
29	500	14450	42	20.23
---	Profile 011			

30	500	14950	42	20.93
31	500	15450	42	21.63
32	500	15950	42	22.33
33	500	16450	42	23.03
34	500	16950	42	23.73
35	500	17450	42	24.43
---	Profile 012			
36	500	17950	42	25.13
37	500	18450	42	25.83
38	500	18950	42	26.53
39	500	19450	42	27.23
40	500	19950	42	27.93
41	500	20450	42	28.63
---	Profile 013			
42	500	20950	42	29.33
43	500	21450	42	30.03
44	500	21950	42	30.73
45	500	22450	42	31.43
46	500	22950	42	32.13
47	500	23450	42	32.83
---	Profile 014			

Deltares

The testing regime followed at Deltares is not similar to Hannover. During the SANDS project, Deltares conducted more than one model setup and profile. This resulted in less profiles taken of the characteristic test. In total half the number of profiles taken at the following semi-regular time intervals:

Table 2.4 *The profile acquisition program used at Deltares. Tests at Deltares were carried out longer than corresponds to Froude scaling to analyze the profile equilibrium.*

Approximate Series Number	Profile	Measurement Time [hr]	
		Actual	Prototype
0	1	0	0.0
3.5	2	1	2.1
10.5	3	3	8.4
28.1	4	8	22.2
56.2	5	16	---
84.2	6	24	---
168.5	7	48	---

In addition, erosion tests were carried out longer than would correspond to Froude scaling of the prototype time because Deltares wanted to analyze the profile equilibrium.

2.4.4 Results and scaling problems

A discussion and analysis of the erosive development results was published by Cáceres, Grüne et al. (2008).

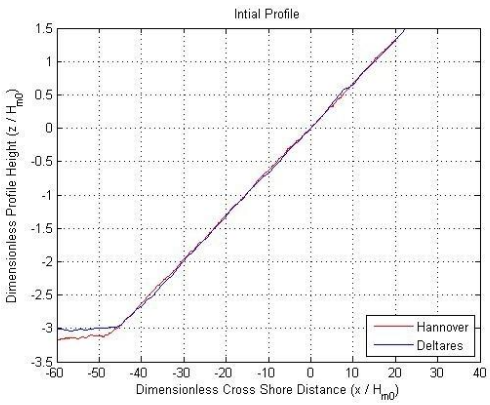

(a) Initial profile

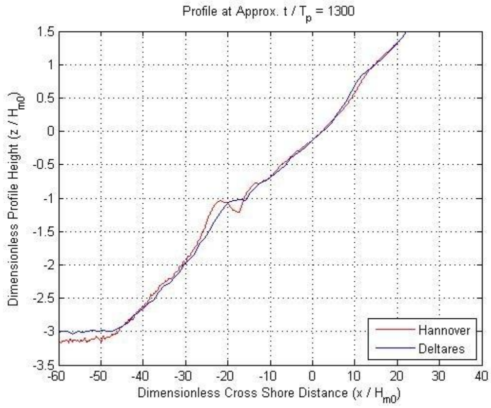

(b) Profile after $t/T_p \approx 3000$

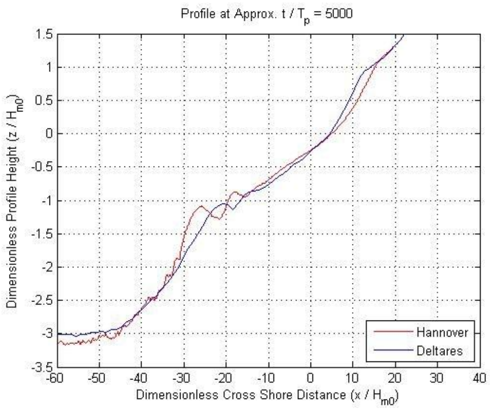

(c) Profile after $t/T_p \approx 5000$

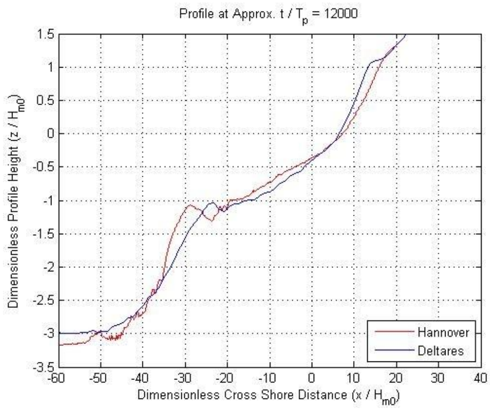

(d) Profile after $t/T_p \approx 12000$

Figure 2.5 *Hannover and Deltares profile development. The Deltares profile shows a discrepancy in the bar height and position.*

Analysis of the profiles between Hannover and Deltares (Figure 2.5) show a discrepancy in the bar height and position. Erosion of the shoreline, however, developed similar to Hannover.

A comparison of the final profiles at the two facilities was also done. This corresponds to a time of 32.8 clock hours at Hannover and 48 clock hours at Deltares (see Table 2.4). While these times are not directly comparable, they show the accentuated differences between Deltares and Hannover. At 48 clock hours, there is a discernable difference in the Deltares developed profile. At Hannover, a depth of closure developed in the flume. However, at Deltares the profile shows movement at the base of the profile and no depth of closure. This is believed to be the result of a shift in the dominant transport regime from bed load dominated at Hannover to suspension dominated at Deltares.

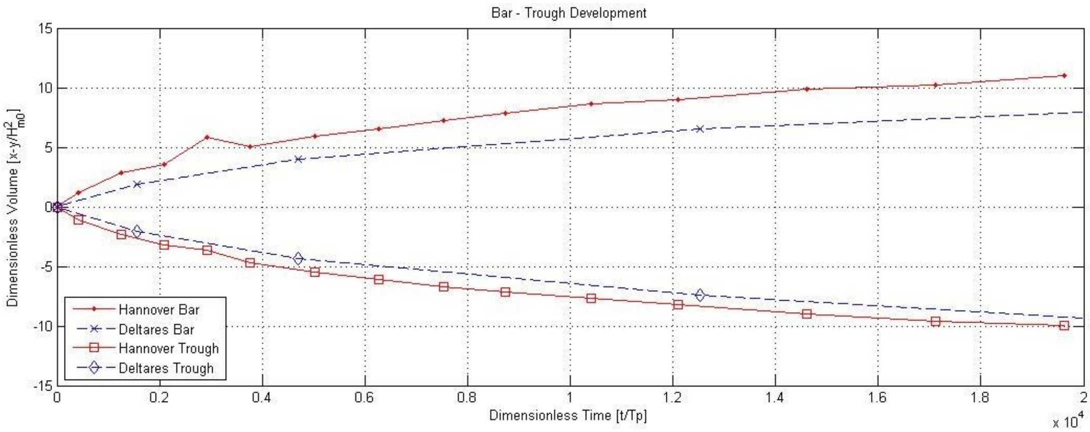

Figure 2.6 *Bar and trough volume development of Hannover and Deltares*

To perform a profile volume analysis, the profile was divided into two representative sections. These sections characterize the erosion, deposition and transport across the profile. The bed level changes were then integrated to determine the volume change with time. Analysis of the volume development (Figure 2.6) show delayed development at Deltares behind the Hannover profile. This also corresponds to delayed horizontal and vehicle bar deployment (see Figure 2.5).

3 METHODOLOGY

3.1 Materials

3.1.1 Flume description

Laboratory experiments were carried out in the Long Research Flume in the Fluid Mechanics Laboratory of the Department of Civil Engineering at Delft University of Technology (*TU Delft*). The wave flume has a total length of 40 m, a width of 0.8 m and a depth of 1 m. At the far end of the flume, an impermeable irregular concrete slope on the order of 1:15 was installed. It started flush with the bottom of the flume about 25 m from wavemaker and extended to the top of the flume.

The Long Research Flume is equipped with a electronically driven paddle type wavemaker. Driving of the wavemaker is computer controlled using WL | Delft Hydraulics generation software. Both regular and irregular waves can be generated. The software is also capable of introducing 2nd order steering and Active Reflection Compensation (ARC) to absorb reflected waves during long tests.

3.1.2 Sediment description

The sediment used during experimentation was made of duroplast, a composite thermoset plastic closely related to bakelite. It is light and strong making it perfect for extended use.

Scaled according the bed load model of Henriquez, Reniers et al. (2008), the model requires scaling of both the sediment diameter and density. Using this method preserves the Shields, Reynolds particle and relative fall velocity parameters resulting in the sediment properties shown below.

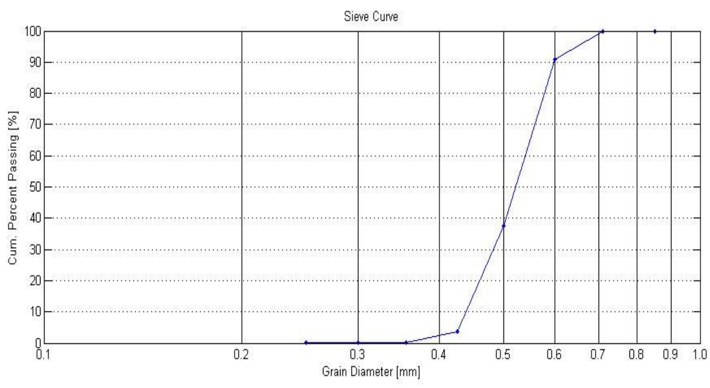

Sediment Properties		
ρ_s	[kg/m^3]	1200
d_{10}	[mm]	0.439
d_{50}	[mm]	0.524
d_{90}	[mm]	0.598
d_{90}/d_{10}	[--]	1.363

Figure 3.1 *Sediment grain size distribution and derived sediment properties*

Figure 3.1 shows that the grain distribution is quite narrow. The sediment had also been used in a number of prior testing campaigns, which causes a loss of some of the finer sediment grains.

3.2 Testing Equipment

3.2.1 Acoustic bed profiler

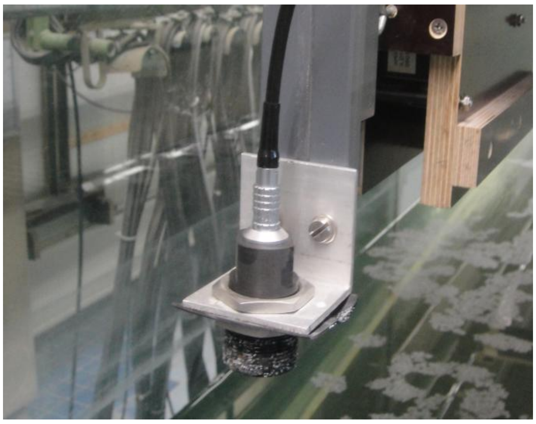

(a) Acoustic bed profiler probe and laser distance meter

(b) Acoustic sound generator and signal transformer housing.

Figure 3.2 *Profile acquisition hardware. An acoustic bed profile was used to obtain in water profile measurements. A laser distance meter was used to obtain measurements in shallow water and dry surfaces. The setup can be seen above (left) with the acoustic bed profiler probe first and laser distance meter behind.*

In water bed profiles were taken with an acoustic bed profiler (ABP). The ABP probe (see Figure 3.2) was placed just below the surface of the water. The probe emits an acoustic sound that travels through the fluid and reflects off the bottom to determine the bathymetry.

Both the minimum and maximum range of the acoustic bed profile are dependent upon a set of predefined input parameters. The minimum distance is based upon two parameters: a delay time (0.001 – 20 ms) and the speed of sound in the fluid (250 – 8000 m/s). During the experiments, it was observed that any distance smaller than approximately 0.036 m was recorded as an error. The maximum distance is dependent upon the measurement window selected (0.001 – 30 ms). The acoustic bed profile is capable of taking profiles up to 23 m water depth.

The resolution of the acoustic bed profiler is +/- 1 mm.

3.2.2 Laser distance meter

Dry measurements and measures in clear water were taken with the use of a laser distance meter (LDM). A light source is generated by the unit (see Figure 3.2) and received by the optical element. A digital signal processer calculates the distance between the light spot and object being measured. This distance is linearized and recorded as measurement.

The LDM has a minimum range of 200 mm and a maximum range of 750 mm. The resolution of the laser is +/- 25 μm however shaking from the carriage decreases this resolution to approximately +/- 1 mm.

3.2.3 Resistive wave gauges

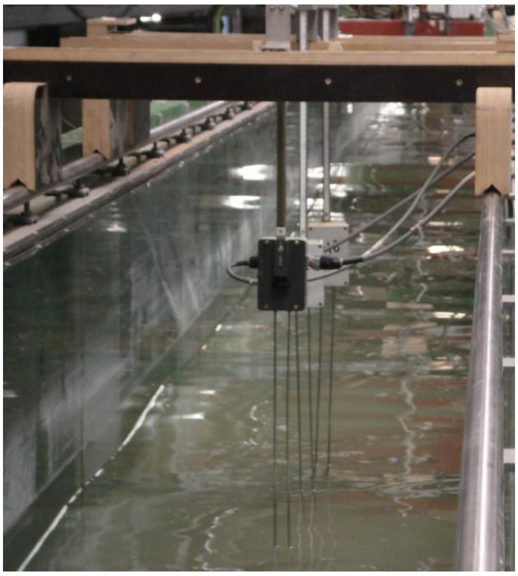

Figure 3.3 *Wave gauges 05 - 07 used during testing. Seen here in situ during Series 001 suspended from above by a wood cradle.*

Surface elevations were recorded using resistive type wave gauges (Figure 3.3). At the beginning of the tests, calibrations were taken daily to check the reliability and robustness of the instrument. Little variation was seen in the calibration factors.

3.3 Testing Setup

3.3.1 Installed sediment profile

In line with the Hannover and Deltares profiles, a plain sloped 1:15 bed was used as a starting point for profile development.

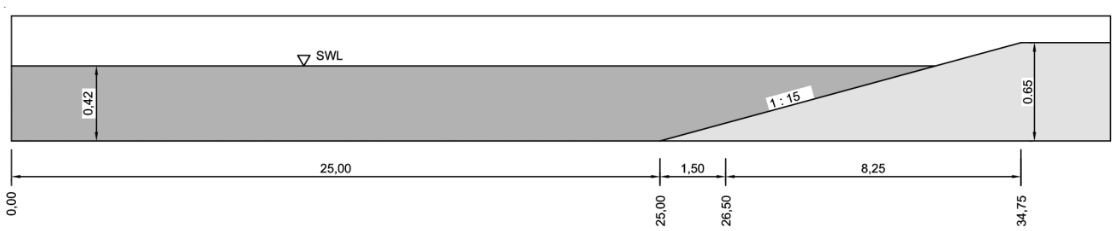

Figure 3.4 *Installed sediment bed and beach profile*

The sediment scaling method used led to a decrease in sediment density and increase in sediment diameter. The increased diameter, coupled with increased bed porosity, Kamphuis (1991) suggests, could lead to increased wave dissipation. Due to concerns over increased wave dissipation, the toe of the profile found in Hannover and Deltares has been removed (see Figure 3.4). With wave properties being scaled according to the outermost edge of the active profile (shown later), development of a depth of closure in Hannover above this toe suggests the modification should have little to no influence on the morphological development.

Two tests were conducted during the experiment. For the first test, the sediment was placed in inside storage and allowed to dry for two weeks. Due to concerns with floating sediment during construction, the sediment bed was constructed in the dry. After construction, the flume was filled with water up to the SWL and allowed to rest two days before testing started.

Post processing of the results showed an initial sinking and compaction of the profile which led to the formation of a large scarp at the upper margin of the profile. To determine if the presences of this large scarp negatively influenced development, a second test was conducted.

Using the final profile of the first campaign, the sediment was moved and placed to reconstruct a 1:15 linear profile. The flume was then filled with water and the sediment agitated to achieve a more realistic compaction. With the flume full, long waves were run over the top to smooth out the profile and achieve an equilibrium compaction. The flume was then partially emptied to the starting SWL and the profile allowed drain three days. This is the profile series analyzed within.

3.3.2 Equipment location

The acoustic bed profiler and laser distance meter were placed on a mechanically controlled sampling carriage which ran over the top of the flume. With each profile measurement, the acoustic bed profiler needed to be raised up to not impact the dry portion of the bed. It was therefore placed on an arm which could be manually raised and lowered. The laser distance meter was placed in line and just behind the echo sounder. It remained in this position throughout the tests. All measurements were taken down the centerline of the flume.

Seven different wave gauges were used during testing to measure surface elevations.

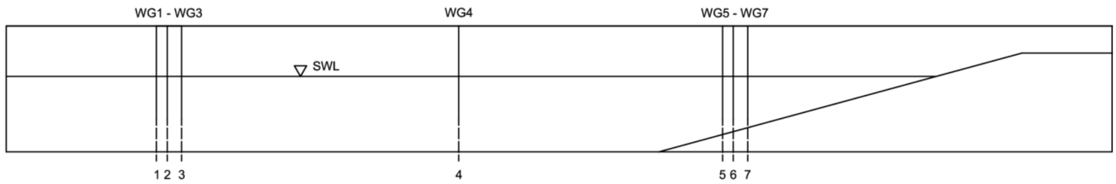

Figure 3.5 *Approximate wave gauge locations*

The location of each wave gauge shown in Figure 3.5 can be found in the following table (Table 3.1). All measurements are relative to the front of the center position of the wave board.

Table 3.1 *In situ wave gauge locations presented correspond to approximate locations in Figure 3.3. Wave gauges 01, 03, 04, and 05 correspond to similar positions within the Hannover wave flume.*

Wave Gauge	01	02	03	04	05	06	07
Location [m]	9.00	9.30	9.70	18.00	26.5	26.8	27.2

Wave gauges 01, 03, 04, and 05 correspond to similar positions within the Hannover wave flume. These gauges were strategically placed to provide a platform for comparison between Hannover and TU Delft.

Wave gauge 05 is located 1.5 m behind the toe of the sediment bed. This position of the sediment bed (both x and z) corresponds to the intersection of the sediment toe and profile at Hannover. With a depth of closure present above this line in Hannover, the plane of this wave gauge is considered the outer margin of the active profile. The primary point for hydraulic scaling, this location will be referenced frequently.

3.4 Testing Regime

3.4.1 Spectrum and forcing

Each testing series comprised of waves generated from a numerical time series used as input to the wave generator. The numerical time series used in TU Delft was the same used in Hannover only scaled using Froude scaling and its respective length scale (1:10). While the modeler provides the frequency to define the length of the time series, before generation, the wave train is internally resampled by the wavemaker software at a sample rate of 2000 Hz. This provides a smooth output signal.

Analysis of this numerical JONSWAP type wave series results in the following wave properties:

Table 3.2 *Scale ratios and parameters used at Hannover and TU Delft. Components were scaled using Froude scaling.*

Parameter	Hannover	TU Delft	Scale Ratio [-]
Wave height, Hs [m]	1	0.10	10
Wave period, Tp [s]	5.70	1.80	3.16
Number of waves, N [-]	500	500	---

Consistent with the hydraulic conditions at Hannover and Deltares, the generation of the time series was limited to 1st order principles.

3.4.2 Data collection schedule

Wave train propagation and subsequent profile collection followed the same semi regular profile sampling program as that of Hannover. The schedule is shown in Table 3.3 below.

Table 3.3 *TU Delft testing and data acquisition program*

Series Number	Date	Number of Waves	Cum. Number of Waves	Clock Hr. [min]	Cum. Clock Hours [hr]
---	07-03-11	Profile 000			
1	08-03-11	500	500	12.28	0.20
---	08-03-11	Profile 001			
2	08-03-11	500	1000	12.28	0.41
3	08-03-11	500	1500	12.28	0.61
---	08-03-11	Profile 002			
4	08-03-11	500	2000	12.28	0.82
5	08-03-11	500	2500	12.28	1.02
---	08-03-11	Profile 003			
6	08-03-11	500	3000	12.28	1.23
7	08-03-11	500	3500	12.28	1.43
---	08-03-11	Profile 004			
8	08-03-11	500	4000	12.28	1.64
9	08-03-11	500	4500	12.28	1.84
---	08-03-11	Profile 005			
10	08-03-11	500	5000	12.28	2.05
11	09-03-11	500	5500	12.28	2.25
12	09-03-11	500	6000	12.28	2.46
---	09-03-11	Profile 006			
13	09-03-11	500	6500	12.28	2.66
14	09-03-11	500	7000	12.28	2.87
15	09-03-11	500	7500	12.28	3.07
---	09-03-11	Profile 007			
16	09-03-11	500	8000	12.28	3.28
17	09-03-11	500	8500	12.28	3.48
18	09-03-11	500	9000	12.28	3.69
---	09-03-11	Profile 008			
19	09-03-11	500	9500	12.28	3.89
20	09-03-11	500	10000	12.28	4.09
21	09-03-11	500	10500	12.28	4.30
---	09-03-11	Profile 009			
22	09-03-11	500	11000	12.28	4.50
23	09-03-11	500	11500	12.28	4.71
24	09-03-11	500	12000	12.28	4.91
25	09-03-11	500	12500	12.28	5.12
---	10-03-11	Profile 010			
26	10-03-11	500	13000	12.28	5.32
27	10-03-11	500	13500	12.28	5.53
28	10-03-11	500	14000	12.28	5.73
29	10-03-11	500	14500	12.28	5.94
---	10-03-11	Profile 011			
30	10-03-11	500	15000	12.28	6.14
31	10-03-11	500	15500	12.28	6.35
32	10-03-11	500	16000	12.28	6.55
33	10-03-11	550	16550	13.51	6.78
34	10-03-11	500	17050	12.28	6.98
35	10-03-11	500	17550	12.28	7.19
---	10-03-11	Profile 012			
36	10-03-11	500	18050	12.28	7.39
37	10-03-11	500	18550	12.28	7.60
38	10-03-11	500	19050	12.28	7.80
39	11-03-11	500	19550	12.28	8.00
40	11-03-11	500	20050	12.28	8.21
41	11-03-11	500	20550	12.28	8.41
---	11-03-11	Profile 013			

42	11-03-11	500	21050	12.28	8.62
43	11-03-11	500	21550	12.28	8.82
44	11-03-11	500	22050	12.28	9.03
45	11-03-11	500	22550	12.28	9.23
46	11-03-11	500	23050	12.28	9.44
47	11-03-11	500	23550	12.28	9.64
---	11-03-11	Profile 014			

With each wave train series, the train was started and allowed to propagate to completion of the numerical series before termination. After the last incident wave had impacted the profile, there was a 15 minute rest before the next series was started or a profile recorded.

With the ARC turned off, there is a high probably of occurrence to have standing waves in the flume. By definition, the flow velocities under the node are purely horizontal whereas the flow velocities under the antinode are purely vertical. This can cause a collection of sand under the antinodes and standing wave induced ripples in the bed. Allowing some of the standing wave energy to dampen out between series is one way to minimize this effect.

The 15 minute rest also has implications in the acquisition of the profiles. There is a small area ($h < 0.036$ m) where the echo sounder receives too many soundings and returns an error. In this area, the laser is able to detect the bathymetry (with some post processing) but only if the water is free of sediment. Therefore, rest time was added to the testing regime to allow for the fine sediment to settle out of the water column.

During Series 033, a small increase in the number of waves can be seen. During this series, the wavemaker failed early into the testing. Because only a small number of waves were released and there was uncertainty about exactly where to restart generation, the testing was restarted from the beginning. This resulted in about 50 extra waves propagating.

4 RESULTS AND ANALYSIS

4.1 Hydrodynamics and Propagation

The following section reviews the hydrodynamic environment present in the TU Delft flume during testing. The hydrodynamics, specifically the waves and water level, play an important role in the morphology. They represent the primary forcing constituent responsible for morphological change. Therefore, it is particularly important to maintain similarity with Hannover.

The hydrodynamics present in the Scheldt flume during testing are not discussed within. For a summary of published average hydrodynamic conditions, see Section 2.4.2 or Grüne, Cáceres et al. (2009).

4.1.1 Generated wave train similarity

Reproduction of the Hannover scaled wave train in TU Delft is a complex and dynamic process. Mechanical variance in the wave generation along with natural variance in the propagating waves makes the series by series similarity not possible. Additionally, not having been present for the Hannover testing series, it is not possible to understand why variance occurs in the Hannover testing campaign. Therefore, the main objective to judge similarity is not to capture the series by series difference but rather to ensure similar average conditions over the course of the testing campaign.

Post processing of the wave gauges in Hannover and TU Delft show good agreement between the dominant hydrodynamic properties. The wave gauge by wave gauge results can be found below in Table 4.1. To ease comparison, the results from TU Delft have been scaled up to prototype using Froude scaling with the depth scale equal to 10.

Table 4.1 *Comparison of average wave conditions in Hannover and TU Delft flumes at four similar positions. Associated distances correspond to positions in Hannover flume. A sufficient degree of similarity exists between the wave height and peak period. The shift in the peak period at wave gauge 05 is due to the presence of a standing wave in the flume.*

Wave Gauge 01 [90.0 m]	Hannover	TU Delft
H_{rms} [m]	0.69	0.71
H_s [m]	0.98	1.01
T_p [s]	5.58	5.58
T_{m02} [s]	3.98	4.62

Wave Gauge 03 [97.0 m]	Hannover	TU Delft
H_{rms} [m]	0.70	0.71
H_s [m]	0.90	1.00
T_p [s]	5.59	5.58
T_{m02} [s]	3.77	4.55

Wave Gauge 04 [180.0 m]	Hannover	TU Delft
H_{rms} [m]	0.68	0.68
H_s [m]	0.96	0.96
T_p [s]	5.58	5.85
T_{m02} [s]	3.45	4.65

Wave Gauge 05 [200.0 m]	Hannover	TU Delft
H_{rms} [m]	0.68	0.68
H_s [m]	0.96	0.96
T_p [s]	5.69	32.68
T_{m02} [s]	3.47	4.75

Some obvious differences can be seen in the Table 4.1. Some of these differences were intentionally implanted into the wave train while others were due to limitations of the testing campaign.

Due to limitations in the availability of sediment, constriction of the sediment bed required that the installed concrete slope be used as a profile base. Comparison of the Hannover and TU Delft flumes show that the wave train in TU Delft needed to propagate an additional 100 m prototype in order to reach similar positions at the outermost boundary of the active profile. Wave gauge 05 was used as the gauge to compare similarity. Its position at the outermost boundary of the active profile ensures hydrodynamic change is due predominantly to propagation and not morphological development (i.e. shoaling due to bar migration). Prior to installation of the sediment bed, a large hydrodynamic testing series was conducted to understand the propagation of the wave train and ensure correct scaling.

Near the wavemaker, both the H_{rms} and H_{m0} wave heights show a slight comparative increase in energy. Early testing of the wave train (i.e. before installation of the sediment bed) showed a consistent underproduction (6%-7%) in the propagating wave train energy. Discussion with the manufacturer of the generation software revealed this known error related to the actualization of the numerical time series. On their recommendation, the gain factor was increased slightly to account for this reduction. Additionally, a small amount of energy was added to the wave train to account for the extra 100 m prototype of propagation. This method resulted in good similarity in both the H_{rms} and H_{m0} wave heights at wave gauge 05 ensuring proportional energy propagates onto the active profile. However, this does cause the wave height close to the paddle be slightly higher when generated.

The produced peak period shows good similarity at wave gauge 01 and 02. Using a JONSWAP spectrum, this similarity ensures the train contains the correct focus of energy when produced. At wave gauge 03, there is a slight increase in the peak period as the peak shifts to 5.85 seconds. At flume scale, this results in only small differences which are difficult to correct for. Once the train reaches wave gauge 05, a large difference can be seen in the comparative peak periods. This is due to the amplification of a standing wave which appeared in the flume early into testing. If the respective spectrums are analyzed with this spike removed, a peak period of 5.85 seconds is produced. Under these conditions, the relatively small differences are considered negligible.

There is considerable disagreement between the Hannover and TU Delft mean periods. For reasons unknown to the author, when the produced Hannover spectrum is compared with its numerical spectrum, a drop of about one second is observed. At TU Delft, the wavemaker is equipped with a method to compensate for high frequency energy to correctly reproduce such a condition. With generation limit to first order principles, compensation is not possible, making the correct reproduction of the Hannover produced spectrum not possible. For similarity analysis, the focus was therefore only on the wave heights and peak period which represent the dominant energy of the spectrum. With this limitation, similarity was achieved.

4.1.2 Reflection analysis and standing wave implications

Observation of the obtained spectrums throughout the testing campaign (Figure 4.1; Appendix A) show the consistent development of a number of well defined low frequency peaks with various energy densities.

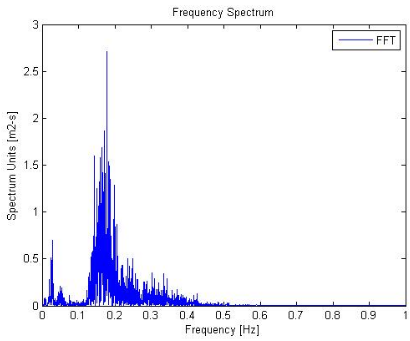

(a) Hannover (1:1)

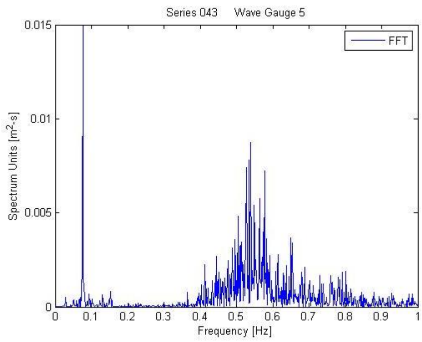

(b) *TU Delft (1:10)*

Figure 4.1 *Hannover and TU Delft spectrums taken from wave gauge 05 during Series 043. Spectrums were derived using standard fast Fourier transform (FFT) analysis. They show the development of long wave and standing modes within each facility.*

The smaller peaks ($S_f < 0.001$ m^2-s) are believed to be the development of bound long waves. Longuet-Higgins and Stewart (1964) were the first to discover the variation of the radiation stresses of grouped waves is the reason for the appearance of long waves. Formed as an equilibrium process, these waves are bound to the wave groups and their height is proportional to the short wave heights. Not unique to the testing, these low frequency groups consistently appear in both spectrums.

The TU Delft spectrum also shows the development of one defined peak at f = 0.0796 Hz (or T = 12.56 s). While Hannover also developed a standing wave, the development at TU Delft was much earlier, continued and had strong implication on the spectral output (Table 4.1; Figure 4.1). The spike was large enough to shift the derived peak period from the high frequency to low frequency component. Further analysis of the time series with a focus on the low frequencies, (defined here as f <0.15 Hz due to scaling) shows continued growth of this spike with increasing number of testing series campaign (Appendix A; Figure 4.2). As this spike is well outside of the Stokes range and continues to grow with time, this spike is not believed to be due directly to wave group induced radiation stresses. The regularity and growth of these points suggested a standing wave mode in the tank.

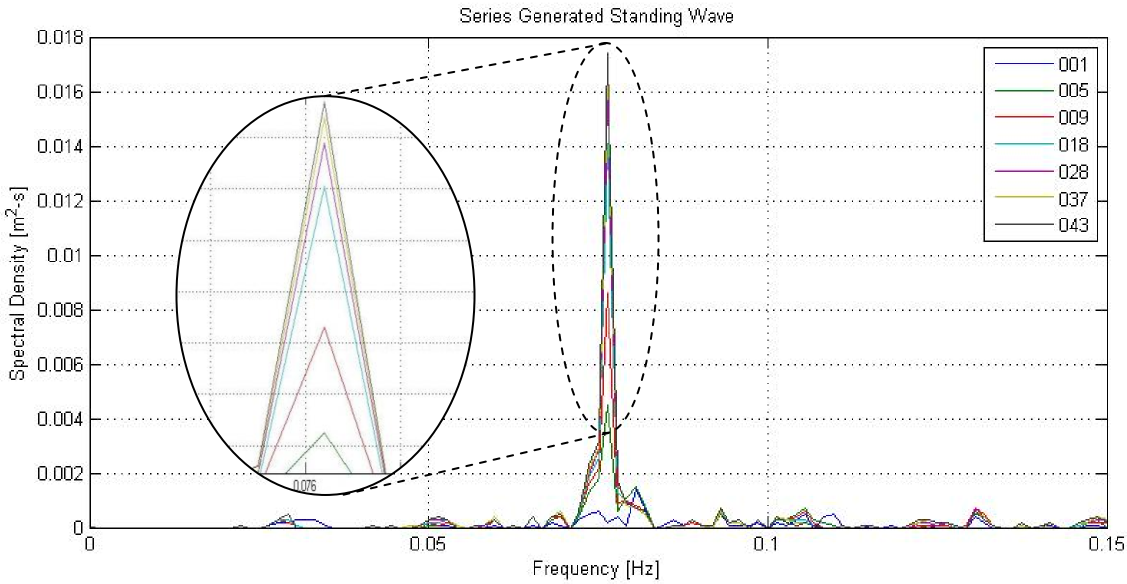

Figure 4.2 *Low frequency spectral components, defined as (f < 0.15 Hz) due to reduced scale, show presence of a standing wave in flume. The development of a standing wave mode can be seen which increases with profile development.*

Standing waves are well documented occurrence in wave flumes [Kirby, Ozkan-Haller et al. (2006)]. Von Dongeren, Battjes et al. (2007) explain that once the wave groups which contain these bound long waves approach the shore and the short waves start to break, the bound long waves are released traveling with their own phase velocity. In the flume, with a closed boundary at both ends and without ARC, these long waves remain trapped and form into a standing wave.

Using the least squares decomposition method of Zelt and Skjelbreia (1992), an estimate of the incident and reflected waves can be made to estimate the present of reflected energy.

Gauges were placed as close to the wave paddle as possible to minimize especially the nonlinear hydrodynamic errors. This corresponded to three wavelengths also ensuring proper formation of the wave train.

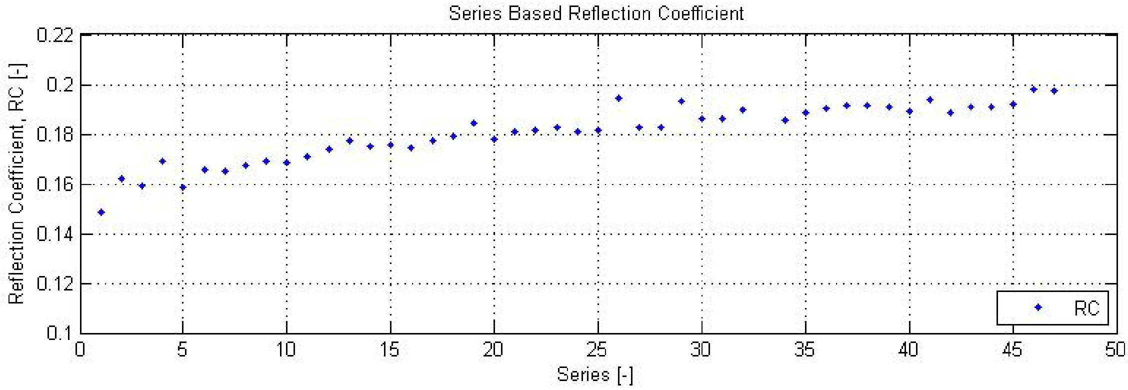

(a) Calculated reflection coefficient (RC = $H_{rms\text{-}ref}$ / $H_{rms\text{-}inc}$) *during testing campaign. Results shown increased reflection with increased profile development.*

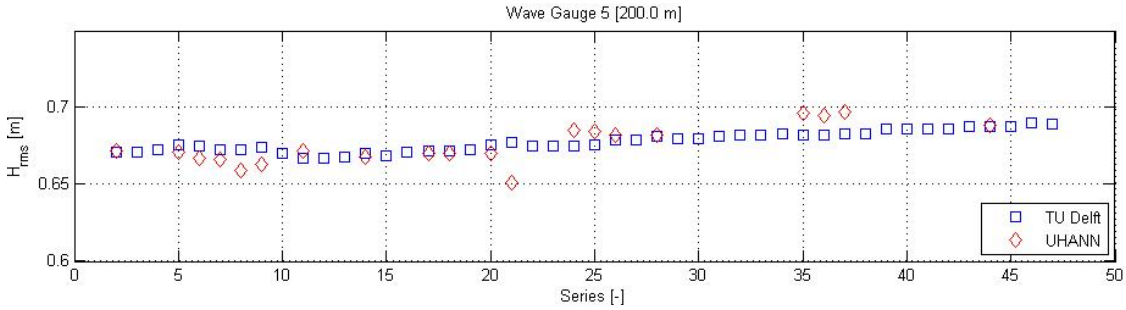

(b) H_{rms} wave height during testing campaign

Figure 4.3 *Increase in reflection coefficient shows a proportional increase in the H_{rms} wave height*

Results of the incident and reflected decomposition of TU Delft (Figure 4.3) show a general increase in the amount of reflection over the course of the testing campaign. The increase in reflection can partially be explained using the concept of beach states (Section 2.2.2). Due to the erosive nature of the wave train, as the testing campaign progresses, the beach profile moves sediment offshore creating a scarp at the upper end. This steepening results in a greater amount of reflected energy. It is this increased reflection which is responsible for the increase in the standing wave amplitude.

Using a short span fast Fourier transformation (discrete FFT) with a hamming window, the development of the standing wave can also be observed (Figure 4.4) over the course of the wave train series.

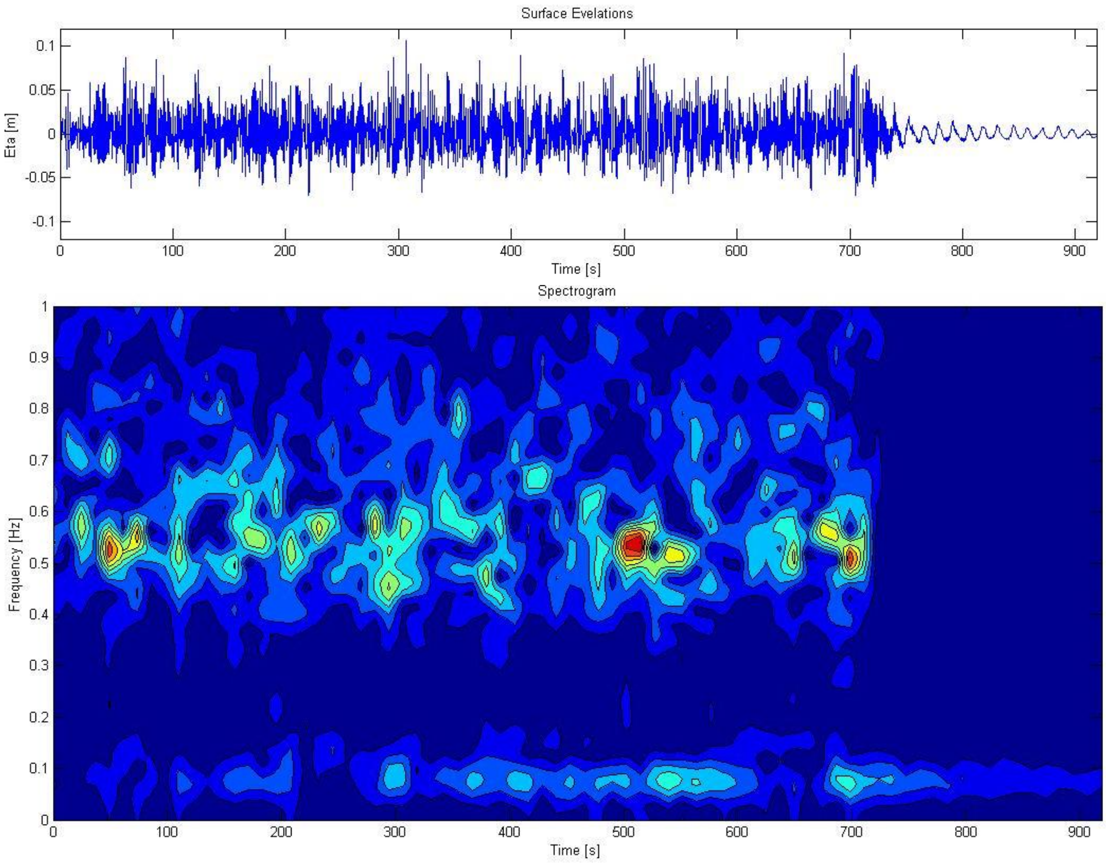

Figure 4.4 *Surface elevation and corresponding spectrogram at wave gauge 05 for Series 043. The peaks in the high frequency waves corresponds with the peaks in the times series. The low frequency components appear to be out of phase with high frequency components suggesting a delayed standing wave mode.*

From this spectrogram a valuable connection can be seen between the peak components of the spectrum and the low frequency standing wave. The spectral energy peaks in the high frequency components correspond well with the larger wave groups in the series. The standing wave shows a continued but variable grow with time. The peaks in the standing wave seem to be delayed with the peaks in the high frequency components. This times the connection of the standing wave with the reflections. It also suggests suggest that the wave needs to propagate a certain distance/time before developing into a standing mode.

Figure 4.3 shows the development of the H_{rms} wave height thought the testing campaign. A consistent increase in weight height can be observed, starting at about Series 005 and continuing until Series 047. This increase is not believed to be due to error by the wavemaker. Rather, it is believed to be a consequence of the standing wave.

To assess the resonance influence, the standing wave energy component can be isolated from the low frequency components. Using a standard zero order moment analysis, derivation of the H_{rms} wave height shows consistent agreement with the observed increase. For illustration, using the spectrum of Series 047, the derived H_{rms} of the standing wave is about 0.02 m prototype. This is approximately the difference between the first and last H_{rms} wave height. This result would tend to suggest that the incident wave height was slightly underestimated due to the presence of the standing wave. However, since the difference in reflected wave heights (the source of the error) is less than one standard deviation, this is not considered a significant error.

4.2 Profiles, Sediment Fluxes and Gradients

4.2.1 Profiles

The profile results of the testing campaigns for all three facilities (Hannover, Deltares and TU Delft) are presented below.

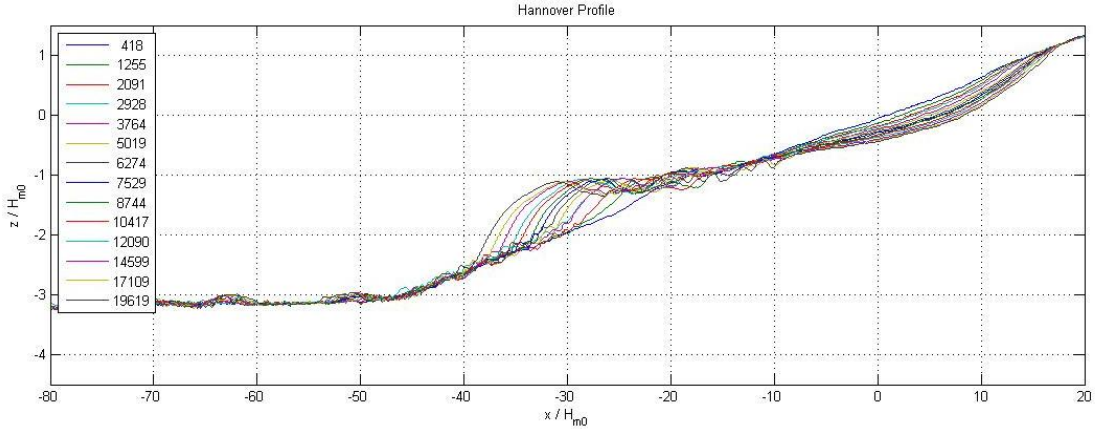

(a) Hannover (1:1)

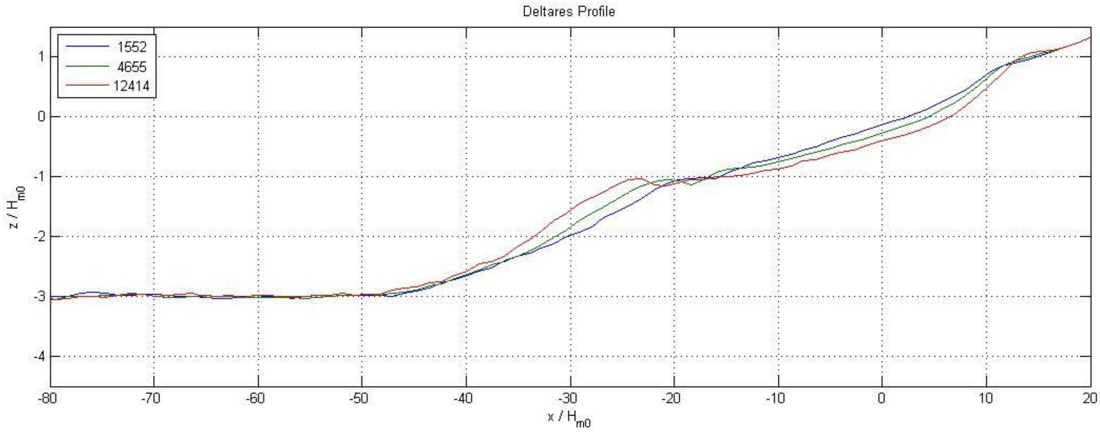

(b) Deltares (1:6)

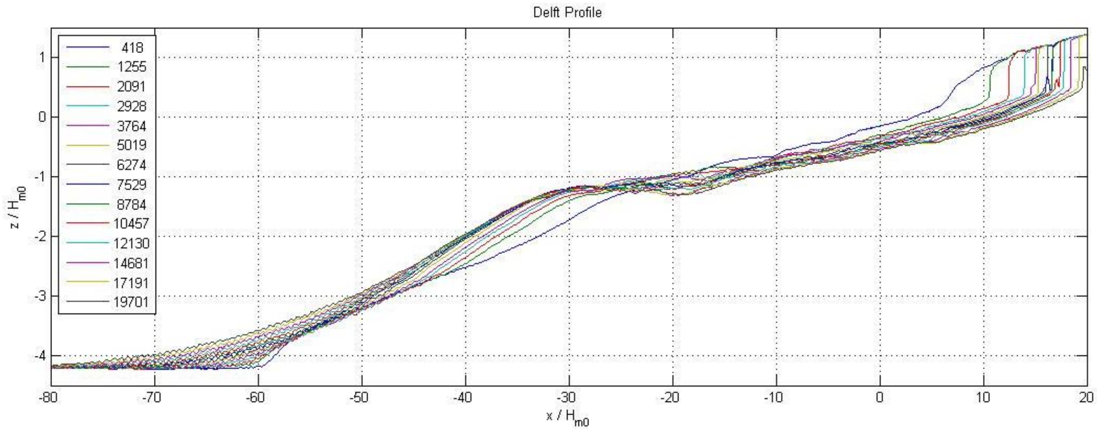

(c) TU Delft (1:10)

Figure 4.5 *Cross sectional (1:15 starting slope) profiles from respective facilities (also see Appendix B). (Legend: Approximate number of incident waves)*

These profiles (Figure 4.5) have been nondimensionalized using the significant wave height and peak period to facilitate comparison. The datum also corresponds to the intersection of the initial profile and still water level.

A marked degree of similarity can be found across all three profiles. Each facility saw the development of a bar and trough system within the first few wave train series. After initial development, this bar subsequently moved offshore and the profile developed. The development of this bar-trough system is vitally important to analysis and represents the main requirement need for further analysis. The focus of subsequent sections will attempt quantify the degree of similarity achieved, where scale effects appeared, and their impact on sediment transport and morphological development.

4.2.2 Transport rates

Using the profiles presented in Section 4.2.1, sediment fluxes can be derived from the bed level changes. In order to derive the transport rates, the following flux formulation was used.

$$F = \int_0^X \frac{\partial z}{\partial t} \, \partial x \qquad 4.1$$

Since the dominant sediment transport fluxes are expected from right to left, the fluxes are integrated in that direction. This provides a zero flux node at the upper margin of the profile to coincide with the physical processes. Using this definition, positive sediment fluxes correspond to onshore transport and negative sediment fluxes correspond to offshore transport.

The initial profile was not used as the datum for flux analysis. A certain number of artifacts appear in some of the initial profiles, which subsequently influence the analysis. The second profile at each facility serves as the datum to attempt to remove the influence of some of these artifacts. Using one initial profile to quantify morphological change is somewhat unrealistic. It creates a degree of artificial smoothing which gives bias toward the later profiles. However, as the main objective of such an analysis is to show general trends in quantities, this method was adopted. As long as the reader is aware of this bias, it should present little influence on the results.

The results of the flux analysis can be found below (Figure 4.6).

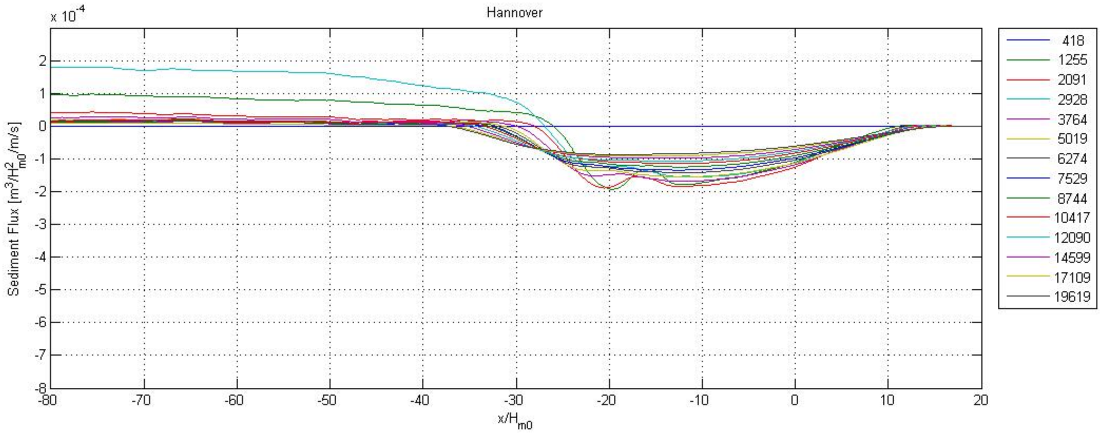

(a) Hannover (1:1)

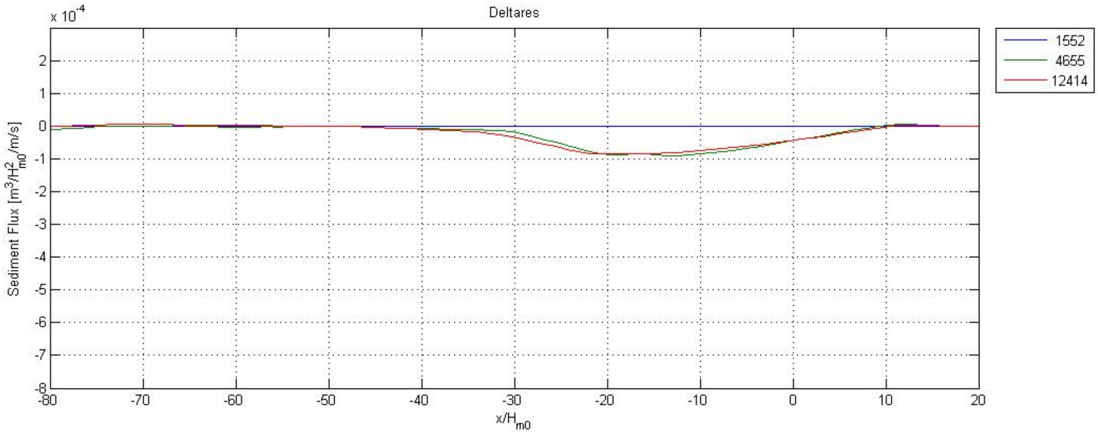

(b) Deltares (1:6)

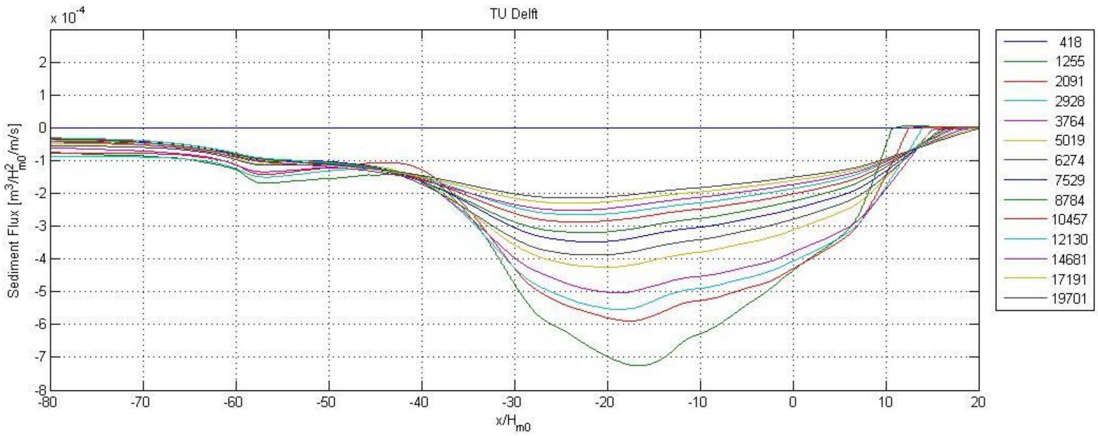

(c) TU Delft (1:10)

Figure 4.6 *Bed-level- change derived transport rates (also see Appendix B). (Legend: Approximate number of incident waves)*

As a flume represents a closed system, the sediment fluxes should converge to zero. However, due to a lack of bathometric data across the length of the flumes, the fluxes were computed to the farthest extent possible. This results in net sediment fluxes crossing the left boundary of the plot.

The Hannover profiles saw a large onshore sediment flux on the lower shoreface during some profiles acquisitions. Observation of the profile change does show a small bed level change in this area. This temporary onshore flux could be due to the presence of the rippled bed in this section of the profile. Ribberink, van der Werf et al. (2008) have shown that depending on the ripple geometry and hydraulic regime, transport in this region can either be onshore or offshore directed. Given the temporary appearance of this flux, measurement error is a more likely cause. However, as the author was not present for testing at Hannover, a definitive conclusion cannot be made at this time.

While the general trends appear to be the same, a degree of dissimilarity is observed in transport rates of both Deltares and TU Delft. The fluxes of Deltares seem to be lower by a factor of two compared to Hannover. Where conversely, the fluxes at TU Delft seem to be thrice as high compared to Hannover.

4.2.3 Transport gradients

The transport gradients can also be derived from the bed level changes. Transport gradients however, are only the derivative of the fluxes.

$$G = \frac{\partial F}{\partial x} \tag{4.2}$$

Transport gradients can be understood as a numerical representation of erosion and accretion. In relation to the profile comparison, this is advantageous as it gives a numerical representation of the bed level changes.

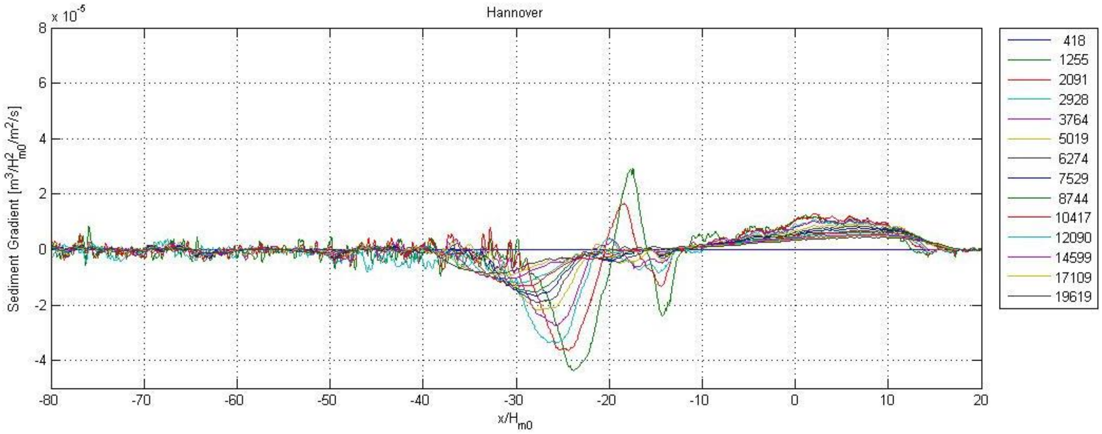

(a) Hannover (1:1)

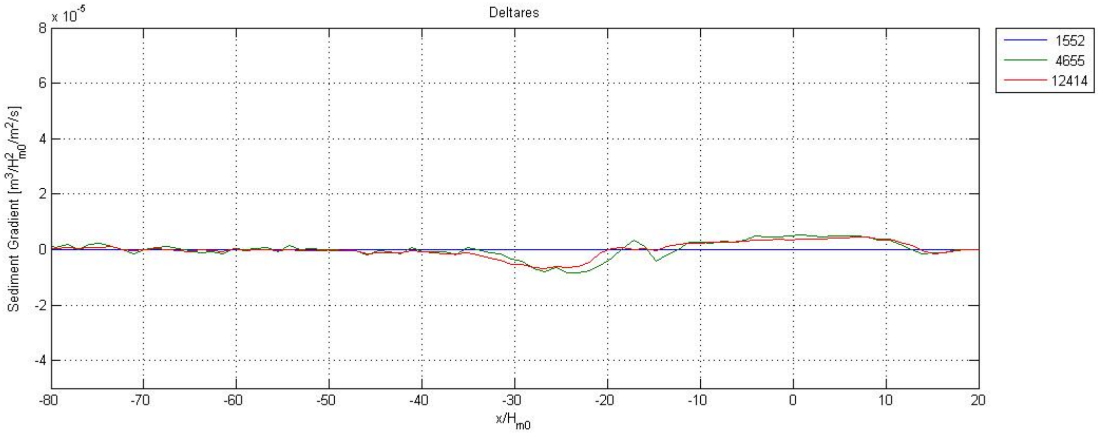

(b) Deltares (1:6)

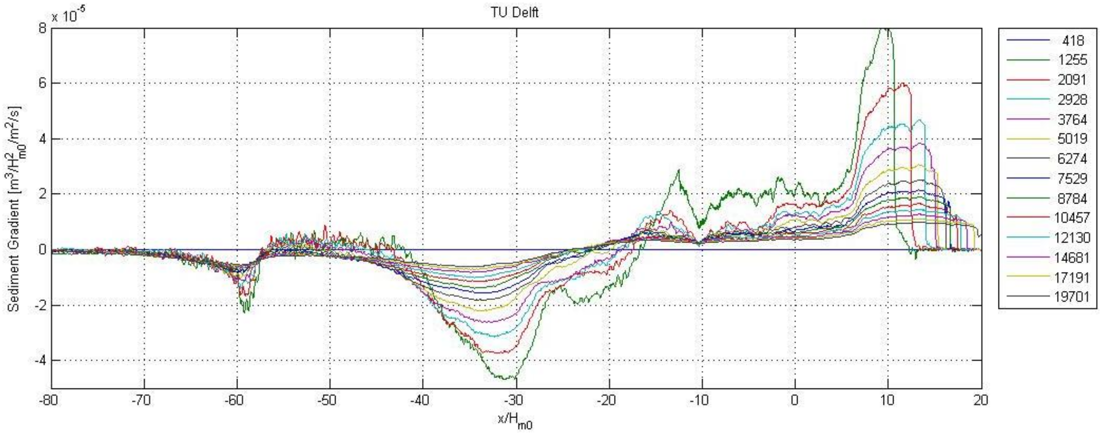

(c) TU Delft (1:10)

Figure 4.7 *Bed-level- change derived gradients (also see Appendix B). (Legend: Approximate number of incident waves)*

The transport gradients at both Deltares and TU Delft appear to be generally divergent when compared with Hannover. Similarly to the sediment fluxes, Deltares shows smaller gradients while TU Delft shows larger. Especially over the bar however, the magnitude between

Hannover and TU Delft appear to be similar. These results are in close agreement with the profile development.

The large transport gradients appear to be especially disproportional in the swash zone. Due to the low density and large diameter sediment used, once wetted, the sediment becomes quite cohesive. This caused a linear scarp to develop in the profile of TU Delft. This scarp is not reflected in the profiles due to the position of the measurement carriage (from above). The scarp which developed was often concave in shape until the cohesive forces could no longer support the lip weight and it collapsed. This caused avalanching to be the main mechanic contributing sediment to the subsurface. Since capillarity and intermolecular forces cause these cohesive effects, once the sediment becomes submerged, this cohesiveness is negated.

4.3 Scaling Parameters

The transport rates presented in Section 4.2.2 appear to be divergent with the degree dependent upon the type of sediment scaling. Ideal scaling theories provide a platform to understand how the sediment scaling affects the individual transport across the nearshore. By definition, if each term of a transport similarity set is preserved ($n = 1$), the transport regime should also be preserved. The ideal scaling set of Kamphuis (1991) and Dalrymple (1989) have been described previously (Section 2.4) which allow for this analysis. Therefore, the cross shore variance of the nondimensional parameters must first be derived.

With profiles obtained during testing, the wave height and wave period are the two main hydrodynamics values required to derive the distribution of the nondimensional parameters across the nearshore. Since the wave period is approximately constant across the nearshore, only the wave heights need to be resolved. The nearshore model of Battjes and Janssen (1978) was selected for this analysis. The cross shore model assumes:

$$\frac{\partial P}{\partial x} + \overline{D} = 0 \qquad 4.3$$

where:

P	Time average energy flux	J /m-s
$\overline{D}$	Time average dissipation power	J/m^2-s

The dissipation power is resolved using the maximum probably wave height and broken wave percentage. Both of these quantities are implicitly resolved in the model using a modified Rayleigh distribution. Boers (2005) has shown with data from flume tests that this model reasonably resolves the time averaged wave heights within the surf zone.

4.3.1 Bed load scaling

The Kamphuis (1991) similarity set was discussed in Section 2.4. The Shields number and particle Reynolds number within the set together characterize boundary layer processes over the bed and therefore the degree of sediment contributed to transport. These terms are therefore identified here as the sediment pickup function. The shear velocity remains the only undefined variable. While there are a number of possible definitions of the shear velocity, for this analysis, the shear velocity is evaluated using solely the combined wave and current shear stress. This method quantifies purely the boundary layer contributions which are of most interest for bed load processes.

Using the sediment pickup function and the relative fall as a dynamic set, it is possible to plot their variation over the nearshore profiles. Displaying nondimensional parameter variance across the nearshore provides a very powerful visual tool. With Hannover representing unscaled (and therefore undistorted) conditions, Deltares and TU Delft give a direct quantification of how the bed load processes are reproduced when sediment is scaled according to their respective sediment scaling theories (e.g. Froude or bed load model). The relative density and bed form parameters are not included as their variation across the nearshore is considered negligible for this analysis.

$$\theta = \frac{\rho\, u_*}{\gamma\, d_{50}}$$

$$Re_* = \frac{u_* d_{50}}{\nu}$$

$$V = \frac{u_*}{w_s}$$

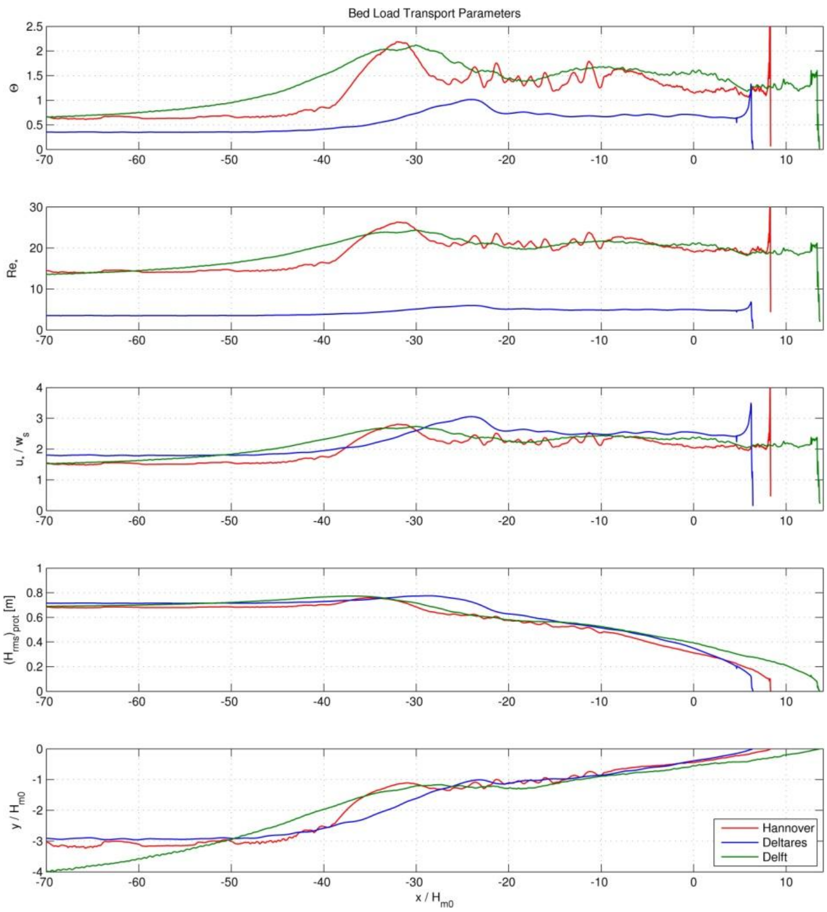

Figure 4.11 *Cross shore variation of bed load scale relations based on the Kamphuis (1991) similarity set. The similarity between Hannover and TU Delft appears to approach unity. Froude scaling at Deltares appears to decrease similarity especially with respect to the sediment pickup function.*

Between Hannover and TU Delft, in Figure 4.11 there appears to be a great degree of similarity. A rippled bed appears low in the profile of the two facilities. Interestingly, at the location where the Shields parameter moves above one, the ripples disappear and the bed becomes plain. After this crossing, the Shields number remains high and the bed plain across the rest of the nearshore. This particular feature is very important to preserve similar near bed processes with Hannover. As discussed above, plain bed sediment pickup is only a function of the boundary layer processes, which by definition, must be present to preserve bed load transport.

Within the inner surf zone of Hannover, large bed waves appear which were not reproduced at TU Delft. These features appear in natural profiles [see Henderson, Allen et al. (2004)] and are not considered to be a model effect. However, their development is poorly understood. When analyzing the Shields parameter, the bed waves generate shear stress fluctuations within the region which can be noted in Figure 4.11. Unlike a rippled bed regime in which a ripple vortex is generated, Van Rijn (2007) suggests that if the ripple length is much greater than the orbital excursion however, the ripples do not contribute to the bed state roughness. The length and height of the ripple suggest that bed load processes give the dominant contribution to sediment pickup and near bed suspension in this region. Since the average of the sediment pickup function remains convergent, it suggests that the scaling parameters are approximately reproduced within this region.

There are however two scaling parameters which are consistently mismatched across the shoreface: the bed form and relative density parameters. The mismatch of the bed form parameter comes directly from the scaling of the grain diameter. While by definition, a scale effect should present itself, it is possible to minimize any unintended effects. Most simply, ensuring that the Shields number remains high across the surf zone. The development and contribution of ripples can be avoided altogether if their development is suppressed. Caution should however be given as this method only applies in cases, such as this, where a plain bed regime is expected.

Kamphuis (1991) has discussed some of the consequences on sediment transport due to the mismatch of the relative density parameter. Focusing only on the submerged transport, Kamphuis (1991) suggests that, due to the reduction in density, the sediment pickup accelerations are not preserved. The result is sediment which, once mobilized, accelerates quickly within the flow. As long as this mismatch remains small, this should be an advantage as accelerated development time would require less clock hours. Observation of the profiles presented in Section 4.2.2 would tend to confirm the presence of this phenomenon. If the mismatch is too large, the particle accelerations can lead to a loss in the granular contact stresses which causes fluidize bed. This can create a layer of almost instantaneous sediment movement, which can cause disproportional erosion volumes. The density mismatch should consequently be minimized to avoid this.

Even scaling sediment density and diameter terms, similarity of all terms in the Kamphuis (1991) similarity set is not possible. To preserve transport, the only physical possibility is to attempt to preserve dominant terms and minimize unintended scale effect. With minimized scale effects coming from the relative density and bed form parameters, the sediment pickup function and relative fall velocity present as the dominant dynamic terms in the similarity set. Their high degree of similarity in Figure 4.11 is therefore very important suggesting bed load transport is preserved. Additionally it also suggests that scaling of sediment according to the scaling law of Henriquez, Reniers et al. (2008) is in fact a valid method to preserve bed load transport (for lengths scales down to and including 1:10).

Comparison of Froude scaling between Hannover and Deltares in Figure 4.11 does not show a large degree of similarity. Cáceres, Grüne et al. (2008) noted that during testing, a larger proportion of suspended sediment was observed. It is believed that Deltares experience a change in the dominant transport regime moving from bed load dominated at Hannover to suspension load dominated at Deltares. Observation of the scale relations could give some insight to why this happened.

Figure 4.11 shows that unlike, Hannover and TU Delft which shift to a high Shields number regime before entering the surf zone, Deltares does not. This would tend to indicate that the entirety of the Deltares profile is under a vortex-ripple regime. Not only is a sediment vortex regime an organized process but is often a defined suspensions process ($w_s/u_* > 0.8$). With vortex shedding releasing sediment into the water column, wave boundary layer contributions are limited. The scaling method's ability to maintain a developed boundary layer and dominant bed load transport regime is no longer possible.

There is also an additional underestimate in the Reynolds particle number at Deltares compared to Hannover. Comparison with the Shields curve shows that the critical Shields number is higher. This underestimation will result in delayed sediment movement and undeveloped concentrations. The relative fall velocity on the other hand does show a good degree of similarity. However with a value greater than 0.8 and a low Shields number, when compared with data presented by Ribberink, van der Werf et al. (2008) would suggest strong vortex dominance. It is hypothesized that with this dominance, the vortex is no longer able to mobilize, transport or suspend proportional amounts of sediment. The implication of this vortex on sediment fluxes and concentrations will be examined in subsequent sections.

These results suggest that Froude scaling completely changes the state of the bed and resultant transport regime. Based on these scaling parameters results, it can be concluded that when sediment is scaled according to Froude scaling (for length scale at and below 1:6) bed load transport cannot be preserved.

4.3.2 Suspended load scaling

The suspended load ideal scaling set proposed by Dalrymple (1989) was discussed in Section 2.4. While the Shields number and relative fall velocity remain unchanged from Section 4.3.1, they are included here to complete the similarity set.

$$\theta = \frac{\rho\, u_*}{\gamma\, d_{50}}$$

$$Re_* = \frac{u_* d_{50}}{\nu}$$

$$D = \frac{H}{w_s\, T}$$

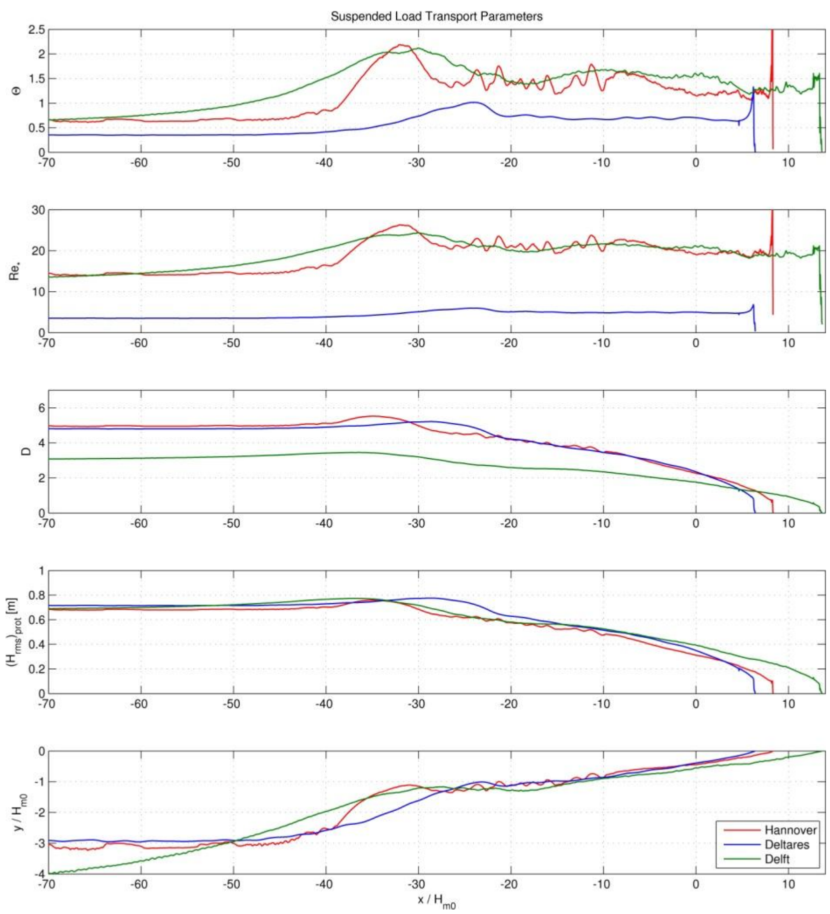

Figure 4.12 *Cross shore variation of suspended load scale relations based on the Dalrymple (1989) similarity set. The use of the bed load model at TU Delft appears to decrease the similarity with Dean number. The use of Froude scaling at Deltares shows good agreement with the Dean number. However, the sediment pickup function remains dissimilar.*

Analysis of the ideal suspension set (Figure 4.12) now shows that the TU Delft Dean number is consistently underestimated compared to Hannover. Since the sediment was scaled specifically to preserved bed load transport, this underestimate is expected. The mismatch comes directly from the fall velocity since the dynamic hydraulic parameters are scaled correctly according to Froude scaling laws. Even though the density of the sediment is much less than natural sediment, the diameter is quite large. When the fall velocity is compared with similar sediment scaled according to Froude scaling, the TU Delft sediment fall velocity is much higher and therefore more suspension resistant. The mismatch in the Dean number therefore results in sediment which underestimates the turbulent contributions to suspension. While the sediment pickup function does remain the same, the mismatch of the Dean number shows that using the bed load scaling method, suspended load scaling is not preserved by the Henriquez, Reniers et al. (2008) scaling method.

With the Dean number introduced, Hannover and Deltares quantities show a high degree of similarity with this parameter. It would suggest, especially in the outer surf zone and inner surf zone where suspension is particularly important, that suspension is reproduced correctly.

However, in order for the suspension set to be reproduced, there should be reasonable similarity between all terms of the similarity set. There is still the mismatch between the sediment pickup function which voids this similarity.

The boundary layer or near bed processes act as a feed to the transport regimes for both a smooth and rippled bed. However, the degree to which sediment is mobilized is usually reduced within a rippled bed. This is due to the underdevelopment of the boundary layer and inability of the rippled vortex to generate proportionally large shear stresses. The thin layer of sediment generates strong gradients close to the bed often characterized by an exponential like profile. An increased critical Shields parameter, and reduced Shields value sediment mobility will also reduce sediment concentrations. The reproduction of the suspension process is therefore not possible.

4.4 Return Flow and Sediment Concentrations

In Section 4.3, the effect of sediment scaling methods on the resultant nondimensional parameter sets were examined. The sediment flux disagreement (Section 4.2.2) presented suggests that the mismatches in both facilities (TU Delft and Deltares) influence the sediment transport from one degree to another. To explore these results, a simple model is used here to decompose the sediment fluxes into time averaged return flow and concentration quantities.

In Section 2.4, a formulation to resolve the morphological time scale was presented based on work by Vellinga (1986). A simple relation to express the suspended sediment flux was used to derive this time scale. Since the derivation is intended to characterize the dune erosion process, a constant concentration profile over the water depth is used as the basis for analysis. Close to the dune face, where water depths are small and turbulence is large enhancing mixing, this is a valid approximation. However, away from the dune face this assumption would increasingly weaken as a power like concentration profile characteristically develops.

Using the Vellinga (1986) approach however, the sediment concentration quantities across the nearshore can be resolved. Instead of the assumption of a linear concentration profile, the profile can be represented by a depth averaged quantity. While this does not change the form of the equation, it is important to understand that the underlying assumptions are inherently different and depend on the flow similarity. This difference allows a depth averaged quantity to approximate the entire nearshore resulting in:

$$\mathrm{F} = h\, U_r\, \bar{C} \qquad 4.4$$

where:

$\bar{C}$	Depth average concentration	m^3/m^3

For a first order analysis, Stive and Battjes (1984) have shown that these magnitude quantities reasonably asses the offshore transport. With the intent to provide a comparison between facilities, the form of this equation can also be transferred into a scale relation:

$$\mathrm{n_F} = \mathrm{n_h}\, \mathrm{n}_{U_r} \mathrm{n}_{\bar{C}} \quad 4.5$$

And using Froude scaling $\left(\mathrm{n}_{U_r} = \mathrm{n_h}^{0.5} \right)$:

$$\mathrm{n}_{\bar{C}} = \frac{\mathrm{n_F}}{\mathrm{n_h}^{1.5}} \quad 4.6$$

The result is an equation that can resolve the sediment concentrations from only the sediment fluxes and length scales based on return flow similarity. This is advantageous since the profile-derived transport rates were presented in Section 4.2.2 and the length scales are known.

4.4.1 Return flow

The return flow represents the main advective component to the sediment fluxes, the magnitude of which can vary greatly across the surf zone. Drawing most of its form from the wave induced turbulence (i.e. eddy viscosity profile), the vertical profile of the flow is influenced only marginally by the sediment transport. It is therefore assumed that the sediment scaling has negligible effects on the return flow. Since the hydrodynamics were scaled according to Froude scaling, breaking characteristics should be preserved (Section 2.2.1) allowing the return flow to be decomposed by a depth averaged quantity.

Stive and Battjes (1984) present a model to decompose the variance of the magnitude of the return flow across the surf zone. They assume that for a random wave field breaking on a beach, the breaking waves have a quasi-steady depth similar flow profile. Stive and Battjes (1984) observed that the flow profile is rather uniform over the lower depths of the flow profile and adopt a depth average approximation. Using a linear wave train, the model approximates that the return flow mass flux is balanced with the net mass flux above trough level. This results in:

$$U_r = \frac{1}{8} Q \left(\frac{g}{h} \right)^{0.5} H_{rms} \quad 4.7$$

where:

Q	Broken wave percentage	-

The percentage of broken waves was introduced as an extension from linear theory to account for a random wave field. This quantity varies with position in the surf zone and is approximated using the modified Rayleigh distribution of Battjes and Janssen (1978). The Battjes and Janssen (1978) model was used previously (Section 4.3) to resolve the wave height within the surf zone and therefore couples nicely with this return flow approximation.

Using the Stive and Battjes (1984) model results in the following cross shore distribution of the time and depth averaged return flow:

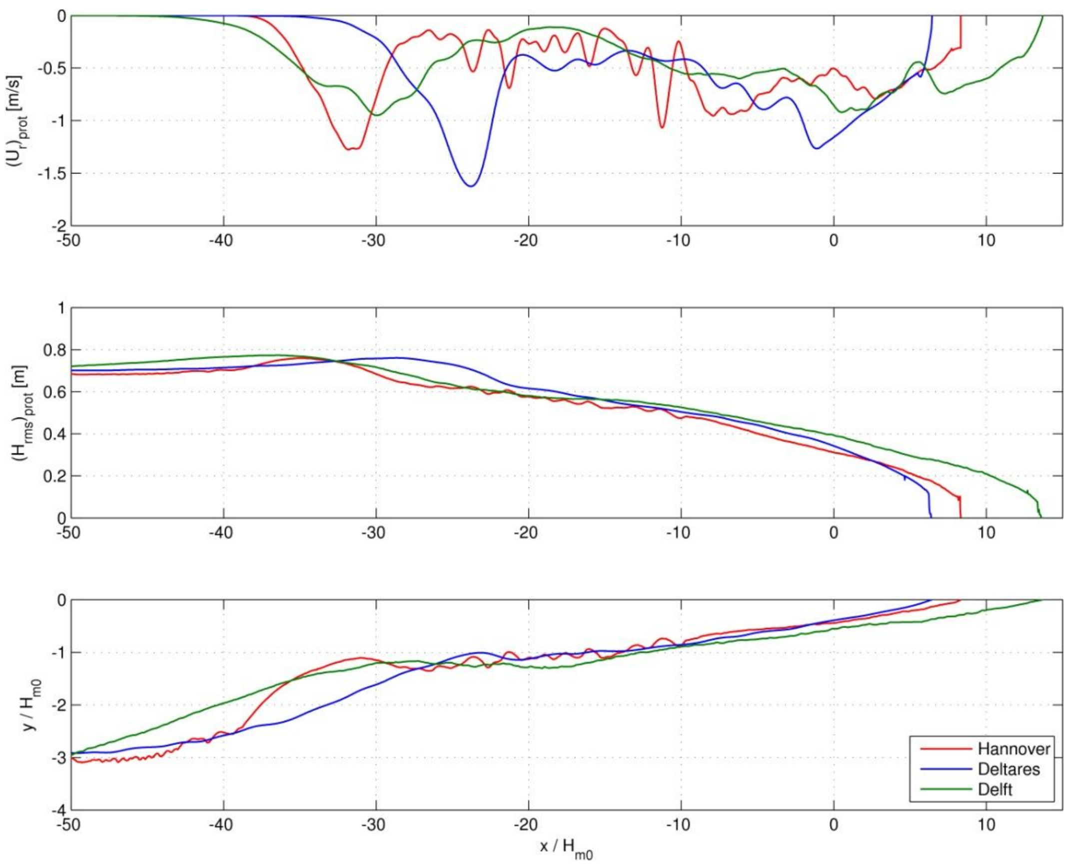

Figure 4.13 *The time averaged flow magnitude of the cross shore return flow show a reasonable degree of similarity especially within the surf zone.*

These results show similar general trends across the three facilities. This is important to note because the validity of Equation 4.6 is based on the return flow similarity.

The most notably feature of the results is the spike in the return flow over the breaker bar. This spike is expected and can be conceptualized using control volume analysis. In order to maintain conservation of mass, the volume of water flowing through each cross section must be equal. As the return flow progresses over the bar, much like fluid flow through a diffuser, the flow must accelerate to maintain this continuity. It is the increase here of the velocities over the bar and rapid dissipation on the outer shoreface which greatly contributes to the offshore bar migration. The effect of this process on transport is mostly characterized by the Dean number since transport here is strongly correlated the amount of suspended sediment.

While there is a defined return flow spike over the bar in all three facilities, the location and magnitude seems to differ. The peak in the return flow of Deltares is much before Hannover or TU Delft. While the cross section is hydraulically early because of differences in the testing campaigns, Cáceres, Grüne et al. (2008) have shown that the bar was consistently located higher in the profile. The bar position caused the return flow magnitude to rise early and because it formed in a shallower location, to increase in magnitude..

At TU Delft, the peak return flow velocity position was comparable to Hannover. However, the magnitude was underestimated. This is predominantly because the bar that formed at TU Delft was more diffusive than Hannover or Deltares. Relating the sediment size and shape Simons and Sentürk (1992) show that due to the increase in grains size, the angle of repose of this sediment is slightly less. This contributes to greater depth over the bar. With the increase in depth, the velocities do not increase which cause the reduction in the magnitude.

4.4.2 Sediment concentrations

With sufficient similarity between the return flow components, the influence of sediment scaling on the concentrations is of great interest. With accelerated development at TU Delft and reduced development at Deltares, the similarity in the return flow suggests that the sediment concentrations contribute firstly to the differences in the fluxes.

Depth averaged concentration

Using the similarity in the return flow (Section 4.4.1), along with Equation 4.6 the depth and time averaged concentration quantities can be resolved. First, however, the sediment flux scale relations need to be derived for both Deltares and TU Delft as input to the equation. Removing the wave height and time scale nondimensionalization from the transport rates (Figure 4.6) allows for easy transfer into flux scale quantities. Combining these fluxes with the associated depth scale results in the following concentration scaling:

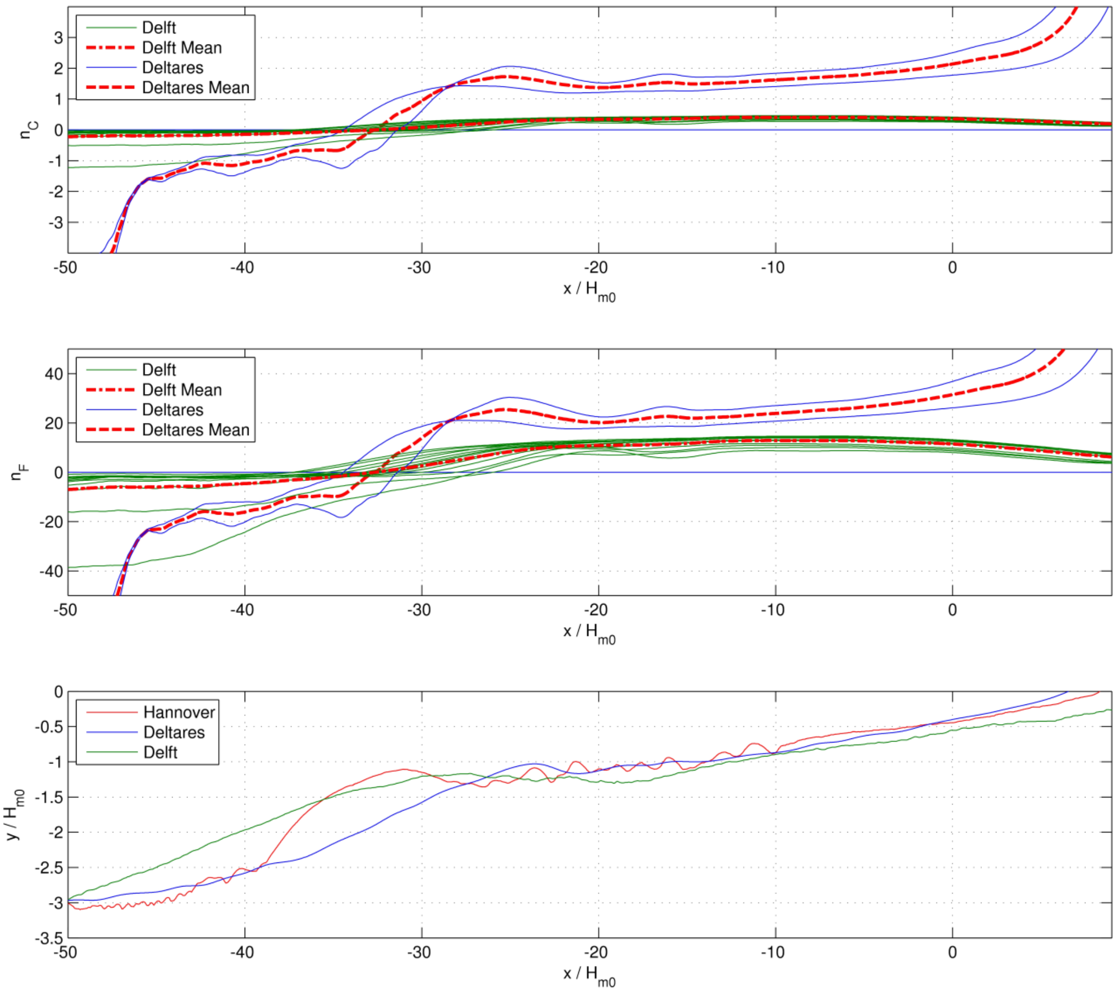

Figure 4.14 *Sediment concentration (n_C) and flux (n_F) similarity. Ideally if all parameter were preserved, the depth averaged concentrations should scale to unity. Concentrations suggest that Froude scaling results in lower concentrations while the density scaling at TU Delft increases the concentrations.*

Observation of the concentration profiles across the nearshore show compartmentalized and defined sediment transport regimes across the surf zone. In each cross shore zone, (the swash zone, inner surf zone, outer surf zone and shore face) the sediment scaling method has a defined influence on the physical sediment transport process. This suggests that sediment cannot simply be scaled for one region and be expected to respond similarly to prototype conditions across the domain. With marked differences, the results suggests sediment will respond differently in each region and also depend on the scaling method.

The bar position and development similarity between Hannover and TU Delft give the best quantification of the influence of scaling across the nearshore. While TU Delft did show consistently high sediment concentrations, this scaling method best highlights the concept of process compartmentalization.

High sediment concentrations within the swash zone (x / H_{m0} < 0) were represented by hastened erosion in the geometrical profiles. The initial shoreline regression was strong but after an initial adjustment period developed much along the same line as Hannover and

Deltares. Due to this initial release however, sediment concentrations remain high within this region as shown in the figure above (Figure 4.14).
The influence of swash processes decreases toward the inner surf zone ($0 < x / H_{m0} < -25$) which correlates with a decrease in sediment concentrations. Sediment concentrations should scale to unity if all suspension and transport processes have been completely reproduced. It is practically interesting here in the inner surf zone they do not. Due to the presence of only surface rollers, wave induced turbulence is focused toward the surface. Wave induced sediment mobility is therefore only a function of bed load processes. Concentrations greater than Hannover suggests that the near bed processes are not reproduced correctly. This conclusion is contradictory to the similarity founded in the scaling parameters. It suggests either that the mismatch between the relative density is more significant than expected or that there is some process not accounted for by the scaling parameters. This mismatch however seems to be both consistent across the inner surf zone and independent of the local breaking process. This would further suggest that the mismatch concentrations are a physical manifestation of the bed load processes.

At the outer surf zone ($-25 < x / H_{m0} < -35$), sediment concentrations increase as transport regimes transition and scale parameters become dissimilar. Unlike the inner surf zone which is defined by bore like surface rollers and mixed transport regimes, transport here is dominated by plugging breakers. With the mismatch in the relative density and increasing particle acceleration, the influence of the wave jet to sediment mobility in this region is significant. Van Rijn (1984) has also suggested that an increased grain diameter will increase the centrifugal forces on individual grains further enhancing mixing. The inherent suspension processes and parameter mismatches generated higher suspension and stronger offshore transport muddling shoreface processes. This effect is so significant that in the region for which sediment was scaled, the lower shoreface, are the largest concentration mismatches. This however highlights that while mobilization and suspension processes are localized, the totality of cross shore transport is holistic. The concentrations show that memory type scale effects can corrupt transport in a subsequent region. Therefore, the macro scale processes and dominant sediment transport directions should subsequently influence the sediment scaling to minimize these effects.

Unlike TU Delft, the sediment concentrations at Deltares are consistently underestimated throughout the profile. Especially from the boundary of the swash zone to breaker bar. The increased critical Shields number and underestimation in the actual Shields values, discussed in previous sections, are also consistent with these findings. The deceased sediment mobility is a result of the critical value with an additional decrease a result of the direct Shields value. This shows that the ripples contribution to sediment mobilization is not enough to compensate for the reduction in shear stress. Even though the vortices mobilize and suspend sediment, the actual mobility layer remains very thin producing strong concentration gradients close to the bed. Vortices are only able to mobilize and suspend a finite amount of sediment defined by each passing wave. With a reduced Shields number, the result is reduced near bed averaged concentrations and suspended sediment concentrations. This is also reflected in the morphological development that is slowed by these underestimations.

Once though the inner surf zone, there is an additional underestimation in the mean concentrations. It is likely that the additional decrease in the concentrations comes from the fact that the Deltares breaker bar remained higher in the profile than Hannover. As was shown previously this caused an early spike in the return flow which would accelerate the sediment flux. Therefore, when the concentrations are matched up, they are not directly geometrical comparable. For this comparison, the decomposition method used is therefore not considered valid past the breaker bar for Deltares.

Reference concentration

In previous sections, it was shown that depth averaged sediment concentrations were not consistent in either facility. At TU Delft, the increased concentrations are partially interesting because of the similarity presented with the near bed parameters. If the bed load processes were in fact preserved, sediment concentrations should scale closer to unity. Introducing an eddy viscosity model, it is possible to resolve the concentration profiles. Then using these profiles and the mean concentration relations, resolve the contributions of sediment from the bed load process.

The boundary layer or near bed motions are most responsible for creating sediment movement and determining the degree of sediment contributed to transport. To resolve the concentration profiles, the boundary layer must be modeled correctly. In the case of Hannover and TU Delft, a smooth bed was present making it is possible to represent the bed roughness as a function of the sediment diameter ($k_s = 3\ d_{50}$). The boundary layer thickness can then be resolved using the formulation of Fredsøe and Deigaard (1992).

$$\delta = f_\delta\ 0.09\ k_s \left(\frac{A}{k_s}\right)^{0.82} \tag{4.8}$$

where:

f_δ	Wave irregularity factor	-

This equation has been derived primarily for regular oscillatory motions. Klopman (1994) showed that random waves tend to increase the boundary layer thickness. A wave irregularity factor was therefore introduced to account for this. This factor was set to three based on recommendations by Reniers, Thornton et al. (2004).

Due to the presence of a rippled bed at Deltares, the above process must be slightly modified. The rippled bed at Deltares does not allow the wave boundary layer and reference level to be resolved directly. Unlike Hannover and TU Delft who use the grain diameter, the ripple height at Deltares becomes the determinate roughness input. Therefore, the ripple height must be first calculated. To determine this ripple height, the formulation by Van Rijn (1993) was used. This equation is based on the mobility parameter:

$$\Omega = \frac{\hat{u}^2}{(s-1)g\ d_{50}} \tag{4.9}$$

Using this mobility parameter, Van Rijn (1993) proposed a piecewise function to define the ripple height:

$$\frac{\Delta_r}{A} = 0.22 \quad \text{for} \quad \Omega \leq 10 \tag{4.10a}$$

$$\frac{\Delta_r}{A} = 2.8 \cdot 10^{-13}(250 - \Omega) \quad \text{for} \quad 10 < \Omega \leq 250 \tag{4.10b}$$

$$\frac{\Delta_r}{A} = 0 \quad \text{for} \quad \Omega > 250 \tag{4.10c}$$

This formulation was derived for irregular waves, which, compared to regular waves, tend to smooth and decrease the amplitude of the bed ripples [Nielsen (1981)]. The upper limit of 250 corresponds to a smooth bed and sheet flow. It should however be noted that Equation 4.10 is valid only for nominal sediment densities ($s = 2.65$). Using data of Yalin and Russell (1962), Nielsen (1981) showed that lightweight sediment tends to smooth ripples earlier than predicted by the mobility parameter. Therefore, only profiles shoreward of the rippled bed region are analyzed here.

With the ripple heights known, a modified bed roughness and reference level can be determined. Van Rijn (1993) present roughness values which range from one to three times the ripple height ($k_s/\Delta_r = 1 - 3$). Based on recommendations of Van Rijn (2007), a value of one was selected as input. This modified roughness quantity was subsequently used as input to the boundary layer model of Fredsøe and Deigaard (1992).

The reference level is also dependent upon the ripple height. Van Rijn (1993) recommended a value equal to half the ripple height ($a/\Delta_r = 0.5$). For a smooth bed regime, the thickness of the boundary layer defines the reference level. The reference level dictates the upper limit of the near bed sediment transport. Therefore, any transport above this level is suspended transport.

Suspended sediment transport is depended upon the vertical concentration and velocity profiles. To resolve the vertical concentration profile, the eddy viscosity distribution must be resolved since it is assumed the turbulent motions keep the sediment in suspension. The piecewise eddy viscosity model of Roelvink and Reniers (1994) was used to resolve the turbulent profile. This model, which uses parabolic shape factors to describe the vertical distribution of the turbulent eddy viscosity, is optional for surf zone applications. It specifically accounts for changes in the eddy viscosity due to wave breaking and currents. This is important as mixing is increased in regions where turbulence is produced (e.g. the outer surf zone). This consequently affects the sediment transport in the area. For a complete presentation of the model, one is referred to Reniers, Thornton et al. (2004).

Using this eddy viscosity model is possible to derive the concentration profiles. Some authors [Van Rijn (1984) & Bosboom and Stive (2010)] have noted however that the turbulent mixing of water and of sediment are in fact two different processes, which individually need to be accounted for. Usually, to account for these differences, a sediment mixing coefficient is used.

$$\frac{\varepsilon_s(z)}{v_t(z)} = \beta(z) \qquad 4.11$$

where:

ε_s	Sediment diffusivity	m^2/s
v_t	Eddy viscosity	m^2/s
β	Sediment mixing coefficient	-

Fredsøe and Deigaard (1992) have shown using theoretical sediment convection analysis that a sediment mixing value can be greater than unity. However, using a mixing length approximation, they also show that the momentum exchange between the fluid and sediment could result in a value less than unity. With these differences, a constant value of one was selected for analysis.

With the eddy viscosity in terms of the sediment diffusivity, the vertical structure of the concentration profile can be resolved.

$$\frac{c\ (z)}{c_a} = \int_a^0 \exp\left[\frac{w_s}{\varepsilon_s(z)}\right] dz \quad for \quad z > a \qquad 4.12a$$

$$\frac{c\ (z)}{c_a} = 1 \quad for \quad z \leq a \qquad 4.12b$$

For this first order analysis, it is assume that concentrations within the boundary layer are constant. Consequently, this model shows that suspended sediment concentrations are only dependent upon the reference concentration, the sediment fall velocity and sediment diffusivity.

Concentration profiles for both smooth and rippled beds were taken at 0.1 unit intervals starting at x / H_{m0} = -35 and ending at x / H_{m0} = 0. A selection of profiles are presented below.

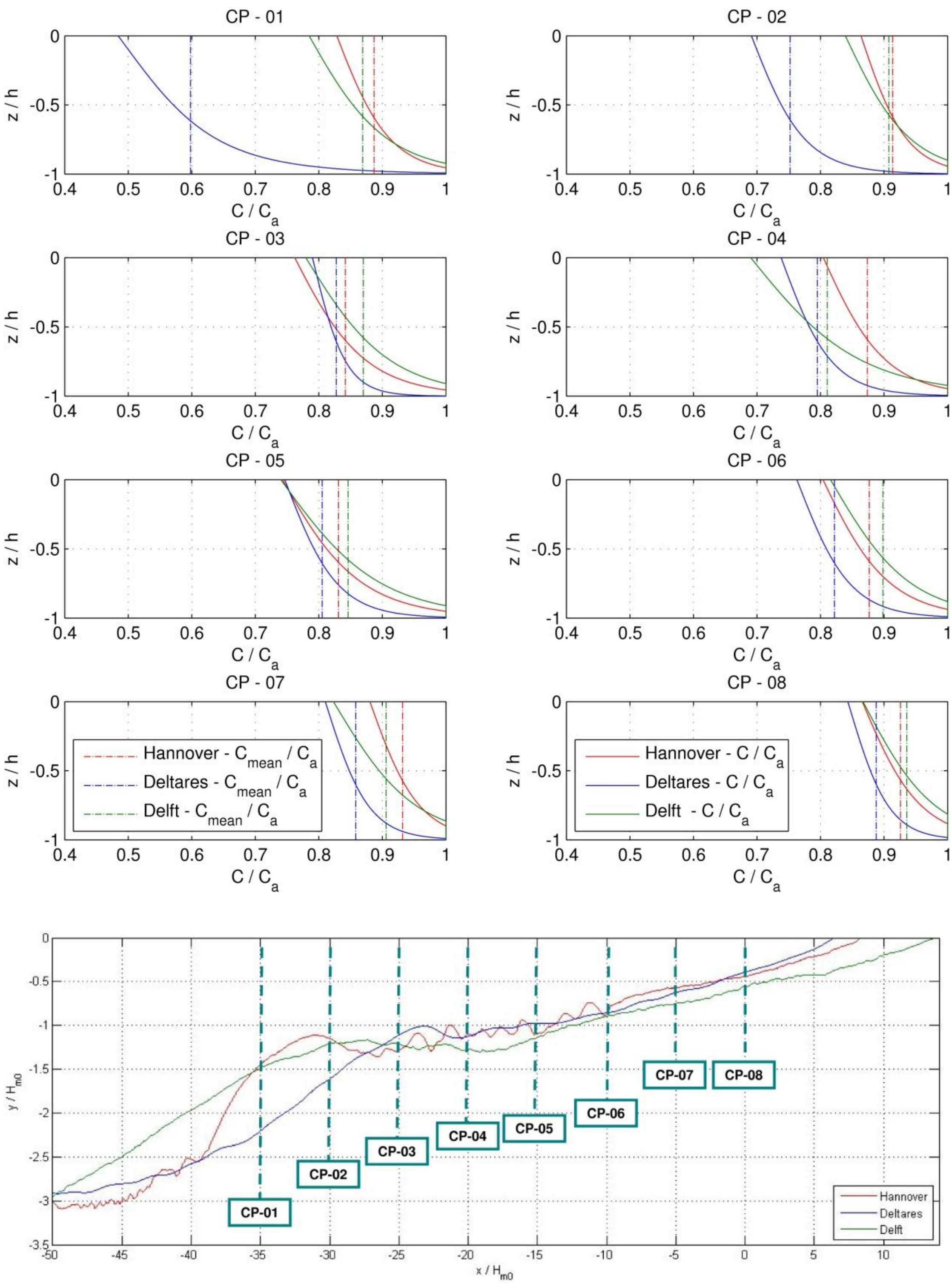

Figure 4.15 *Concentration profiles across the surf zone.*

Combining the mean concentrations resolved during the bed profile analysis and the concentration profiles resolved from the eddy viscosity model, the two quantities were used to determine the reference concentration. Concentrations here are of interest since the reference level represents the upper boundary of the bed load layer. Resolving the level and concentration relates how much material was mobilized to how much was brought into suspension.

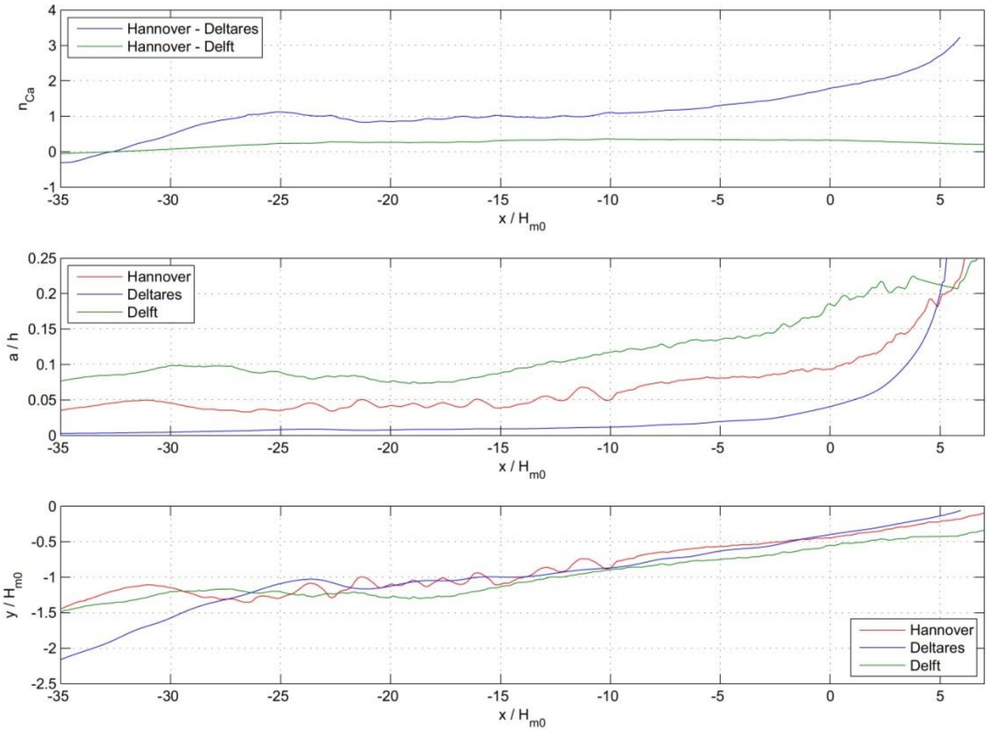

Figure 4.16 *Reference level and concentrations across the inner surf zone. The influence of the ripples at Deltares are reflected in the characteristic reference level curve. At TU Delft, both the reference level and concentration show increased mobility.*

Results of the profile model at TU Delft show there was a larger reference level and higher concentrations at this level. This result is in direct conflict with the similarity presented by the scaling parameters. Further complicating mobile bed scaling, the results show that even with matching dynamic terms (Shields number, particle Reynolds number and relative fall velocity), near bed sediment scaling was not preserved. This would tend to indicate that there was increased influence from one of the static similarity terms or there is a process not considered by the ideal similarity set.

The increase in the reference level is a direct result of the sediment diameter scaling. With the bed roughness scaled to ensure correct shear stress and turbulent regimes, the layer thickness is not accounted for. Equation 4.8 shows that the boundary layer thickness is a function of the bed roughness and orbital excursion. With the excursion scaled according to Froude scaling, the bed roughness remains as a free variable. The result is an increased boundary layer thickness and subsequent reference level. With the increased reference level, the eddy viscosity model suggests there is enhanced boundary layer turbulence at the boundary between the two regimes. The sediment has shown to be particularly susceptible to turbulent processes specifically due to the mismatch of the relative density. This could have influence on the near bed sediment concentrations. However, the nature of the present data does not allow a definitive decision to be made.

The reference level and concentration at Deltares confirms many of the principles, which have been previously discussed. While the reference concentration is very similar to Hannover, there is a strong mismatch in the reference level. Without the combination of these two parameters, the sediment contributions were reduced resulting in delayed development.

Within a rippled bed, this reference level is defined by the characteristic ripple curve. Shown above, similar curves have been presented by Neilson. Most noticeable is the reduced thickness of the reference level compared to Hannover or TU Delft. For a rippled bed, the reference level increases with an increased mobility parameter. The transition to a smooth bed is defined by the point the rippled vortex no longer can support the ripple walls and the ripple consequently collapse in on itself. This transition is not shown in Figure 4.8 because of the presence of ripples across the extent of the profile.

The near bed concentrations also indicated the underdevelopment of a boundary layer and the vortex's inability to compensate to mobilize sediment. Most importantly is the combination of the reference concentration and level. Within a rippled regime, the near bed concentrations characteristically develop in an exponential profile (unlike the power like profile of a smooth bed). Without the developed boundary layer and shear stresses, the ripple vortex cannot mobilize proportionally similar amounts of sediment. The quantities that it does mobilize remain very close to the bed. Sediment which is mobilized and brought into suspension by the ripple vortex creates strong concentration gradients. It is this process, confirmed by the scaling parameters, which is reflected in the sediment fluxes and delayed development.

5 CONCLUSIONS & RECOMMENDATIONS

5.1 Achievements

Profiles were obtained at TU Delft (scale 1:10) following the testing regime used during the SANDS project. This set made use of density and diameter scaled sediment ($\rho_s = 1200\ kg/m^3$ and $d_{50} = 0.52\ mm$); scaled according to the bed load model of Henriquez, Reniers et al. (2008). The complete set used for analysis here includes the Hannover (prototype scale 1:1) and Deltares (Froude scale 1:6) profiles obtained during the SANDS project. Using these profiles, the present work looked to extend state of knowledge regarding the impact of sediment scaling on nearshore transport processes.

Analysis of the profiles showed a marked degree of geometrical similarity between all three facilities. More specifically, the development of a bar-trough system and subsequent offshore migration. The development of this bar-trough system was vitally important to analysis and represents the main requirement needed for further analysis.

The depth and time averaged sediment fluxes were derived from the bed level changes. While there was similar geometrical development, the morphological time scales and transport rates were divergent. Compared to Hannover, the transport rates of Deltares were underdeveloped reflecting delayed morphological development. Conversely, TU Delft saw rapid bar development and offshore migration. This is reflected in the sediment fluxes which were approximately twice as large as Hannover.

To understand how sediment scaling influence the resultant morphology, the ideal scaling sets of Kamphuis (1991) and Dalrymple (1989) were presented. Using these as a basis, the cross shore distribution of the Shields number, particle Reynolds number and relative fall velocity showed good agreement at TU Delft. Similarity between these nondimensional parameters suggested that both sediment mobility and near bed suspension were similar with prototype. However, due to a large fall velocity, a mismatch in the Dean number suggested sediment suspension was underestimated. The use of Froude scaling at Deltares suggested that neither near bed nor suspended load transport regimes were reproduced correctly. Most significantly was the drop in the Shields number. This resulted in a comparative transition of the bed through the surf zone from smooth in prototype to rippled at 1:6 model scale. An erosive process which was largely bed load dominated in prototype, the rippled state of the bed inhibits the development of this bed load dominance.

A simple depth and time averaged model was also used to decompose the average sediment concentrations near the bed. These concentrations were used to check the consistency of the nondimensional parameter agreement with the manifestation of the physical process.

Inconsistent with the nondimensional results, TU Delft showed that near bed sediment mobility and suspension was overdeveloped. This is in direct conflict with the previous conclusions founded in the similarity between the dynamic scaling parameters. This would tend to indicate increased influence from the static parameters or that there are significant processes not accounted for in the scaling sets. The rippled bed at Deltares shows decreased sediment mobility and suspension. This was confirmed with the scaling parameters by the reduction in the Shields number and increased critical Shields value.

Finally, the depth averaged concentrations revealed significant cross shore variance in the resultant concentration quantities. This variation was dependent upon the sediment scaling method used. There was also distinct variation across the surf zone with each reflecting the compartmentalized nature of the cross shore. The combination suggests that a region based approach should be used for sediment scaling considering both the transport regime and dominant sediment transport direction. It is believed this would better capture the desired transport processes.

5.2 Recommendations

In regards to the conclusions drawn in the present work, further experimentation is needed to understand the near bed fluid-sediment interaction. Most important is the effect of sediment scaling on mobility and near bed suspension. The agreement between the Shields number, particle Reynolds number and relative fall velocity suggest theoretically that bed load processes should be preserved. However, the manifestation of the physical processes revealed a large increase in sediment mobility. It was suggested that this was due to both an increased boundary layer thickness and significant influence from the relative density mismatch. With only a broad level understanding, further investigation is needed to provide in depth knowledge related to this small scale process in order to better understand this contradiction.

Since it is not physically possible to scale every process across the nearshore, scale effects will continue. At present, this is an unavoidable consequence of physical model scaling. With their constant influence, a quantification of their influence on true processes is not well understood. The diversity and quantity of parameter mismatches/scale effects across the spatial domain are simply too great to provide a clear understanding of the processes. As transport processes transition from zone to zone, the results here show sediment will respond differently. Therefore, once the sediment no longer corresponds with unity, it will introduce some level of distorting within the macro scale processes.

This highlights one of the main difficulties with projects which attempt to use large scale means to understand small scale processes. Due to the diversity of scale effects, tying to understand smaller scale processes based on purely the macro scale processes will continue to muddle results and our comprehension of scaling knowledge. Therefore, the current objective of small scale sediment modeling (in regards to scaling) should not attempt to recreate the complete macro scale processes. Rather, the key to dealing with these problems is finding a way to minimize sources of error using a more focused approach.

The complexity of the surf zone and the impact on the sediment scaling suggests that experiments should take a more compartmentalized approach focusing on scaling zone by zone. With the inclusion of the density and diameter term, results have shown that scaling methods allow for the preservation of scaling parameters within individual transport zones. By compartmentalizing and focusing on individual transport zones (e.g. the inner surf zone) while maintaining localized similarity, we can better represent localized processes within. This will reduce the variety and quantity of scale effects and refine the complexity of the processes, increasing the quality of results.

A wave flume and mobile bed present unique advantages and opportunities to exploit these abilities. The combination of the two allows coexistent suspension and advection processes to contribute to sediment transport. Influences such as return flow advection, boundary layer turbulence and wave breaking are all included simultaneously. These are affects which must be decoupled and/or simplified in other small scale facilities such as an oscillatory wave tunnel. This makes it difficult to understand the localized interactions especially in regards to scale effects which are quite important to sediment transport modeling. With localized scaling, we can reduce the variety and quantity of scale effects. This simplified approach will ease our ability understand how scale effects manifest and influence the transport processes without losing the primary process. With a better zone by zone understanding we can eventually understand the totality of the macro scale process. This will lead to an eventual ability for complete interpretation at prototype scale which is the ultimate goal.

To extend the current state of scaling knowledge, more data sets are needed which include especially density term scaling in nearshore morphodynamic processes. The nature of the present work took a general approach, which was able to show cross shore process compartmentalization. However, this general nature limits the ability to progress deeper into the process interactions. A number of experiments have been carried out with lightweight sediment that attempt to understand individual processes (i.e. ripple development in an oscillating water tunnel). However due to both the compartmentalized and holistic nature of the nearshore, processes interactions are significant. Varying density and diameter terms and focusing on the localized transport processes should continue to reveal how parameter mismatches physically manifest and what scale effects are significant. Investigating localized processes and scaling while allowing for interactions should eventually lead to more comprehensive scaling knowledge and fruitful research endeavors.

6 REFERENCES

Battjes, J. A. (1974). "Surf similarity." *Proceedings of the 14th International Conference on Coastal Engineering*, Copenhagen, American Society of Civil Engineers.

Battjes, J. A. (1975). "Modeling of turbulence in the surf zone." *Proceedings of the Symposium on Modeling Techniques*, San Francisco, American Society of Civil Engineers.

Battjes, J. A. and J. P. F. M. Janssen (1978). "Energy loss and set-up due to breaking of random waves." *Proceedings of the 16th International Conference on Coastal Engineering*, Hamburg, American Society of Civil Engineers.

Boers, M. (2005). Surf Zone Turbulence. Department of Civil and Geotechnical Engineering. Delft, Technical University of Delft. PhD**:** 180.

Bosboom, J. and M. J. F. Stive (2010). Coastal Dynamics I. Delft, VSSD.

Cáceres, I., J. Grüne, et al. (2008). "Mobile bed tests. The SANDS project." *Proceedings of the 31nd International Conference on Coastal Engineering*, Hamburg.

Church, C. C. and E. B. Thornton (1993). "Effects of wave-breaking induced turbulence within a longshore current model." Coastal Engineering(20): 1-28.

Dalrymple, R. A. (1989). Physical modelling of littoral processes. Recent Advances in Hydraulic Physcial Modelling. R. Martins. Dordrecht, Kluwer Academic Publishers**:** 567-588.

Dean, R. G. (1973). "Heuristic models of sand transport in the surf zone." Conference of Engineering Dynamics in the Coastal Zone.

Deigaard, R., J. Fredsøe, et al. (1999). "Net sediment transport under wave groups and bound long waves." Journal of Geophysical Research 104(C6): 13,559-513,575.

Dingler, J. R. (1974). Wave Formed Ripples in Nearshore Sands. San Diego, University of California at San Diego. Ph.D.

Flores, N. Z. and J. F. A. Sleath (1998). "Mobile layer in oscillatory sheet flow." Journal of Geophysical Research 103(C6): 12783-12793.

Fredsøe, J. and R. Deigaard (1992). Mechanics of Coastal Sediment Transport. Singapore, World Scientific.

Grasso, F., H. Michallet, et al. (2009). "Physical modeling of intermediate cross-shore beach morphology: Transients and equilibrium states." Journal of Geophysical Research C: Oceans 114(9).

Grüne, J., I. Cáceres, et al. (2009). Data (plus megadata) set from flume- instrumentation erosion/accretion tests. Integrated Infrastructure Initiative HYDRALAB III. Hannover - Barcelona - Delft, Coastal Research Center FKZ - Universitat Politècnica de Catalunya - Deltares**:** 1-60.

Hallermeier, R. J. (1981). "Terminal settling velocity of commonly occurring sand grains." Sedimentology 28(6): 859-865.

Henderson, S. M., J. S. Allen, et al. (2004). "Nearshore sandbar miggration predicted by an eddy-diffusive boundary layer." Journal of Geophysical Research 109.

Henriquez, M., A. J. H. M. Reniers, et al. (2008). "On the scaling of sediment transport in the nearshore." *COASTLAB 2008*, Tech. Univ. of Bari, Bari, Italy.

Hughes, S. A. (1993). Sediment transport models. Physical Models and Laboratory Techniques in Coastal Engineering. P. L. F. Liu. Singapore, World Scientific. 7.

Hughes, S. A. and J. E. Fowler (1990). "Validation of movable-bed modeling guidance." *Proceedings of the 22nd International Conference of Coastal Engineering*, Delft, The Netherlands, American Society of Civil Engineers.

Hoyng, C. (2008). Erosive and Accretive Coastal Profile Response. Department of Hydraulic Engineering. Delft, Technical University of Delft. Master of Science in Engineering.

Iribarren, C. R. and C. Nogales (1949). "Protection des Ports, Section II." *XVIIth International Navigation Congress*, Lisbon, Portugal.

Ito, M. and Y. Tsuchiya (1986). "Time scale for modeling beach change." *Proceedings of the 20th International Conference on Coastal Engineering* 2: 1196-1200.

Jonsson, I. G. (1966). "Wave boundary layers and friction factors." *Proceedings of the 10th International Conference on Coastal Engineering*, Tokyo, Japan, American Society of Civil Engineers.

Kamphuis, J. W. (1972). "Scale selection for mobile bed wave models." *Proceedings of the 13th International Conference on Coastal Engineering*, Vancouver, Canada.

Kamphuis, J. W. (1975). "Coastal mobile bed model - does it work." *Proceedings of the 2nd Symposium on modeling techniques*.

Kamphuis, J. W. (1985). On understanding scale effects in coastal mobile beds. Physical Modeling in Coastal Engineering. A. A. Balkema. Rotterdam**:** 141-162.

Kamphuis, J. W. (1991). Phyisical Modeling. Handbook of Coastal and Ocean Engineering. H. B. Herbich. Houston, Gulf Publishing Company. 2.

Klopman, G. (1994). Verticle structure of the flow due to waves and currents, WL-Delft Hydraulics. Part II.

Kirby, J. T., H. T. Ozkan-Haller, et al. (2006). “Seiching in a large wave flume.” *Proceedings of the 30th International Conference on Coastal Engineering*. J. McKee Smith. San Diego, American Society of Civil Engineers**:** 1159-1171.

Longuet-Higgins, M. S. (1953). "Mass Transport in Water Waves." Philosophical Transactions of the Royal Society of London. Series A, Mathematical and Physical Sciences 245(903): 535-581.

Longuet-Higgins, M. S. and R. W. Stewart (1964). "Radiation stresses in water waves: a physical discussion, with applications." Deep Sea Research 11: 529-562.

Mogridge, G. R. (1974). "Scale laws for bed forms in laboratory wave models." *Proceedings of the 14th International Conference on Coastal Engineering.* American Society of Civil Engineers.

Nielsen, P. (1981). "Dynamics and Geometry of Wave-Generated Ripples." Journal of Geophysical Research. 86(C7): 6467-6472.

Noda, E. K. (1972). "Equlibirum beach profile scale-model relationship." Journal of Waterways, Harbors and Coastal Division WW4: 551-528.

Reniers, A. J. H. M., E. B. Thornton, et al. (2004). "Verticle flow structure during Sandy Duck: obervations and modeling." Coastal Engineering(51): 237-260.

Ribberink, J., J. J. van der Werf, et al. (2008). "Sand motion induced by oscillatory flows: Sheet flow and ripple vortex." Journal of Turbulence 9(20): 1 - 32.

Roelvink, J. A. and A. Reniers (1994). "Upgrading of a quasi-3D hydrodynamic model." *MAST G8-M overall workshop*, Gregynog.

Simons, D. B. and F. Sentürk (1992). Sediment Transport Technology, Water Resources Publications.

Stive, M. J. F. and J. A. Battjes (1984). "A model for offshore sediment transport." *Proceedings of the 19th International Conference on Coastal Engineering*, Houston, American Society of Civil Engineers.

Sutherland, J. and R. Soulsby (2010). Guidlines for Physical Modeling of Sediment Dynamics, HR Wallingford.

Swart, D. H. (1974). "A schematization of onshore-ofshore transport." *Proceedings of the 14th International Conference on Coastal Engineering*, Copenhagen, Denmark, Coastal Engineering Research Council.

Thornton, E. B., R. T. Humiston, et al. (1996). "Bar/trough generation on a natural beach." Journal of Geophysical Research 101(C5): 12,097-012,110.

Ting, F. C. K. and J. T. Kirby (1994). "Observation of undertow and turbulence in a laboratory surf zone." Coastal Engineering 24(1-2): 51-80.

Van Rijn, L. C. (1984). "Sediment transport, part II: Suspended load transport." Journal of Hydraulic Engineering 110(11): 1613-1643.

Van Rijn, L. C. (1993). Principles of Sediment Transport in Rivers, Estuaries and Coastal Seas. Utrecht, Aqua Publications.

Van Rijn, L. C. (2007). "Unified view of sediment transport by currents and waves I. Intiation of motion, bed roughness and bed load transport." Journal of Hydraulic Engineering 133(6): 649-667.

Van Rijn, L. C., P. K. Tonnon, et al. (2010). "Scale laws for beach and dune erosion processes." Coastal Engineering.

Vellinga, P. (1986). Beach and Sune Erosion During Storm Surges. Delft, Delft University of Technology. Doctoral Thesis**:** 200.

Von Dongeren, A., J. A. Battjes, et al. (2007). "Shoaling and shoreline dissipation of low-frequency waves." Journal of Geophysical Research 112.

Wright, L. D. and A. Short (1984). "Morphodynamic variability of surf zones and beaches: a synthesis." Marine Geology(56): 93-118.

Yalin, S. and R. C. H. Russell (1962). "Similarity in sediment transport due to waves." *Proceedings of the 8th Coastal Engineering Conferences*, London, American Society of Civil Engineers.

Zelt, J. A. and J. E. Skjelbreia (1992). "Estimating incident and reflected wave fields using an arbitrary number of wave gauges. *Proceedings of the 32nd International Conference of Coastal Engineering*." B. L. Edge, American Society of Civil Engineering**:** 777-789.

APPENDIX A: HANNOVER AND TU DELFT SPECTRUMS

Input to the wavemaker is given in the form of a numerical time series. A FFT analysis of that series results in the following spectrum.

Numerical Spectrum

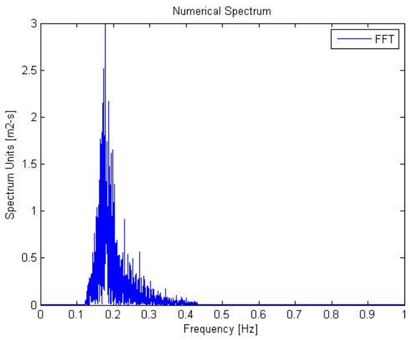

(a) *Prototype numerical spectrum*

Eight surface elevation time series are presented below. These were chosen to show the representative changes during both testing campaigns. Since not all time series were taken at Hannover, the selection was limited to only those found in both Hannover and TU Delft.

For each series, analysis is also done at a number of wave gauges over the length of the flume. Similarly, analysis in only presented for gauges that approximately concede in UHANN and TU Delft. A table of the four gauges and locations in respective facility flumes can be found below.

Table A.1 *Position of wave gauges in Hannover and TU Delft flumes. All distances are relative to the center position of the wavemaker.*

	Hannover	TU Delft	
Wave gauge	Prototype [m]	Actual [m]	Prototype [m]
01	90.25	9.00	90.0
03	97.30	9.70	97.0
04	180.00	18.00	180.0
05	200.00	26.50	260.5

For a complete analysis of results, see Section 4.1

Series 001

Hannover TU Delft

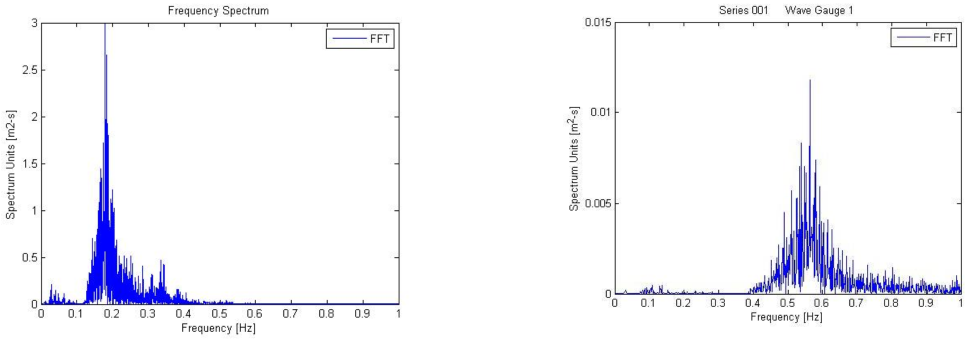

(a) Wave gauge 01

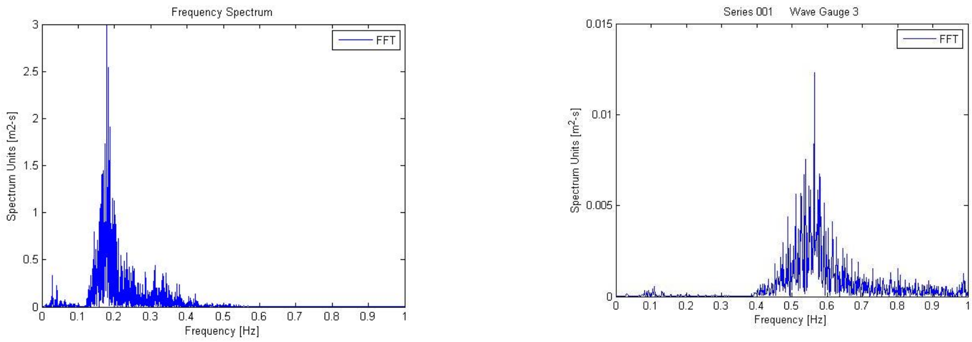

(b) Wave gauge 03

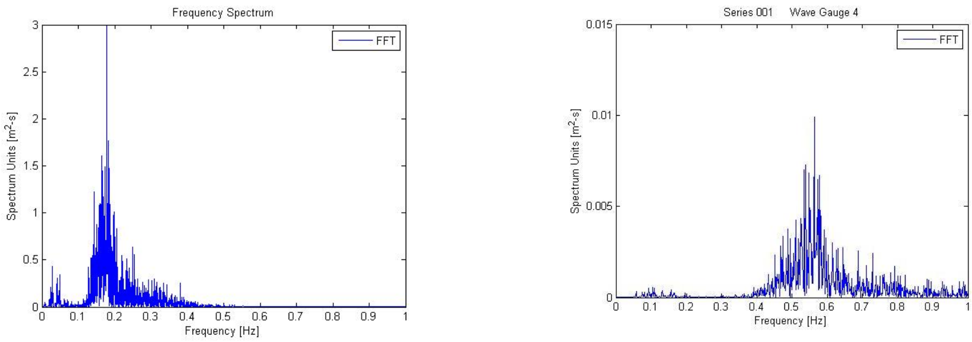

(c) Wave gauge 04

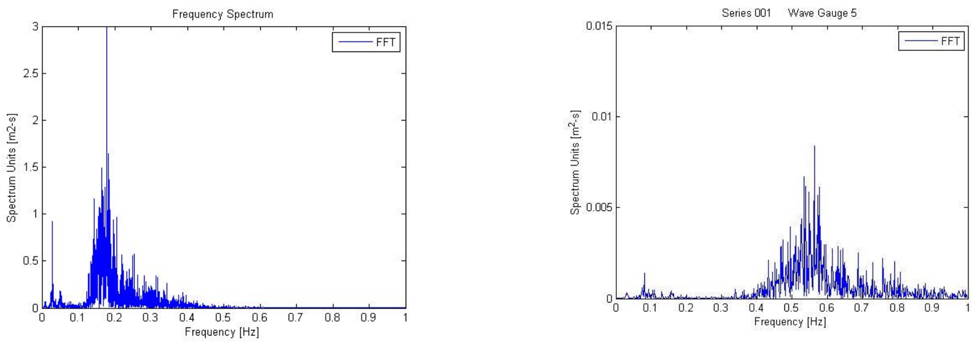

(d) Wave gauge 05

Series 005

Hannover TU Delft

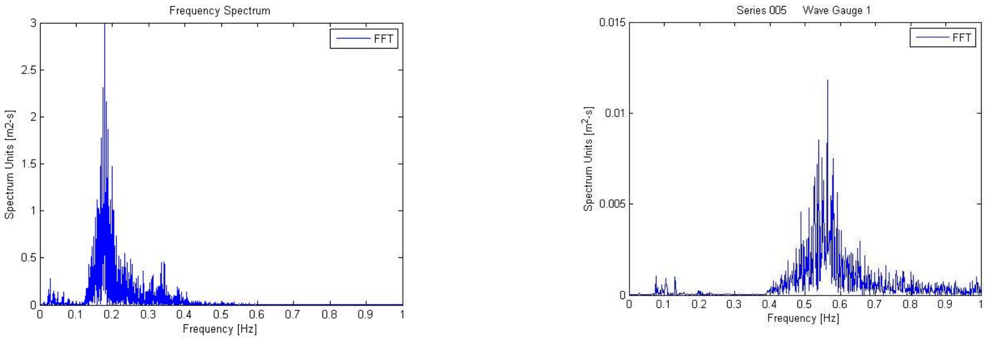

(a) Wave gauge 01

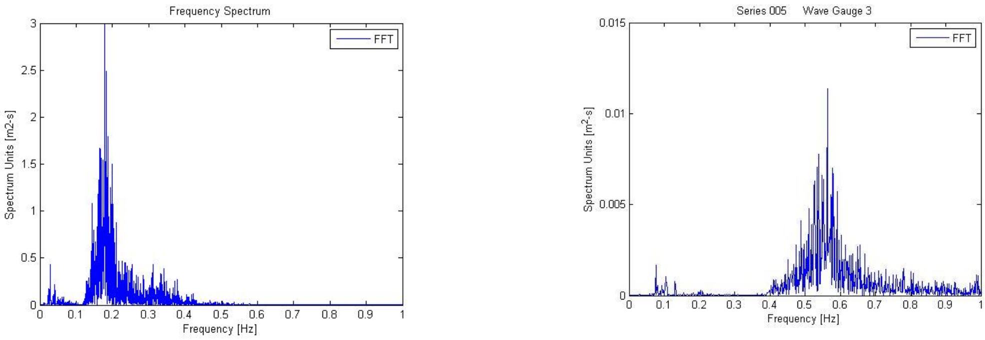

(b) Wave gauge 03

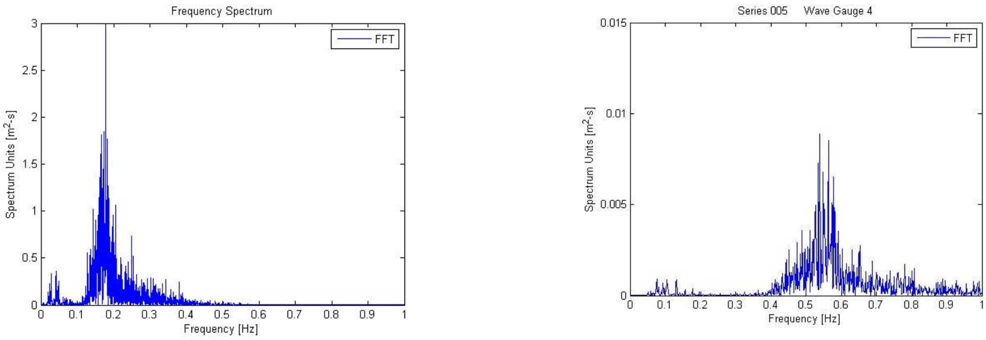

(c) Wave gauge 04

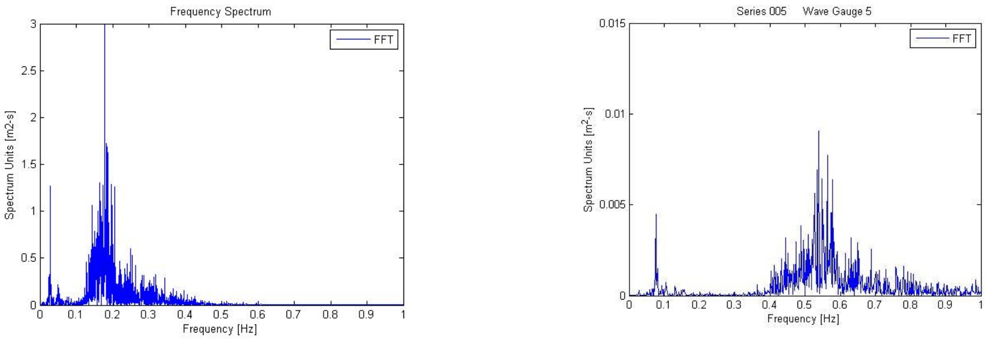

(d) Wave gauge 05

Series 009

Hannover TU Delft

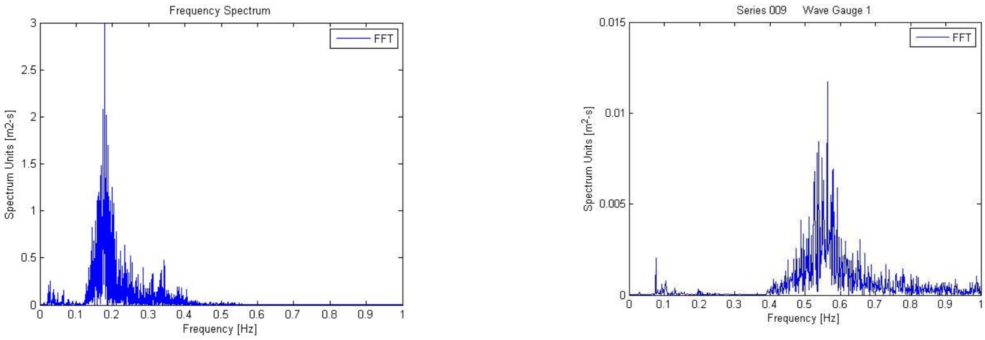

(a) Wave gauge 01

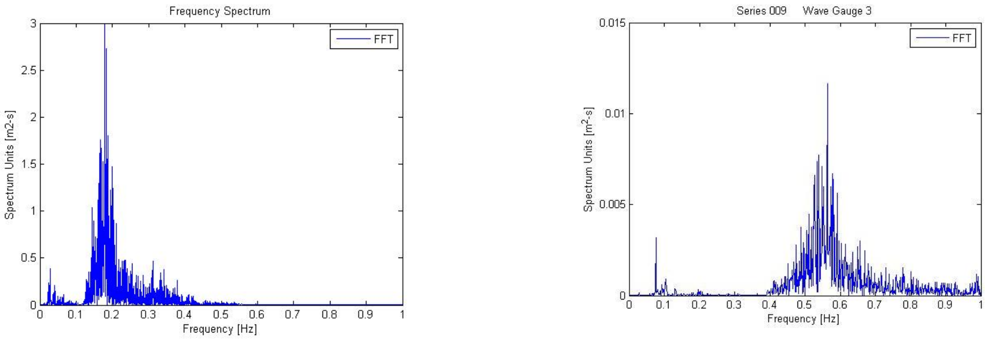

(b) Wave gauge 03

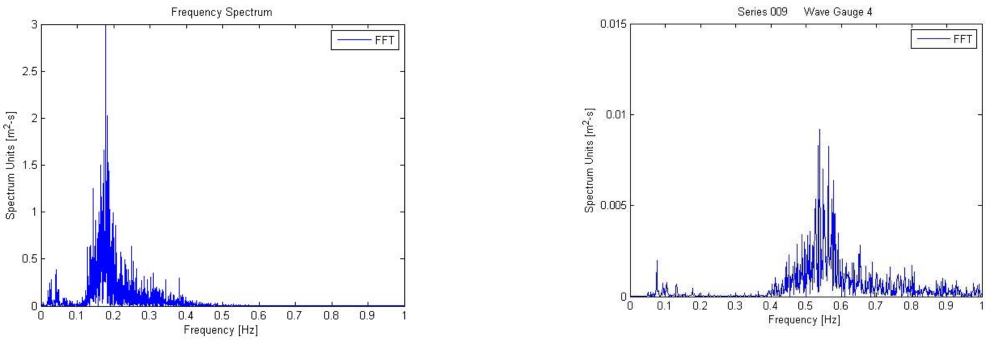

(c) Wave gauge 04

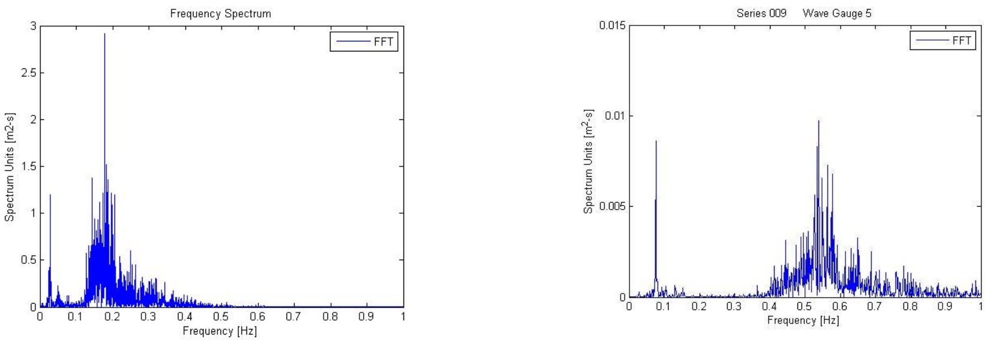

(d) Wave gauge 05

Series 017

Hannover TU Delft

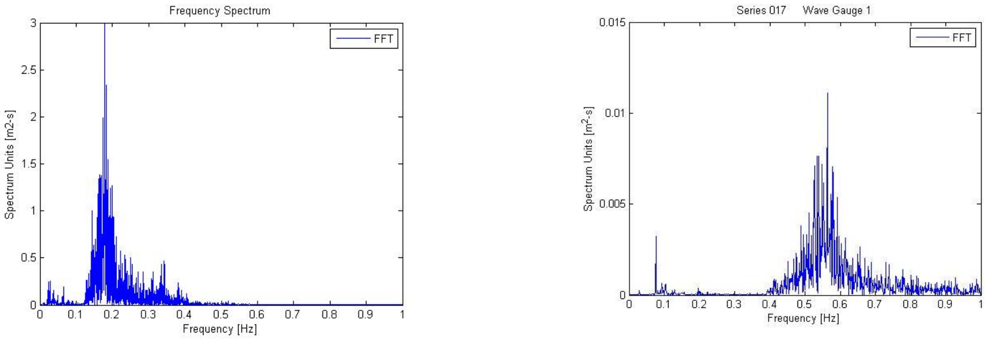

(a) Wave gauge 01

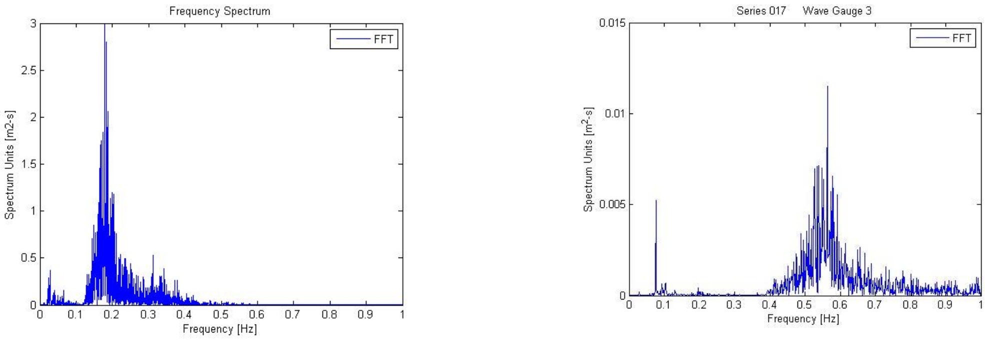

(b) Wave gauge 03

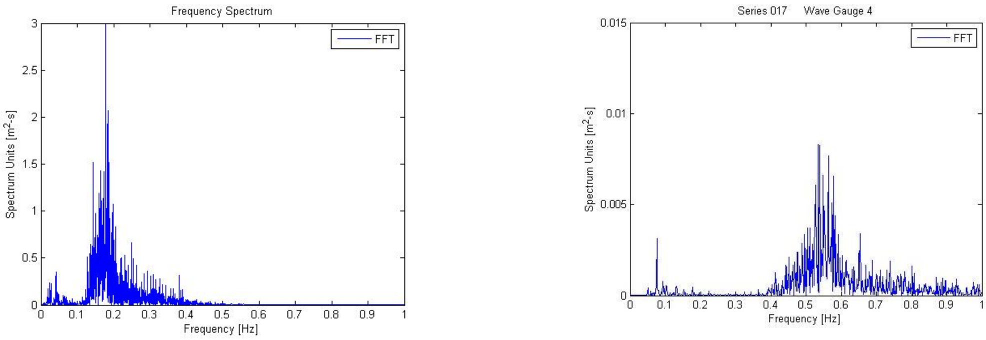

(c) Wave gauge 04

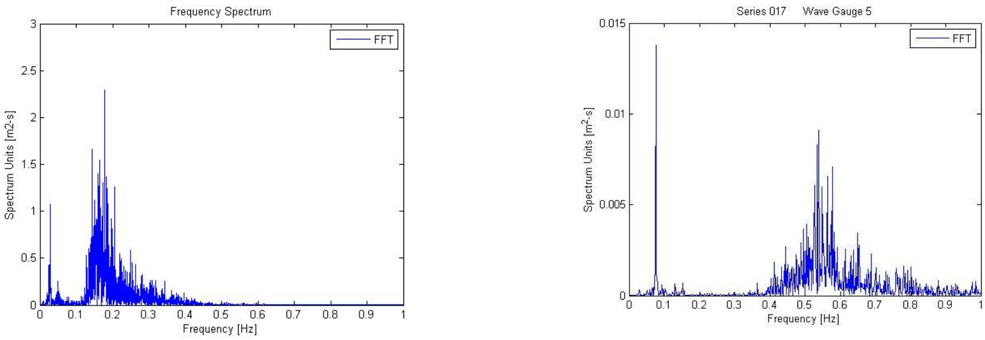

(d) Wave gauge 05

Series 021

Hannover TU Delft

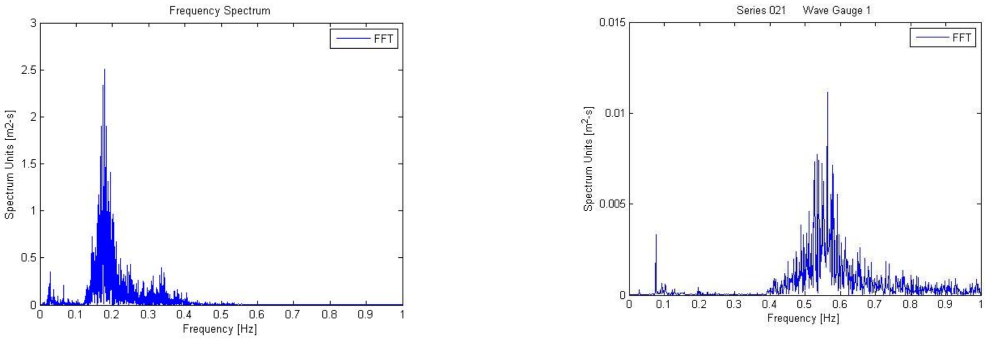

(a) Wave gauge 01

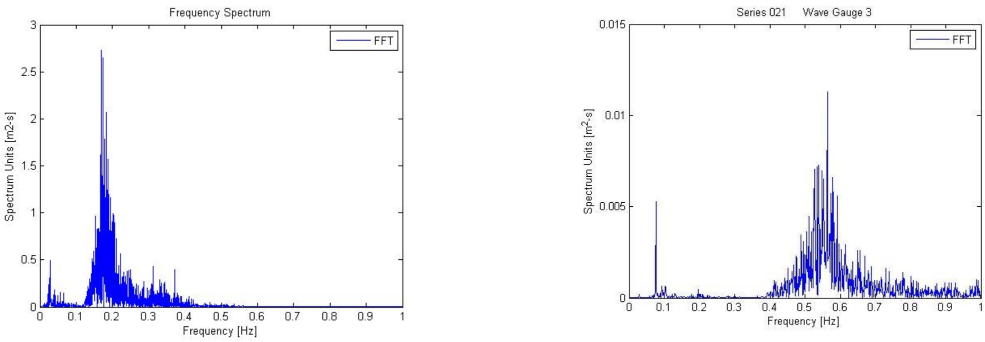

(b) Wave gauge 03

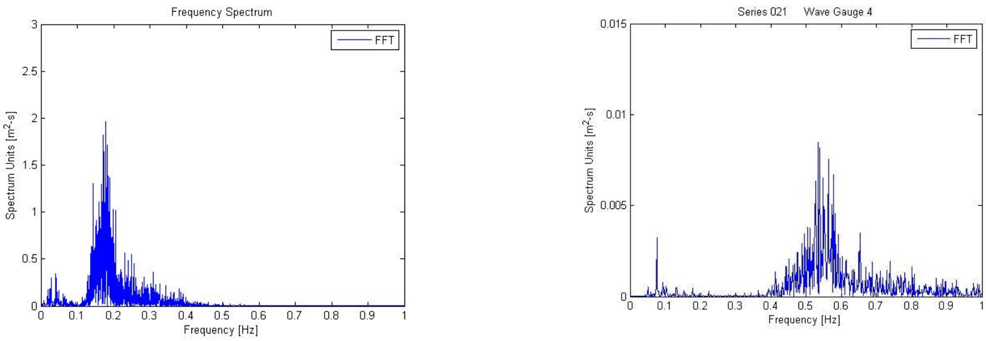

(c) Wave gauge 04

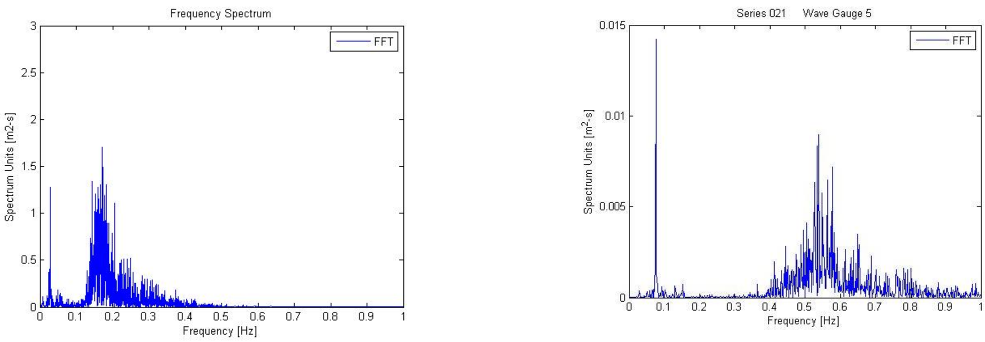

(d) Wave gauge 05

Series 028

Hannover TU Delft

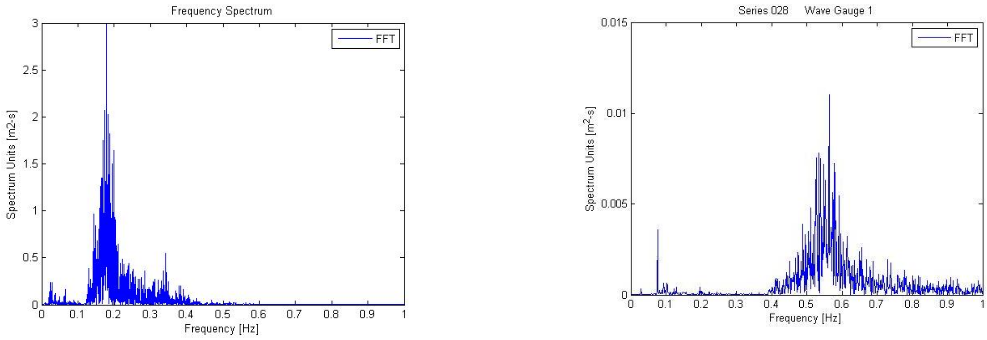

(a) Wave gauge 01

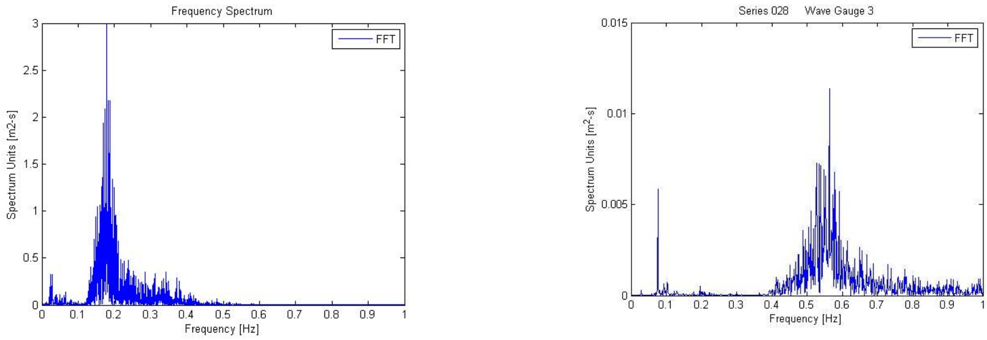

(b) Wave gauge 03

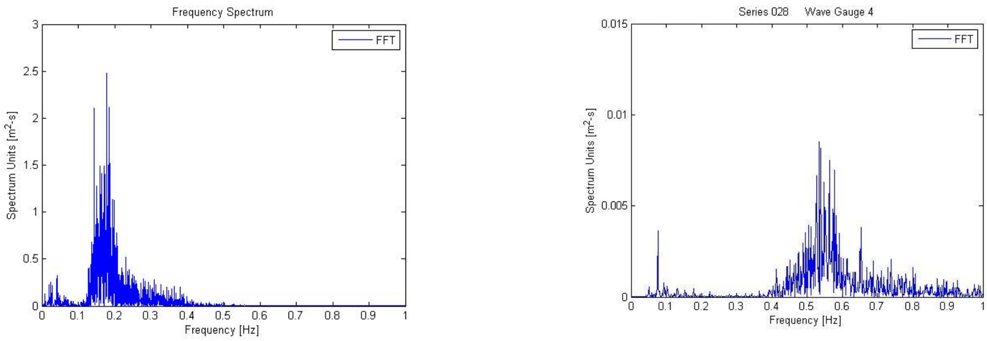

(c) Wave gauge 04

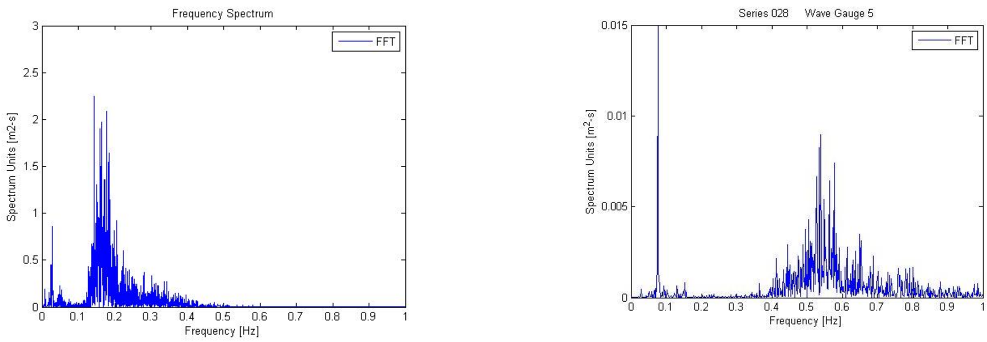

(d) Wave gauge 05

Series 035

Hannover | TU Delft

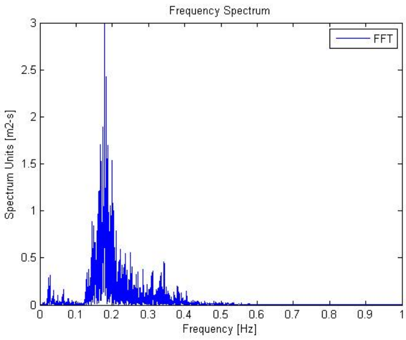

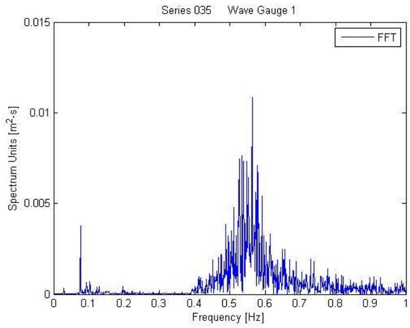

(a) Wave gauge 01

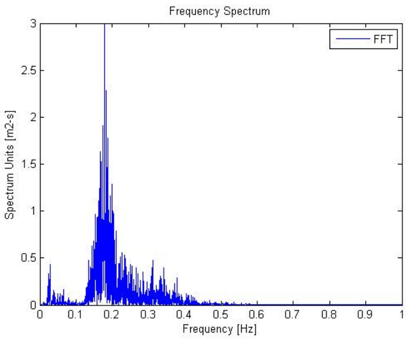

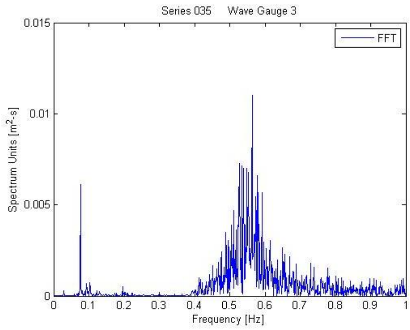

(b) Wave gauge 03

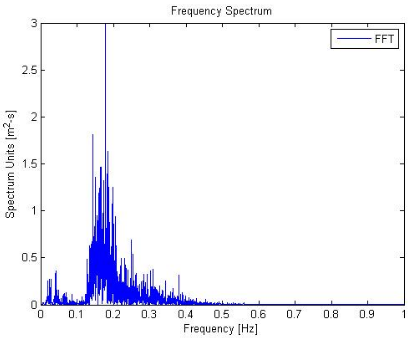

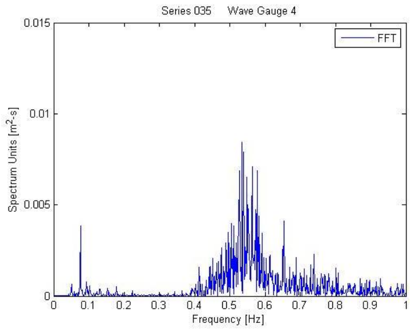

(c) Wave gauge 04

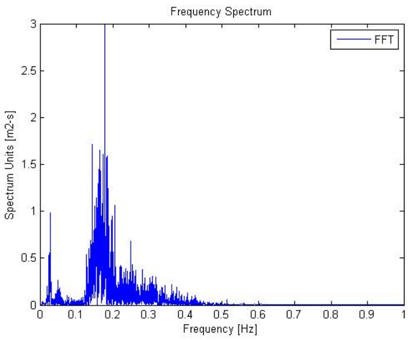

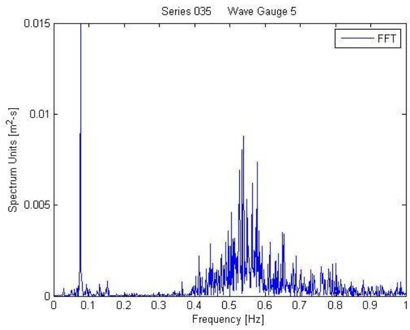

(d) Wave gauge 05

Series 043

Hannover TU Delft

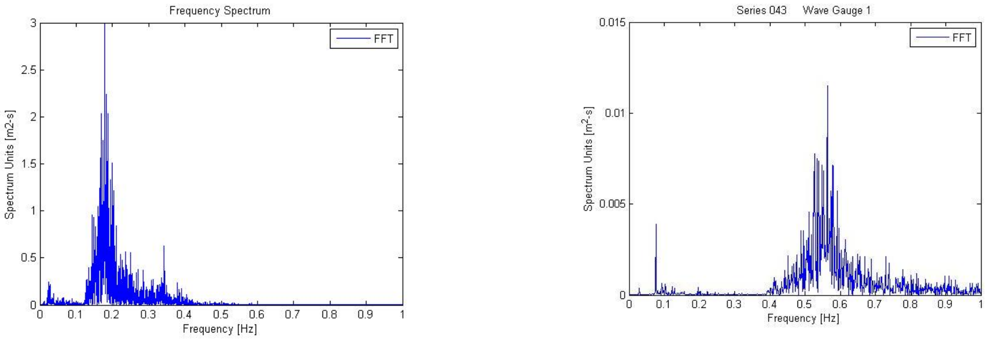

(a) Wave gauge 01

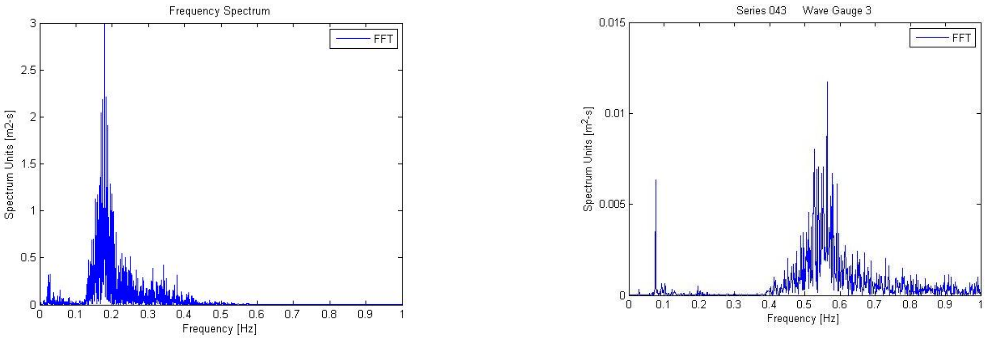

(b) Wave gauge 03

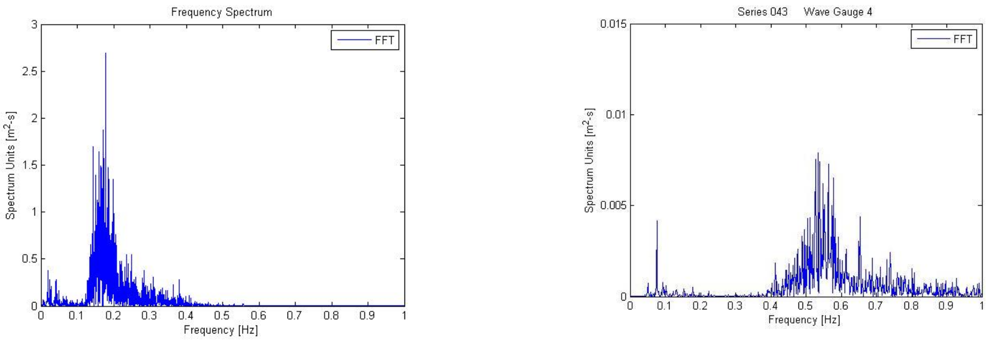

(c) Wave gauge 04

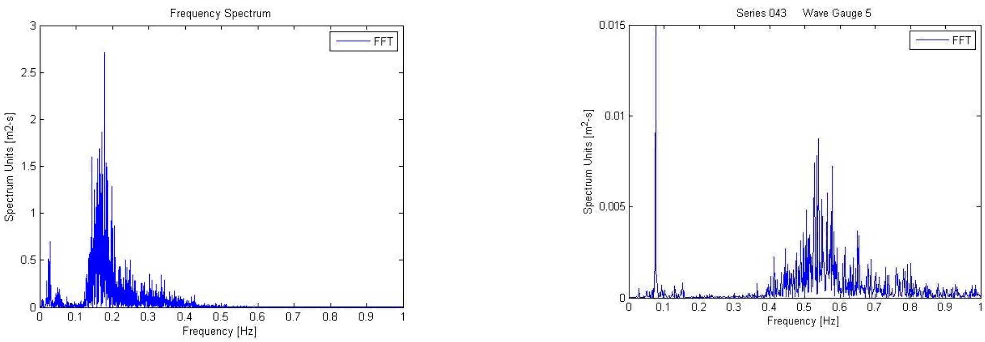

(d) Wave gauge 05

APPENDIX B: CROSS SECTIONS, SEDIMENT TRANSPORT AND GRADIENTS

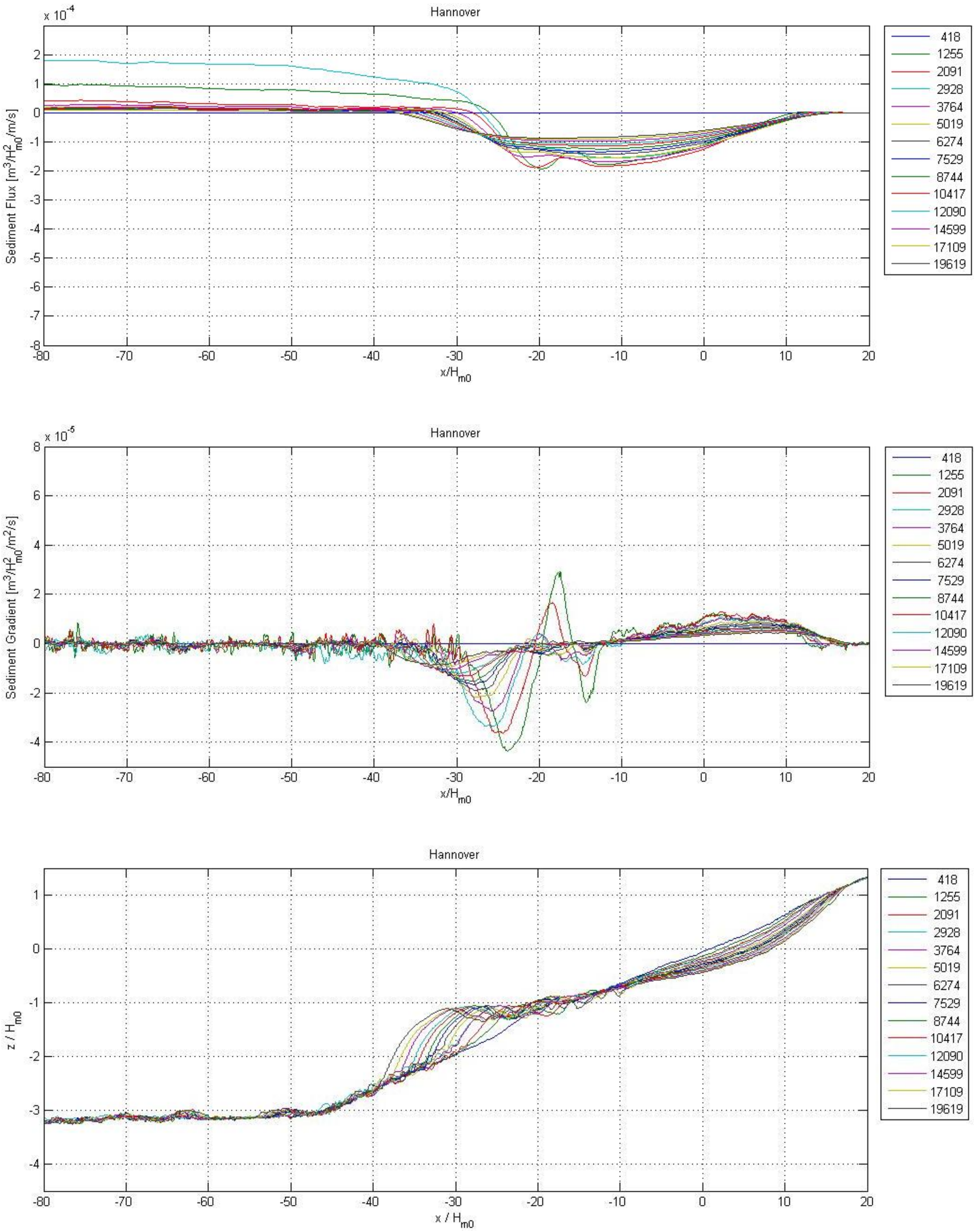

Figure B.1 *Hannover profile data*

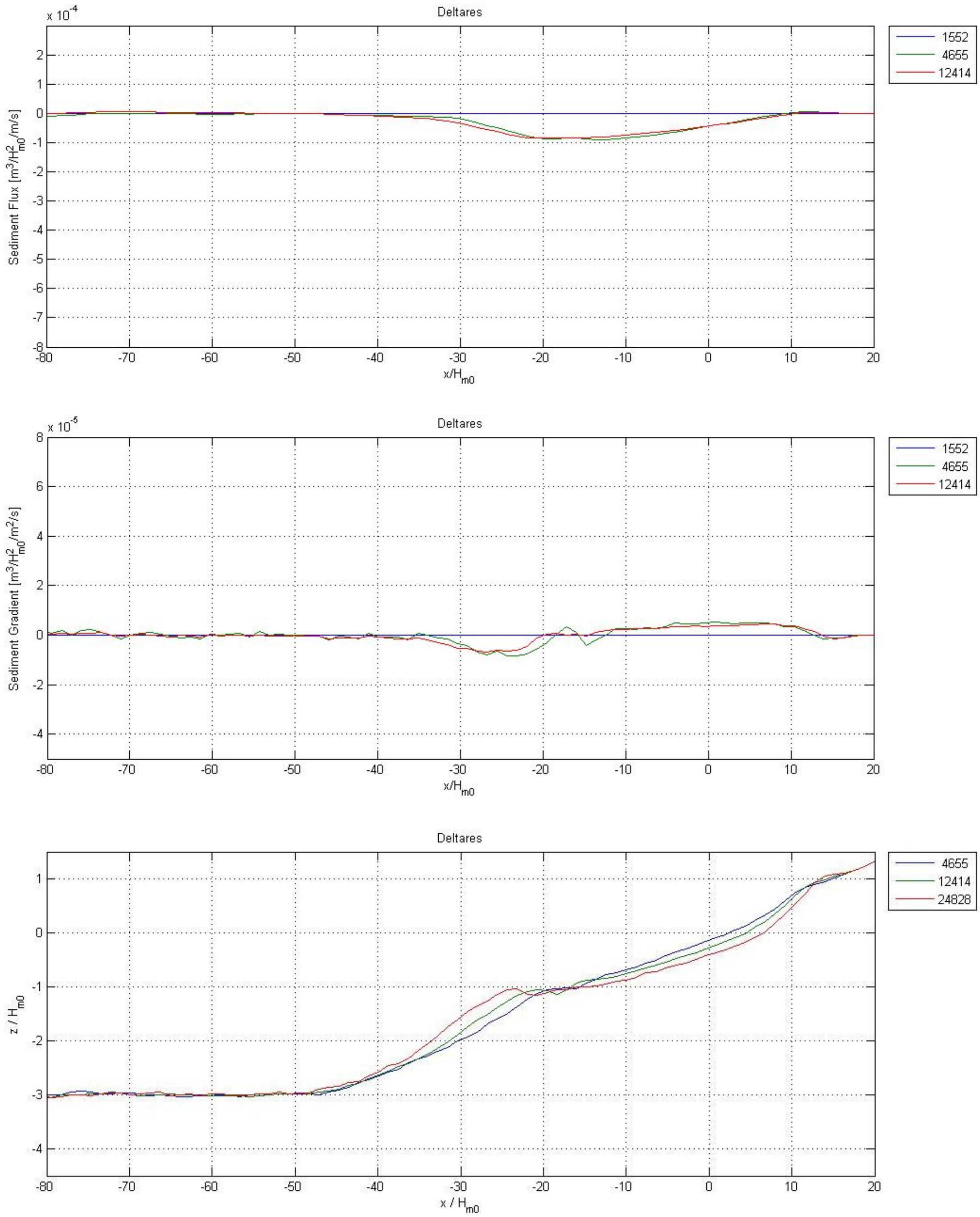

Figure B.2 *Deltares profile data*

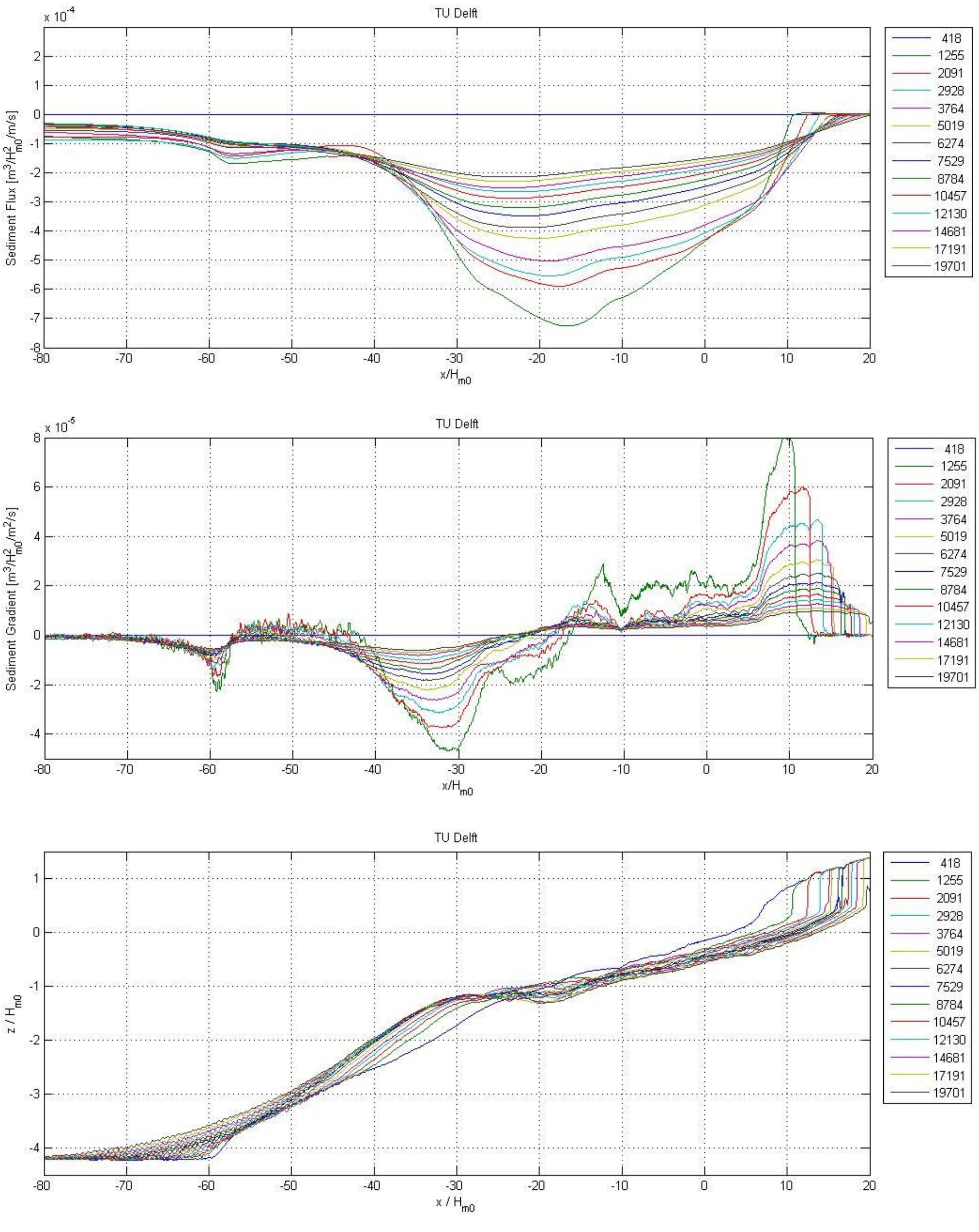

Figure B.3 *TU Delft profile data*

APPENDIX C: LIST OF SYMBOLS

Symbol	Unit	Meaning
LATIN BASED CHARACTERS		
A	m	: Orbital excursion
A_e	m^2	: Dune erosion area
C	m^3/m^3	: Sediment concentration
$\bar{C}$	m^3/m^3	: Mean sediment concentration
$\bar{C}$	J/m^2-s	: Time average dissipation power
d_{50}	m	: Mean sediment diameter
Fr	-	: Froude number
F	m^3/s	: Sediment flux
f_w	-	: Wave friction factor
f_δ	-	: Wave irregularity factor
G	m^3/s-m	: Sediment gradient
g	m/s^2	: Gravitational acceleration
H	m	: Wave height
H_o	m	: Wave height in deep water
H_{rms}	m	: Root mean square wave height
h	m	: Water depth
k	rad/m	: Wave number
k_s	m	: Effective bed roughness
l	m	: Characteristic length
L	m	: Wavelength
L_o	m	: Wavelength in deep water
n	-	: Prototype to model scale ratio
P	J/m-s	: Time average energy flux
p_m	-	: Parameter value in laboratory model
p_p	-	: Parameter value in prototype
Q	-	: Broken wave percentage
Re	-	: Reynolds number
Re_p	-	: Particle Reynolds number
SL	-	: Bed slope
S	-	: Sleath parameter
s	-	: Relative density
T	s	: Wave period
T_m	-	: Morphological time scale
U	m/s	: Characteristic velocity
U_0	m/s	: Mean flow velocity
U_r	m/s	: Return flow velocity
u	m/s	: Orbital velocity
$\hat{u}$	m/s	: Peak orbital velocity
u_*	m/s	: Bed shear velocity

V	-	: Relative fall velocity
w_s	m/s	: Sediment fall velocity

<u>GREEK BASED CHARACTERS</u>

β	-	: Beach slope outside of surf zone
μ	kg/m-s	: Dynamic viscosity of fluid
θ	-	: Shields number
θ_F	-	: Densmetric Froude number
λ	m	: Characteristic length
Δ_r	m	: Ripple height
δ	m	: Boundary layer thickness
ε_s	m^2/s	: Sediment diffusivity
γ	-	: Buoyant weight of sediment
ν	m^2/s	: Kinematic viscosity of fluid
ν_t	m^2/s	: Eddy viscosity of fluid
ξ	-	: Surf similarity parameter
ρ	kg/m^3	: Fluid density
ρ_s	kg/m^3	: Sediment particle density
τ_b	N/m^2	: Bed shear stress
ω	rad/s	: Angular frequency
Ψ	-	: Dean number
Ω	-	: Mobility parameter